EXPERIMENTAL TESTING OF A LIGHTLY REINFORCED CONCRETE SHEAR WALL

A Project

presented to

the Faculty of California Polytechnic State University,

San Luis Obispo

In Partial Fulfillment

of the Requirements for the Degree

Master of Science in Architectural Engineering

by

Jerry Luong & Rory de Sevilla

Fall 2020

COMMITTEE MEMBERSHIP

TITLE:	Experimental Testing of a Lightly Reinforced Concrete Shear Wall
AUTHORS:	Jerry Luong & Rory de Sevilla
DATE SUBMITTED:	Fall 2020
COMMITTEE CHAIR:	Anahid Behrouzi, Ph.D. Assistant Professor of Architectural Engineering
COMMITTEE MEMBER:	Peter Laursen, Ph.D., PE Professor of Architectural Engineering
COMMITTEE MEMBER:	Cole McDaniel, Ph.D., PE Professor of Architectural Engineering

ABSTRACT

Experimental Testing of a Lightly Reinforced Concrete Shear Wall

Jerry Hue Truong Luong & Rory Sebastian de Sevilla

This project report summarizes the findings of a half-scale laboratory test on a slender lightly reinforced concrete (LRC) shear wall subjected to cyclic loading. LRC shear walls, specifically those of pre-1980's type design, have longitudinal and horizontal reinforcement ratios near the code minimum, while often lacking confinement in the wall end-zones. These walls are thought to exhibit brittle compressive failure mechanisms such as rebar buckling or concrete crushing based on observations from past earthquakes. Non-ductile concrete buildings are a large contributor to earthquake losses around the globe, as noted in the San Fernando (1971) and Christchurch (2011) earthquakes, to name a few. In the U.S., buildings constructed before the 1976 UBC are at risk for collapse and pose a significant threat to occupant life-safety and community resilience. Thus, there is a pressure among structural engineers to create feasible and economical design solutions to address these non-ductile concrete performance issues.

The wall test performed in this paper reproduced a unique failure mechanism of LRC walls tested at the University of Auckland, University of Illinois, and University of Canterbury where there is a limited distribution of plasticity, such that there are few, wide primary cracks and secondary cracks do not develop. Also, the several of these tests (Cal Poly and Auckland) exhibit higher than anticipated displacement ductilities due to rocking at the wall-foundation interface. The experimental test results from this project enable the examination of current industry practice for conducting nonlinear analysis of LRC walls as discussed in Doan & Williams (2020).

Keywords: [Non-ductile concrete shear wall, lightly-reinforced shear wall, slender wall, pre-1980's detailing, rectangular structural wall]

ACKNOWLEDGMENTS

This project was mainly funded through the Research, Scholarly, and Creative Activities (RSCA) Grant Program of Cal Poly San Luis Obispo. Additional funding from the Structural Engineering Foundation was also helpful during this project. The Architectural Engineering Department Parents Learn by Doing Fund was also a major contributor to this project.

Garrett Hagen of Degenkolb Engineers deserves a tremendous acknowledgement for consistently answering our questions and for giving us valuable analysis guidance, despite being in Chile during preparations for experimental testing. Scott Arnold, Rey Ortiz, Victor Reyes, and Christian Molina of FYFE also deserve many thanks for providing us with much needed FRP expertise. Thanks also to our advisors, Anahid Behrouzi, Peter Laursen, and Mike Deigert for giving us assistance with the project and keeping it moving along.

Regarding material support, we are grateful for Simpson Strong-Tie's extremely generous donations including two-story custom strong-frames and other hardware. We are also grateful to LMS Reinforcing Steel Group for donating all our rebar on the project as well as to CalPortand for donating all the concrete. Additional thanks are owed to McClone Construction for providing designs, drawings, and hardware for the wall and footing formwork, Zircon for donating a rebar scanner, and Ryan Stolz Concrete Pumping for their services during the wall and footing pour.

Special thanks also to Cal Poly lab tech and electro-mechanical expert Vince Pauschek who donated so much of his time to help us get the test setup in shape. Our project kept him in the lab late on Friday night probably one too many times. Similarly, Tim Dieu and Dave Kempken gave us incredible fabrication assistance and made sure we were safe throughout the project.

We are thankful for the many students that supported our project: Jenna Williams and Tracy Doan for assistance with instrumentation, fabrication, and testing; Ryan Schwartz for his coordination and setup of camera equipment during testing; Carlos Espitia, Johnny Ott, and Ian McCandless who helped to greatly

reduce the construction timeline by constructing the footing and wall formwork; Luke Ostrom who effectively procured material and labor donations for the project and helped us perform the parametric study that led to the final specimen design. Additional thanks to undergraduate Colin Ridgley for designing the axial load application system and to Marin Govett for support during experimental preparations. A final thanks to Aiden Bernhardt, Rachel Chandler, and Sydney Gallion for giving us an extra hand during both concrete pours.

TABLE OF CONTENTS

LIST OF TABLES

LIST OF FIGURES

LIST OF SYMBOLS

A_g	Gross area of concrete section, in^2
b	Width of wall, in
c	Depth of compression zone in wall, in
d	Distance from extreme compression fiber to centroid of longitudinal tension reinforcement, in
d_b	Diameter of longitudinal tension reinforcement, in
E_c	Elastic modulus of concrete per ACI 318, calculated as $57{,}000\sqrt{f_c'}$
E_s	Elastic modulus of steel (29,000 ksi)
f_c'	Specified compressive strength of concrete, psi
f_r	Modulus of rupture of concrete per ACI 318, calculated as $f_r = 7.5\lambda\sqrt{f_c'}$
f_u	Specified ultimate strength of reinforcement, psi
f_y	Specified yield strength of reinforcement, psi
h	Wall height, the distance from the base of the concrete footing to the top of the concrete wall, in
l_w	Wall length, the length of the concrete wall parallel to the ground plane, in
N_a	Axial Load Ratio, the ratio of axial load to specified compressive strength of concrete multiplied by the gross concrete area, calculated as $100*P/(f_c'*A_g)$, %
t_w	Wall thickness, the shortest dimension of the concrete wall, in
h/l_w	Shear span, a ratio of wall height to wall length
l_w/t_w	Cross sectional aspect ratio (CSAR), the ratio of wall length to wall thickness
V_c	Nominal shear capacity of member provided by concrete, lb
V_n	Nominal shear capacity of member, lb
V_s	Nominal shear capacity of member provided by steel, lb
ρ_l	Longitudinal reinforcement ratio, the ratio of longitudinal rebar to gross concrete cross sectional area
ρ_h	Horizontal reinforcement ratio, the ratio of horizontal rebar to gross concrete area along the height of the wall

1. INTRODUCTION

1.1. Background

Reinforced concrete (RC) buildings are common in California, especially in the most populated cities of Los Angeles, San Francisco, and San Diego. The construction of RC buildings is not new, with the late 1800's marking their first construction in California (Wermiel, 2009). Since that time, engineers have faced challenges designing them for zones with high seismicity. Each major earthquake has propelled a greater understanding of seismic RC design, but often at the cost of collapsed structures and lost lives.

Non-ductile RC buildings are the most vulnerable concrete structures to catastrophic earthquake damage or collapse. These buildings have insufficient detailing to allow the lateral force resisting system (LFRS) to withstand large earthquake forces and displacement demands. The LFRS can be comprised of either concrete frames or concrete shear walls, and while each system has its own design concerns to achieve adequate performance when subject to seismic loading this report will focus on shear walls.

The code-mandated design of RC shear wall systems in California per the American Concrete Institute (ACI) Building Code Requirements for Structural Concrete (ACI 318) has evolved dramatically over time. Some of the most important updates happened after the San Fernando earthquake in 1971. As a result, RC buildings built around this time and before (or, pre-1980s construction in general) are specifically susceptible to damage in a major seismic event. Unfortunately, many pre-1980s RC buildings exist in the greater Los Angeles and San Francisco areas. Recent efforts by the Concrete Coalition to quantify the number of vulnerable RC buildings in California yield estimates indicating between 16,000-17,000 pre-1980s RC buildings exist in California with over 3000 in Los Angeles alone (Comartin, 2011). The survey also confirms a large percentage of these structures utilize RC shear wall systems as the LFRS.

Pre-1980s non-ductile RC shear walls have distinct detailing flaws which are most concerning to the engineering community, including low longitudinal reinforcement ratios and no boundary elements. These walls have undesirable failure mechanisms when subjected to large earthquake lateral forces: lightly

reinforced walls may not develop plastic hinges necessary for ductile behavior to occur, and walls without modern boundary element detailing are susceptible to sudden failure due to rebar buckling or concrete crushing in the highly stressed wall end zones. The occurrence of these failure mechanisms can be observed in the Alaska earthquake of 1964, San Fernando earthquake of 1971, Chile earthquakes of 1985 and 2010, and others (Birely, 2012). The consequences of these non-ductile failures are catastrophic to the building and its inhabitants.

Structural engineers have been aware of the dangers associated with non-ductile RC shear walls for several years, but the public is slower to respond to this danger. Financial reasons are a barrier to building owners retrofitting their property to prevent building collapse before a large seismic event occurs (Bernstein, 2005). As a result, the structural engineering profession is seeking to better understand the performance of pre-1980s RC shear walls to economically mitigate the related risks.

1.2. Objective and Scope

The primary objective of this project was to investigate the behavior of flexure dominated lightly reinforced concrete (LRC) shear walls subjected to cyclic loading. The secondary objective is to understand current methodologies available on increasing performance of LRC shear walls, mostly with retrofits involving fiber-reinforced polymer (FRP). The experimental findings from this project were utilized to review current industry practice for nonlinear analysis of LRC walls in Doan & Williams (2020).

1.3. Organization of Contents

The contents of this paper are centered around the full-scale LRC wall test performed by the project team.

Chapter 1 provides insight into the background and the issues with LRC and non-ductile RC walls.

Chapter 2 presents typical failure modes of LRC walls after seismic events, a survey of relevant ACI-318 code changes surrounding concrete walls, existing literature involving experimental testing of LRC walls, and existing literature involving experimental testing of modern walls.

Chapter 3 overviews the dimensions, materials, and sectional capacities of the tested wall specimen. Chapter 4 provides details on the experiment setup, loading systems, instrumentation, and construction of the test specimen.

Chapter 5 describes the experimental testing of the wall specimen including the loading protocol, damage progression, and results.

Chapter 6 presents the analysis methods chosen to predict the wall specimen's global behavior.

Chapter 7 summarizes key findings of the experimental testing performed and provides recommendations for further research.

The appendices contains supplementary information used during the design and implementation of the experimental test.

2. LITERATURE REVIEW

This chapter presents a review of the seismic design and performance of flexurally-dominated, lightly-reinforced concrete (LRC) walls. Section 2.1 presents an overview of LRC damage types observed after significant earthquakes. Section 2.2 presents a focused overview of the progression of the ACI 318 design provisions for detailing boundary element rebar. Section 2.3 provides an overview of experimental tests that examine the response of LRC walls which do not contain boundary elements. Section 2.4 contrasts the performance of modern walls to vintage walls.

2.1. Earthquake Damage of Lightly Reinforced Concrete Shear Walls

The documentation of building damage after earthquakes is mainly attributable to engineers who perform reconnaissance and disseminate these observations in journal articles. The information in these reports or articles is often sparse regarding structural wall damage, yet there are a number of researchers that have synthesized data about recorded structural wall damage to identify trends and for comparison to experimental testing of walls (Wood et al., 1987; Kaplan et al., 2004; Moehle, 2011; Kam, Pampanin, & Elwood, 2011; Birely, 2012). This section summarizes the most relevant types of damage specifically for flexure-dominated LRC shear walls.

2.1.1. Compressive Boundary Element Damage

Compressive boundary element damage is evident when the end zones of a rectangular wall have become highly stressed usually due to excessive cyclic loading. Flexural-compression failures typically result from this type of damage and are visually identifiable by bar buckling and/or concrete crushing in the wall end zone. Examples of this failure mode are shown in Figure 2-1. A survey of 91 damaged buildings with reinforced concrete walls spanning between the 1957 Mexico City Earthquake to the 2010 Chile Earthquake reveals that this damage type was the governing behavior in about 50% of the damaged walls in the U.S. and Chile (Birely, 2012). Similarly, the 2011 Christchurch Earthquake produced many flexural-compression wall failures, especially in pre-1980s construction (Kam et al., 2011). It is widely accepted

that these failures are due to poor ductility detailing as well as inadequate horizontal and vertical reinforcement at critical regions of the walls.

Figure 2-1: Compressive Boundary Element Damage in the 2011 Christchurch Earthquake, Kam et al. (2011)

2.1.2. Flexural Tension Damage / Rebar Fracture

Flexural tension damage is evident when the rebar typically in the end zones of a rectangular wall have fractured due to excessive cyclic loading and/or axial tension. These failures are visually identifiable in locations where concrete has spalled, exposing fractured rebar segments. Significant horizontal cracking is another indicator of axial tension and thus possible rebar fracture. Minor rebar buckling prior to rebar fracture is common. Examples of this failure mode are shown in Figure 2-2.

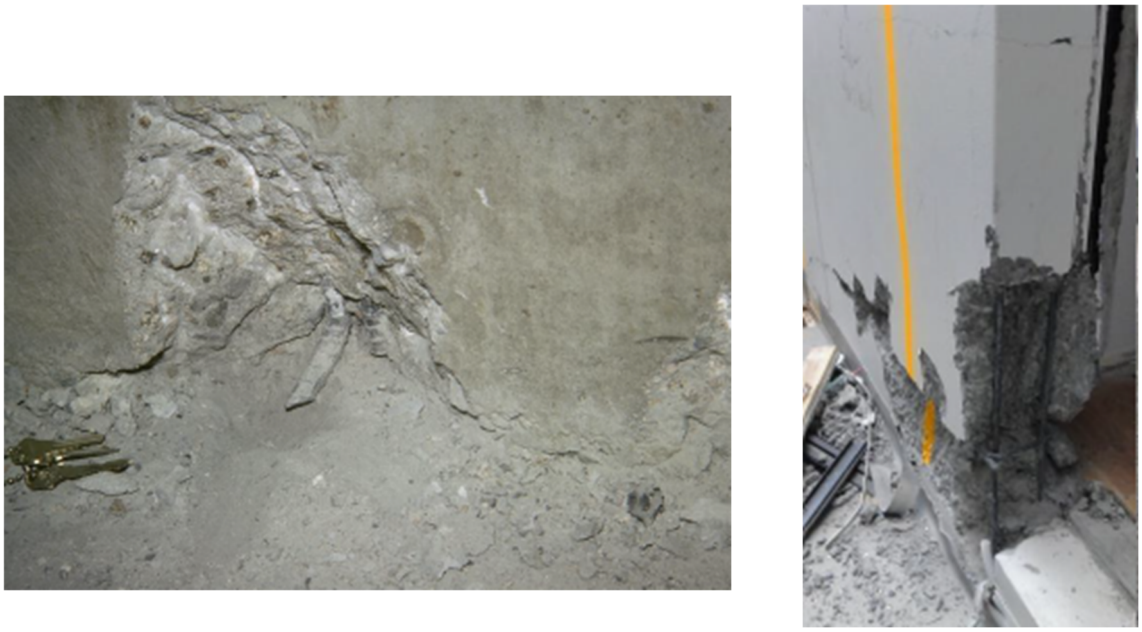

Figure 2-2: Fracture of Longitudinal Reinforcement in Major Earthquakes
(Left) Longitudinal rebar fracture following the 1971 San Fernando Earthquake (Birely, 2012) and
(Right) Longitudinal rebar fracture following the 2011 Christchurch Earthquake (Kam et al., 2011)

Figure 2-2 (right) shows a structural wall in the Gallery Apartments building in Christchurch is a particular case of flexural tension damage where vertical rebar fractured along a single primary crack plane (Kam et al., 2011; CERC, 2012; Hoult et al., 2018). The concentrated yielding of the vertical rebar crossing the primary crack was due to the lack of secondary crack formations (CERC, 2012). This failure mode was also observed in the El Faro building 1st floor shear walls during the 1985 Chile Earthquake (Hoult et al., 2018).

2.1.3. Summary of Earthquake Damage

In general, flexural-dominated LRC walls have exhibited two types of failure modes after earthquakes: compressive boundary element damage resulting in flexural-compression failures, vertical rebar buckling, and concrete crushing; and flexural tension damage resulting in vertical rebar fracture and a lack of secondary crack formations. Engineers believe these failures are non-ductile given how suddenly they can occur and because significant lateral strength capacity is lost. If vintage LRC walls are shown to have non-ductile failures after earthquakes, it is relevant to investigate the progression of structural wall detailing to understand the context in which these walls could be constructed.

2.2. Progression of Structural Wall Detailing in ACI 318

The design provisions from ACI 318 for detailing of reinforced concrete (RC) shear walls have changed significantly between the years 1971 and 2019. Note that only ACI 318-63, 71, 14, 19 are considered as it compares and contrasts walls design requirements for what is considered non-ductile and ductile detailing. More information on the historical changes in ACI 318 can be found in Behrouzi (2016). The most important changes came as earthquakes occurred and more knowledge about effective seismic design became available. This section presents a summary of the changes in relevant code provisions regarding wall reinforcement and boundary element detailing.

2.2.1. ACI 318-63

ACI 318-63 allows for two methods of design – via structural analysis or based on empirical formulas. The wall design requirements, per ACI 318-63 Chapter 22, are as follows:

- Minimum vertical wall reinforcement: 0.0015*reinforced section of the wall, if of reinforcement (ACI 318-63 §2202(f)).
- Minimum horizontal wall reinforcement: 0.0025*gross area (ACI 318-63 §2202(f)).
- Minimum curtains of reinforcement: Walls more than 10 inches thick need two curtains (ACI 318-63 §2202(g)).
- Spacing of reinforcement: No. 3 at 18” o.c. (ACI 318-63 §2202(g)).

2.2.2. ACI 318-71

ACI 318-71 allows for two methods of design – via structural analysis and empirical formulas. Changes to the empirical wall design requirements, per ACI 318-71 Chapter 14, are as follows:

- Minimum vertical wall reinforcement: 0.0015*gross area but may be reduced to 0.0012 if of a specified yield strength of 60 ksi and No. 5 or smaller reinforcing is used (ACI 318-71 §14.2(f)).
- Minimum horizontal wall reinforcement: 0.0025*gross area but may be reduced to 0.002 if of a specified yield strength of 60 ksi and No. 5 or smaller reinforcing is used (ACI 318-71 §14.2(f)).

2.2.3. ACI 318-14

ACI 318-14 has two chapters regarding the design of walls resisting gravity and lateral forces – ordinary and special structural walls. Special structural walls require increased detailing and are required in regions with high seismicity. Modifications to the wall design requirements are listed in the following sections.

2.2.3.1. Requirements for Ordinary Structural Walls

ACI 318-14 Chapter 11 provides design requirements for non-prestressed cast-in-place walls.

- Minimum vertical and horizontal wall reinforcement: based on ratio of concrete strength to ultimate shear demands (ACI 318-14 §11.6).
- Minimum spacing of longitudinal reinforcement: Minimum spacing of 18 inches on center or 3 times the wall thickness. If shear reinforcement is required, spacing is limited to 1/3 times the wall length (ACI 318-14 §11.7).
- Minimum spacing of transverse reinforcement: Minimum spacing of 18 inches on center or 3 times the wall thickness. If shear reinforcement is required, spacing is limited to 1/5 times the wall length (ACI 318-14 §11.7).
- Transverse ties: If longitudinal steel is required for axial strength or if A_{st} exceeds $0.01A_g$, longitudinal reinforcement will be tied with transverse ties. (ACI 318-14 §11.8).

2.2.3.2. Requirements for Special Structural Walls

ACI 318-14 Chapter 18 provides design requirements in §18.2.1.5, §18.2.1.6(g), and T. R18.2 for special structural walls.

- Shear-span and aspect ratio: Geometry of wall affects the governing design provisions of walls (ACI 318-14 T.R18.10-1).
- Minimum vertical and horizontal wall reinforcement: the required reinforcing ratio, ρ_l, is 0.0025 (ACI 318-14 §18.10.2) but may be reduced to values found in ACI 318-14 §11.6 based on the expected shear demand.

- Boundary element detailing: Special boundary reinforcing is required for flexural dominated walls where concrete strains exceed those prescribed by ACI 318-14 §18.10.6.2. Boundary element shall extend horizontally into the compression zone (ACI 318-14 §18.10.6.4(a)). Transverse reinforcement shall satisfy requirements for columns of special moment frames ACI 318-14 §18.10.6.4(e)).

2.2.4. ACI 318-19

With the release of ACI 318-19, there are even more requirements on detailing of the boundary elements. Detailing issues with under-reinforced concrete shear walls are addressed to prevent rupture of rebar at a crack plane. As a result of more knowledge of better detailing and nonlinear performance of concrete shear walls, several changes were implemented.

2.2.4.1. Requirements for Special Structural Walls

- Longitudinal reinforcement: boundary reinforcement steel is limited to the region of 0.15 l_w from the ends of the wall, which is intended to promote the formation of secondary flexural cracks in the plastic hinge region, as noted in ACI 318-19 §18.10.2.4.
- Boundary element detailing: the geometry and drift capacity of the wall are considered in the boundary detailing, as discussed in ACI 318-19 §18.10.6.2. Additionally, more stringent requirements for detailing of horizontal rebar in the boundary element is provided (ACI 318-19 §.18.10.6.4(e).

2.2.5. Comparison of ACI 318 Requirements for Structural Walls

This section compares the requirements of pre-1980's shear wall reinforcement and detailing to modern requirements per ACI 318-14/19. Structural concrete walls designed to ACI 318-71 and prior were not required to have boundary element detailing. However, it is not uncommon to have columns integrated into the ends of the wall. This may have created issues with walls being over-reinforced, which may experience a shear-controlled failure or non-ductile failure. Earlier code provisions did not explicitly require limit state analysis and ductile detailing.

The shear span and cross-sectional aspect ratio are factors that have considerable effects on inelastic performance of walls. ACI 318-14 requires checks on shear-span and cross-sectional aspect ratio to ensure that the wall behaves in a ductile manner. Additionally, ACI 318-14 requires special detailing for rebar in the regions experience high compressive strains and the region experiencing high inelastic deformation. When compared with ACI 318-63/71, ACI 318-14 has more stringent requirements for the design of concrete shear walls.

ACI 318-19 furthers that by providing additional requirements for boundary element detailing, as well as minimum reinforcement requirements to prevent under-reinforced concrete shear walls. Based on recent studies, ACI 318-19 has modified requirements for detailing of rebar in the boundary zones and in the expected plastic hinge region. One significant change, with regards to the performance of flexure-dominated lightly reinforced concrete shear walls, is the requirement of minimum longitudinal reinforcement in the boundary element. Additionally, no lap splices and tighter spacing is required in the region where plastic deformations is expected. These provisions are intended to improve distribution of plasticity, specifically secondary flexural cracking.

2.3. Testing of Lightly Reinforced Concrete Shear Walls

This section reviews the existing literature for experimental tests of rectangular, lightly reinforced concrete shear walls. The purpose of this section is to synthesize the procedures and results from the most relevant wall tests for comparison with the wall test performed in this paper. The tests are presented in chronological order and are summarized regarding each researcher's purpose, test setup, specimen design, materials, and results with specific attention given to the LRC walls in each experiment. A summary table concludes the section along with final discussion. Relevant parameters of interest are discussed below as a preface:

- Longitudinal Reinforcement Ratio: this parameter is the primary factor of interest for this paper. For reference, the minimum longitudinal reinforcement ratio per ACI 318-14 is 0.0025 for moderately loaded cast-in-place walls (§11.6.2). Therefore, the LRC walls explored in this literature review have just above or below this minimum ratio and have no substantial boundary element reinforcement.

- Wall Failure Mode: flexure-tension, shear, shear-compression, or web crushing (Birely, 2012). When a failure mode has caused the lateral load capacity of the wall to drop by at least 20% of the maximum achieved load in a laboratory experiment, this is considered a failure (Park, 1989).

2.3.1. Cardenas & Magura (1973)

Cardenas and Magura were researchers from the University of Illinois investigating the flexural strength of concrete shear walls for high-rise buildings, testing six rectangular walls under quasi-static unidirectional loading. The test setup for the six specimens included loading rods attached to the laboratory floor for lateral load and post-tensioning rods for gravity load (Figure 2-3). The loading was meant to replicate the shear force diagram shown in Figure 2-4, acting on a lower portion of a taller wall. For ease of testing, the specimens were rotated 90 degrees to fit into the testing space. LVDT's were used to measure base rotations, graduated scales measured lateral deflections, load cells measured axial and lateral loads, and strain gages measured longitudinal strains in the vertical rebar.

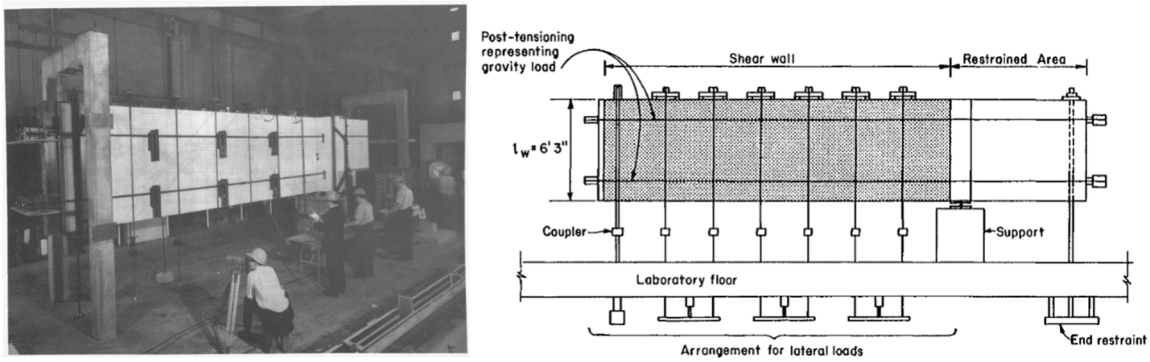

Figure 2-3: Test Setup for Shear Wall Investigation, Cardenas & Magura (1973)

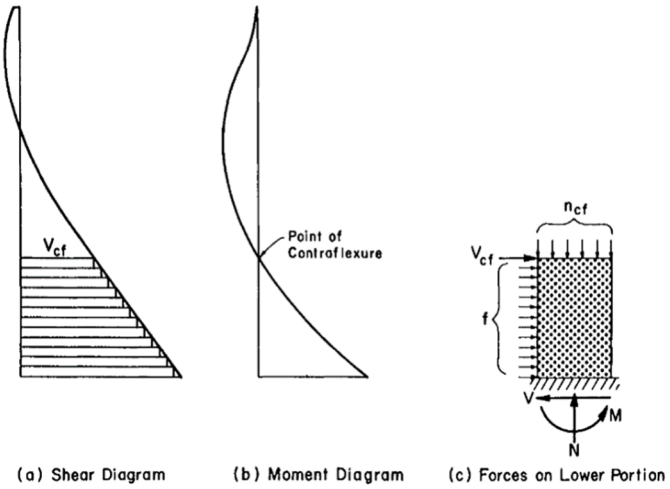

Figure 2-4: Shear and Moment Diagrams for a Typical High-Rise wall, Translated to an Equivalent Model for a Shorter Wall, Cardenas & Magura (1973)

The specimen designs were based upon a survey of high-rise buildings in the Chicago area and cities on the West Coast. The main difference between the specimens was the amount of longitudinal reinforcement in the wall cross section: Specimen SW-1 had the lowest ratio at $\rho_l = 0.0027$. Other parameters for SW-1 can be found in Table 2-1. SW-1 failed in flexure governed by fracture of tension reinforcement at the base of the wall where one large crack formed (Figure 2-5). The researchers attributed this failure mode to the low amount of reinforcement and the relatively high cracking strength of the concrete. All the other specimens with higher reinforcement ratios failed due to concrete crushing.

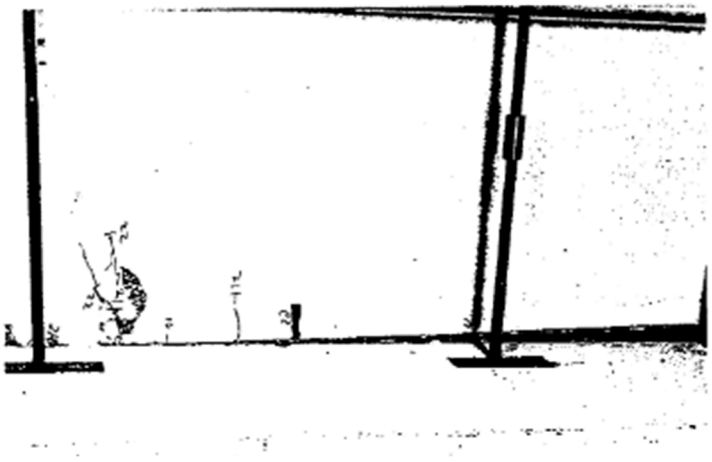

Figure 2-5: Single Crack Plane at the Support of LRC Wall Specimen SW-1 After Testing, Cardenas & Magura (1973).

Cardenas and Magura calculated and measured ductility by comparing the ratio of curvatures at ultimate and at first yield of the rebar. These calculated values were based on Chapter 10 of ACI 318-71, and measured values were averaged over a 40 in. gage length near the base of the walls. In general, curvature ductility decreased with increasing longitudinal reinforcement ratio in the wall specimens, meaning that SW-1 had the greatest ductility equal to 7.0 (Figure 2-6). The next highest ductility was equal to 3.9 for specimen SW-6 with 8.5 times more reinforcement.

In summary, this research and testing by Cardenas and Magura illustrated how changing the longitudinal reinforcement ratios and reinforcement schemes in concrete walls can drastically affect the curvature ductility and energy absorption characteristics of the walls. They also discovered a unique failure mechanism for lightly reinforced walls where a single horizontal crack plane forms at the wall-foundation interface and secondary cracks do not occur.

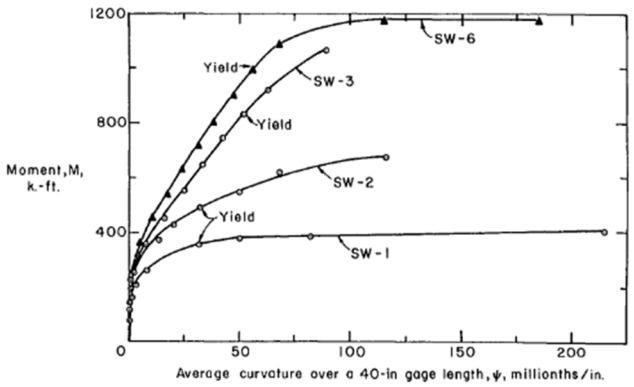

Figure 2-6: Moment-Curvature Relationships, Cardenas & Magura (1973)

2.3.2. Ireland et al. (2007)

Ireland and collaborating researchers at the University of Canterbury in New Zealand investigated an unconventional method of shear wall retrofitting using selective weakening techniques. As part of their shear wall program, they designed, constructed, and tested several benchmark walls via quasi-static cyclic uni-directional loading at two-thirds scale. Specimen W1 was the baseline specimen (with no selective weakening techniques) and had a low reinforcement ratio consistent with a typical pre-1980's New Zealand structural wall.

The loading setup and instrumentation layout for specimen W1 can be seen in Figure 2-7. The tested wall was loaded to represent the lower portion of a much taller wall. The wall was subjected to a constant axial load via two post-tensioning rods on either side of the wall which spanned between a spreader beam and a steel foundation. The lateral force was applied with the horizontal actuator shown, and the wall's movement was restricted by low-friction steel channels alongside the loading beam. Wall response was recorded using linear potentiometers, rotary potentiometers, load cells, and strain gauges on the rebar.

The loading protocol used for specimen W1 was displacement controlled and is shown in Figure 2-8. At each drift level, two complete cycles were performed. The researchers based this loading protocol off the ACI T1.1-01, 2001 recommended regime but used two-cycle sets instead of three-cycle sets, expecting the three-cycle set to be too demanding on the wall.

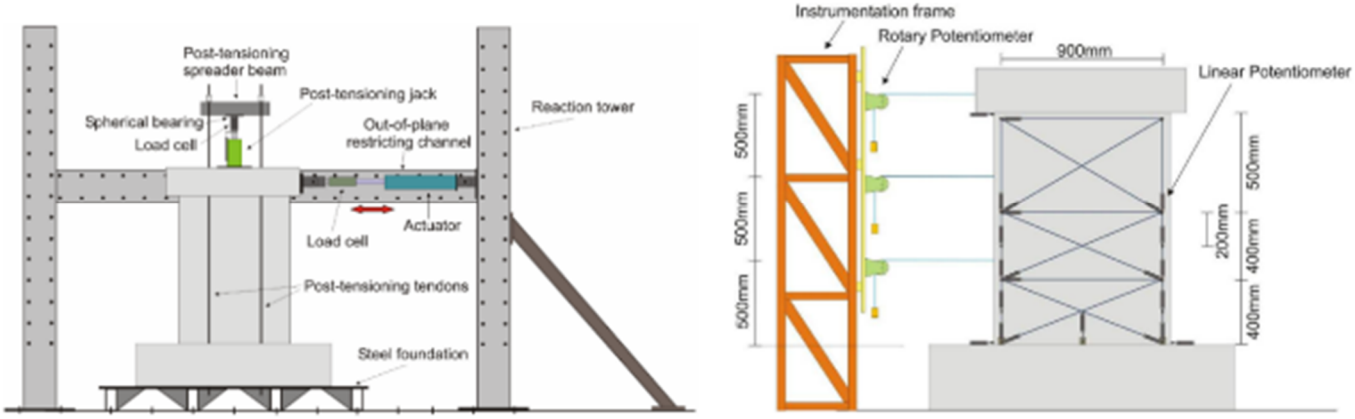

Figure 2-7: Experimental Setup, Ireland et al. (2007)

The specimen design was based on reinforcement details typical of construction practice from the pre-1980's period in New Zealand. The longitudinal reinforcement ratio of specimen W1 was 0.47%, rebar was plain round reinforcement and spliced at the foundation level; additionally, the wall had no boundary elements (see Figure 2-9). Other parameters for W1 are found in Table 2-1.

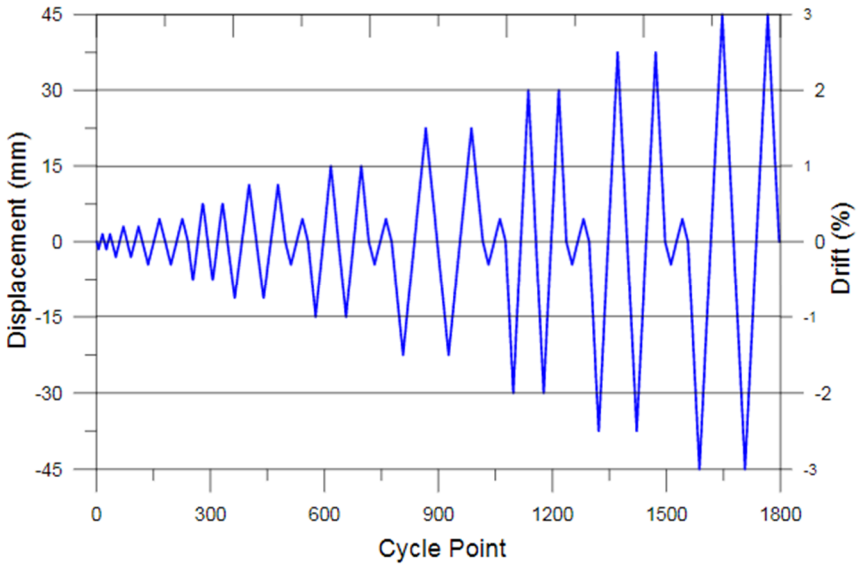

Figure 2-8: Loading Protocol for Specimen W1, Ireland et al. (2007).

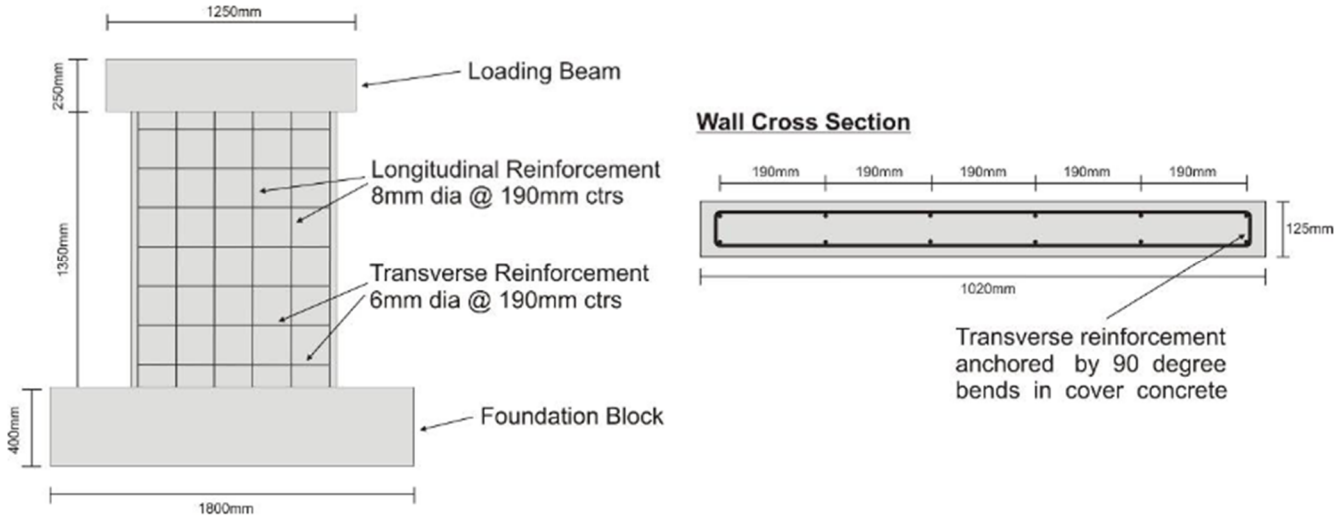

Figure 2-9: Specimen W1 Reinforcement Scheme. Ireland et al. (2007)

The failure of specimen W1 was triggered by buckling and subsequent rupture of longitudinal reinforcement at the wall ends governed by a single crack plane at the wall-foundation interface. A ductile force versus displacement response was achieved up to 2.5% drift, although the wall was tested up to 3% drift (Figure 2-10). When considering the failure of the wall to occur at 2.5% drift, the displacement ductility of specimen W1 was about 10.

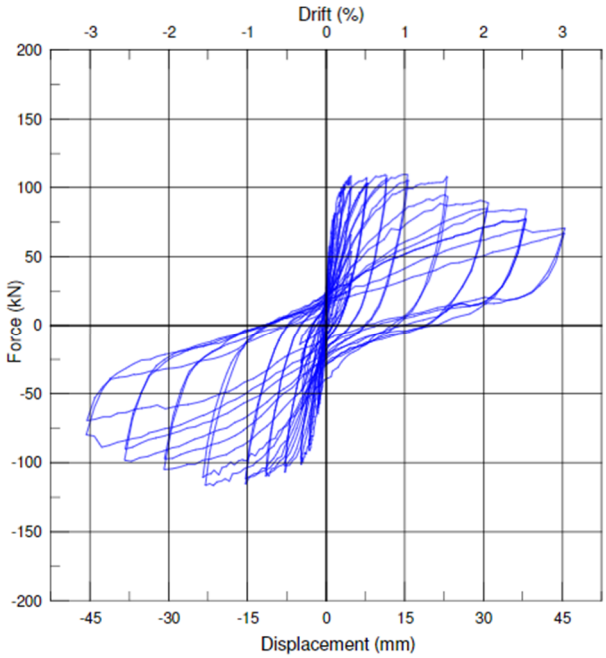

Figure 2-10: Experimental Hysteresis of Specimen W1, Ireland et al. (2007)

2.3.3. Lu et al. (2017)

Lu et al. were researchers at the University of Auckland evaluating the appropriateness of the current minimum longitudinal reinforcement requirements for structural RC walls per the New Zealand Concrete Structures Standard (NZS 3101:2006). They performed a series of tests on six RC walls designed with minimum longitudinal rebar to investigate the failure mode observed by flexure dominated walls during the 2010/2011 Canterbury earthquakes.

The test setup for the wall specimens is shown in Figure 2-11 below. A horizontal actuator applied lateral load at the top of the wall, vertical actuators at each end of the wall applied axial load and moment, and a steel frame surrounding the wall provided out-of-plane stability. The loading was meant to replicate

the net forces acting on a lower portion of a taller wall. String pots were used to measure horizontal drift at the top of the wall, portal gauges (displacement gauges attached to embedded steel studs) were used to measure axial strains and curvatures, and load cells monitored load throughout the tests. The cyclic loading protocol for testing was created in accordance with ACI 374.2R-13 and ACI ITG-5.1-07. All cycles after the theoretical cracking moment was reached were displacement controlled with three cycles per drift level.

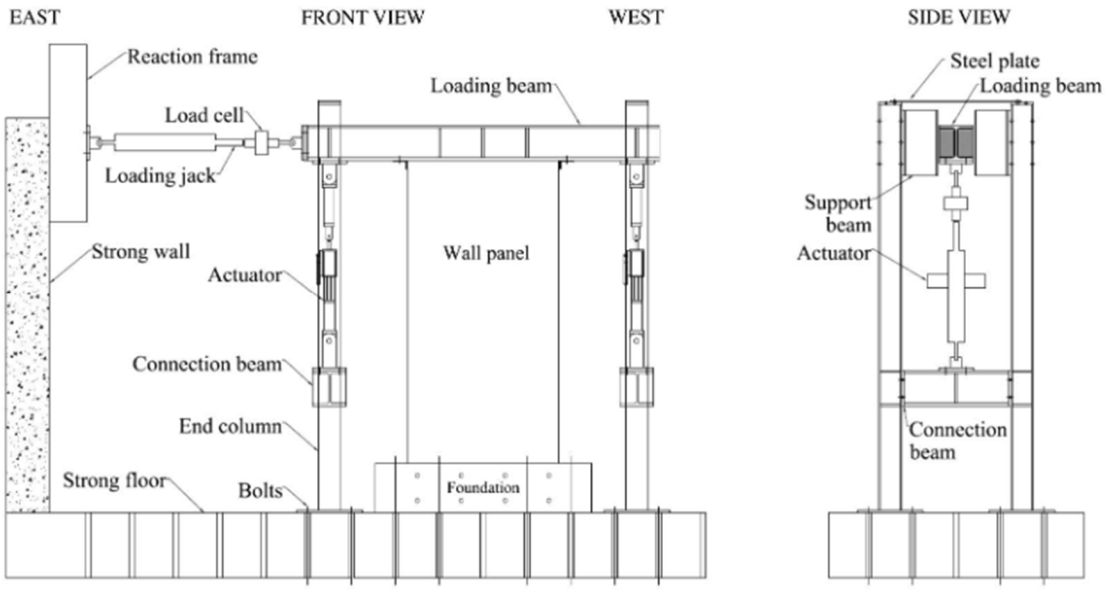

Figure 2-11: Test Setup for Shear Wall Testing, Lu et al. (2017)

The six specimens varied by shear span from two to six, axial load ratio from zero to 6.6%, and usage of end ties from none to about 2.5 inches on center. The walls also had a longitudinal reinforcement ratio of 0.53% and a thickness of about 6 inches. The dimensions of the test specimens were chosen at about half-scale relative to the prototype wall. All specimens failed by rebar buckling and subsequent fracture of the longitudinal reinforcement. The researchers conclude that rebar buckling is particularly likely for LRC walls at moderate drifts. The drift capacity of all specimens except one was 2.5%, defined by a 20% global strength loss (see Figure 2-3 for a hysteresis of specimen C1). The researchers describe this seemingly ductile response to be overestimated by scaling issues of the reinforcement / crack widths and caution readers to expect full-sized walls to perform much worse.

In summary, the behavior of all six test walls was controlled by one to three large flexural cracks at the wall base. The axial load and transverse reinforcement were varied between specimens but had little effect on cracking patterns. Transverse end ties had no significant effect on global ductility. The plastic hinge was estimated using conventional methods but proved inaccurate for these lightly reinforced walls due to the lack of secondary cracking in the plastic hinge region. The researchers recommend that the minimum longitudinal reinforcement per ACI-318, Eurocode 8, and NZS 3101:2006 be revised due to the undesirable failure mode of these walls.

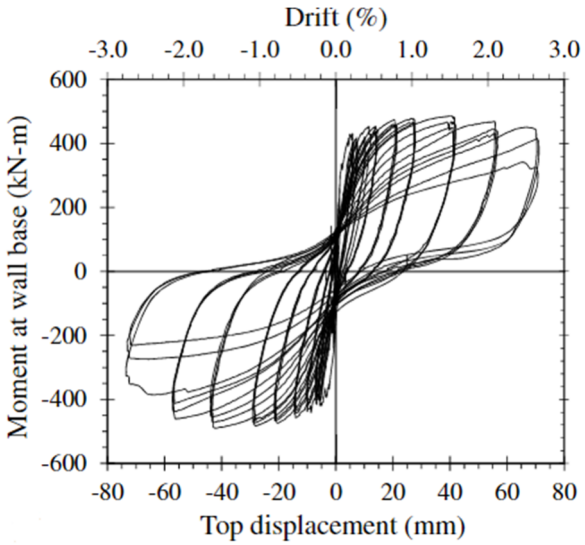

Figure 2-12: Experimental Hysteresis of Wall Specimen C1, Lu et al. (2017)

2.3.4. Summary of Lightly Reinforced Walls

A summary of relevant conclusions regarding the lightly reinforced walls is presented below in addition to a table of important parameters for each test. In general, the walls had similar global ductility and failure mode. Each wall exhibited a distinct failure plane between the foundation block and the base of the wall. Most of the walls exhibited non-ductile behavior compared to the behavior of walls with modern detailing; however, the vintage walls reached higher than anticipated ductility values. Despite this, Lu et al. (2017) notes that the drift capacity of scaled experimental tests may be inaccurately high when compared to the full-size prototype walls they represent.

Table 2-1:Summary of Wall Tests of Lightly Reinforced Concrete Walls

Researcher	Specimen	ρ_l (%)	N_a (%)	f'_c (ksi)	CSAR	SS	Ductility	Failure Mode
Cardenas & Magura (1973)	SW-1	0.27	5.6	7.42	25	2.0	7.0[1]	FT
Ireland et. al. (2007)	W1	0.47	4.7	3.63	8.2	1.3	10	FC
Lu et. al. (2017)	C1	0.53	3.5	5.58	9.3	2.0	12.5	FC
	C2	0.53	3.5	5.00	9.3	4.0	12.5	FC

[1] *Listed value is curvature ductility.*
[2] *FT indicates flexural-tension failure (rebar fracture). FC indicates flexural-compression failure (bar buckling / concrete crushing).*
[3] *A flexural tension failure can occur after bar buckling and/or concrete crushing have occurred.*
[4] *Failure defined as 20% of maximum lateral force loss.*

2.4. Performance of Modern Concrete Shear Walls

This section reviews the existing literature for comparisons between modern and vintage design requirements and analytical and experimental tests of modern reinforced concrete shear walls. The purpose of this section is to provide insight to the differences between modern walls and LRC walls with regards to the performance and failure modes, as reviewed in the previous section.

2.4.1. Dashti and Dhakal (2013)

Dashti and Dhakal (2013) compared analytical models of the performance of reinforced concrete shear walls designed under various standards. The main differences noted in the various standards are the detailing of the boundary elements and minimum reinforcement requirements. The authors distinguish two types of walls – pre-1980s and post- 1980s walls. They describe that pre-1980s generally perform poorly in seismic events due to lack of confinement detailing, inadequate reinforcement, and poor material properties. Consequently, pre-1980s walls were observed to experience concrete crushing and rebar buckling failures. Post-1980s walls were noted to fail from wall web buckling and fracture of vertical rebar in the boundary element.

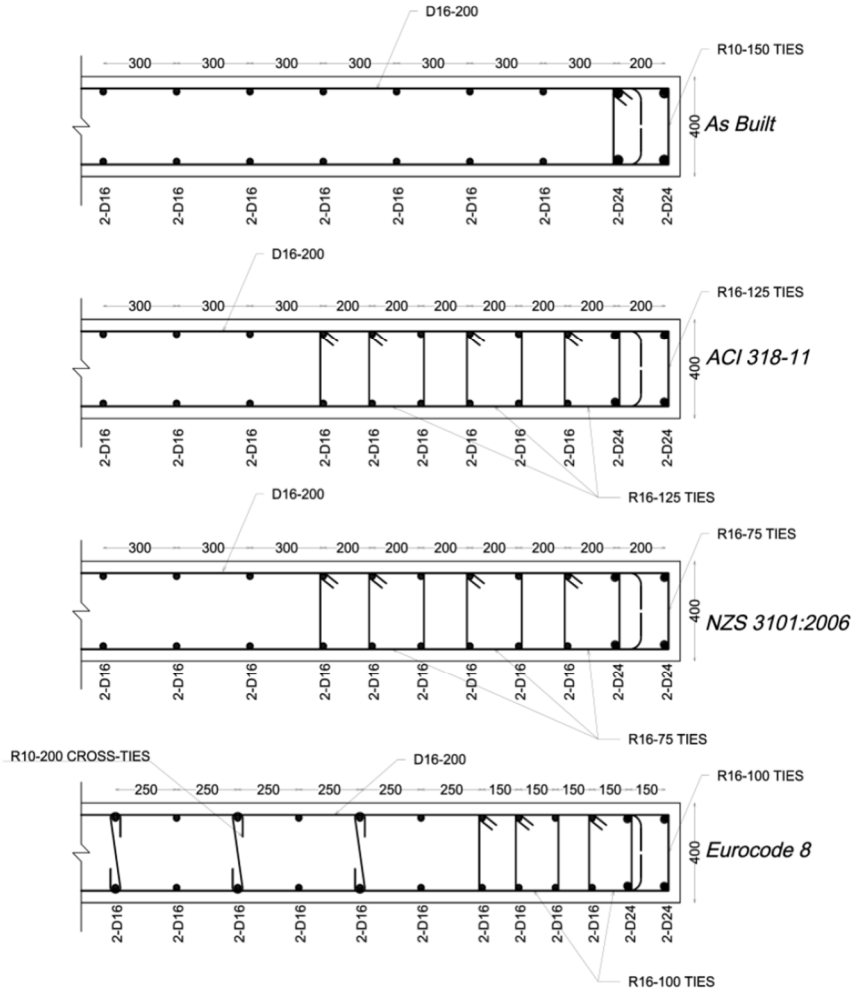

Figure 2-13: Wall Sections, Dashti and Dhakal (2013)

The various standards compared in the study were ACI 318-11, NZS3101:2006, and Eurocode 8. Additionally, the standards were compared to a case study wall built according to the NZS3101:1982, as shown in Figure 2-13. The walls were all slightly modified, such that shear and flexural capacities were similar. An axial load ratio, N_a, of 25% was applied to the analytical models.

From the comparison of the analytical models, it was noted that all the walls performed similarly in the linear range, specifically at cracking and yielding of rebar. Walls with boundary reinforcement detailing that extended beyond the compression depth were able to achieve larger curvature and displacement ductility. Walls lacking the required horizontal confinement length resulted in abrupt strength degradation and lower ductilities, regardless of the volumetric reinforcement ratio in the boundaries.

In summary, analytical models were created to compare the performance of various modern structural standards for concrete shear walls, specifically with regards to boundary element detailing. From the finite element modeling, the walls with the longest length of confined boundary reinforcement were able to achieve displacement and curvature ductilities on the magnitude of 2 and 8x larger than the original wall, respectively.

2.4.2. Seismic Performance Limitations of Slender Reinforced Concrete Structural Walls

Segura (2017) presented experimental results of modern walls and their deficiencies. Segura mentions that modern walls have the potential to achieve high drift ductility and is assumed that modern walls are governed by tension-controlled failures. However, field observations of buildings in regions with similar seismic design standards, when compared to ACI 318-14, demonstrated that modern walls are susceptible to compression-controlled failures.

The experimental testing consisted of two phases. The first phase considered walls WP1-4, which were designed to ACI 318-14 provisions, and the second phase considered walls WP5-7, which included detailing to enhance the performance. The wall specimens are shown in Figure 2-14. Both phases were subjected to reversed-cyclic loads and axial load ratios, N_a, of 10%.

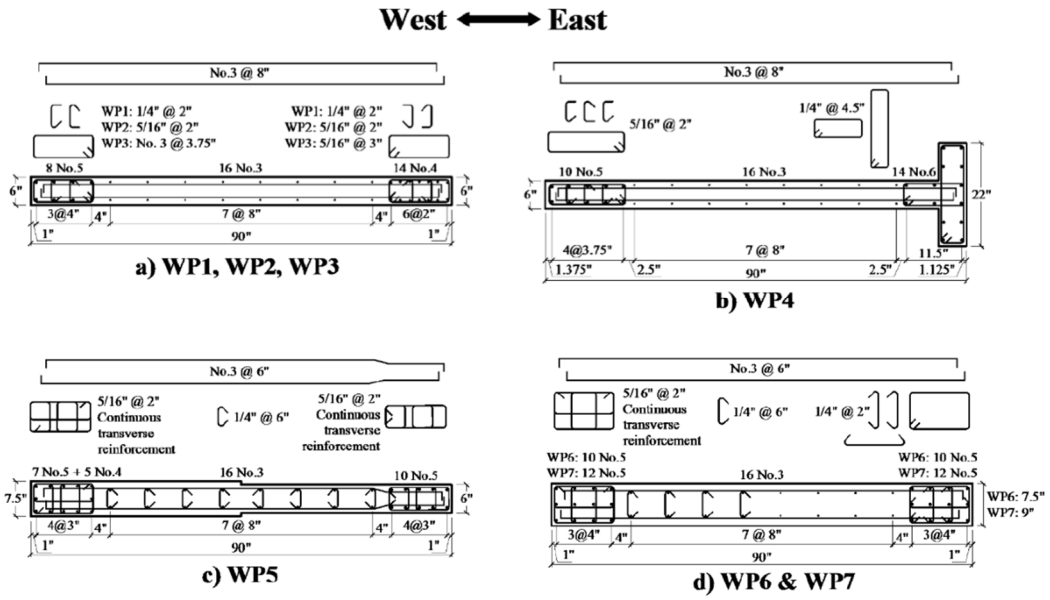

Figure 2-14: Wall Sections, Segura (2017)

Slender walls meeting the minimum thickness requirements of ACI 318-14, are unlikely to exhibit ductile failure modes. Also, slender walls are more unlikely to achieve the desired plastic rotations, such as those prescribed in ASCE 41-13 and ASCE 7-10, and likely to experience out-of-plane instability. Furthermore, modern walls may experience abrupt compression failures when transverse boundary elements are detailed with single hoops and crossties, as opposed to continuous transverse reinforcement, due to non-uniform distribution of transverse strains. In general, walls with lower compression depth-to-wall thickness ratios, *c/b*, will remain stable in compression and achieve larger plastic deformations.

2.4.3. Summary of Performance of Modern Walls

The literature from this section summarized existing analytical and physical studies involving modern reinforced concrete walls. The intent of modern code provisions for concrete shear walls is to prevent non-ductile failure and implies that walls will be tension-controlled (Segura, 2017). However, it is possible for walls designed to current code to still experience non-ductile behavior. Segura states that flexural yielding for slender walls, usually in the formation of a single critical region near the base of the wall and also known as the plastic hinge, is the ideal mechanism for ductile behavior. The intent of ACI 318-14 design provisions for structural walls is to prevent premature compression failures and suggests that walls will be governed by tension-controlled failures. From field observations, walls designed to similar provisions experience concentrated damage near the base, which includes longitudinal reinforcement buckling, out-of-plane instability at boundary elements and crushing of the wall boundary and web.

When walls are well-detailed, such that transverse strains are uniformly distributed, buckling of longitudinal reinforcement is limited, and strains are limited to the region where boundary elements are detailed, more ductile behavior can be expected (Segura, 2017; Dashti and Dhakal, 2013). One notable difference is that LRC walls will develop isolated flexural crack planes, including at the base of the wall, whereas modern walls tend to have distributed flexural cracks, which is a typical indicator of ductile behavior.

2.5. Discussion of Literature Review

This chapter presented a review of the existing literature involving reinforced concrete walls, including a review of prominent earthquake damage types (Section 2.1), previous and current versions of ACI 318 code-based design of structural shear walls dating back to ACI 318-63 (Section 2.2), a review of previous experimental testing of lightly reinforced concrete shear walls in the laboratory (Section 2.3), and an overview of the performance of modern-detailed concrete shear walls (Section 2.4). The following summarizes the observations made:

1. ACI 318 has changed significantly since 1963 regarding the appropriate design of concrete shear walls and thus raises concern for the walls designed to the previous standard.
2. Past earthquakes have revealed the typical failure modes of lightly reinforced concrete (LRC) walls, including compressive boundary element and flexural tension failures.
3. The failure behavior of LRC walls is not easily predicted per contemporary analysis means and the displacement ductility of these walls can be overestimated in the lab due to scaling effects.
4. Thin walls with poor boundary element detailing are unlikely to achieve moderate levels of displacement and curvature ductility, and in some cases may experience out-of-plane stability. ACI 318-19 imposes restrictions on minimum wall thickness (ACI 318-19 T.11.3.1.1). However, thinner walls are acceptable if strength and stability can be proven via structural analysis (ACI 318-19 §11.3.1.1). Additionally, detailing requirements for boundary reinforcement were adopted in ACI 318-14 to account for lateral instability failures seen in recent earthquakes (ACI 318-14 R.18.10.6.4)
5. When compared to LRC walls, walls designed to modern standards can potentially experience compression-controlled behavior, rather than the intended tension-controlled failure modes, despite differences in reinforcement requirements and increased distributed cracking (Segura, 2017).

3. WALL DESIGN & MATERIALS

This chapter outlines the design process, material properties, and geometric parameters chosen for the final wall specimen. Section 3.1 provides an overview of the prototype pre-1980's building used as a basis of design. Section 3.2 discusses scaling of the prototype wall, the parametric study used to refine wall parameters, and lab constraints considered to achieve a feasible test specimen wall. Section 3.3 describes the sectional capacities of the model wall. Section 3.4 describes the footing design used in conjunction with the wall design. Section 3.5 outlines the material testing for both the rebar and concrete used in the project.

3.1. Prototype Building

Many mid-rise buildings built pre-1980s utilize reinforced concrete shear walls as the main lateral force resisting system (Comartin, 2011). As previously mentioned in Section 2.1, ACI 318 had no requirements for special detailing of concrete shear walls at that time. These walls were typically designed to either have minimum longitudinal web and boundary reinforcement (i.e. lightly reinforced) or are often tied to columns at the ends of the wall (overly reinforced). The discussion found in this paper focuses on pre-1980s lightly reinforced concrete shear walls.

The design of the half-scale wall specimen for this project began with plans for a 6-story building constructed in 1958 with story heights of 13.5 feet (Hagen, 2019). The LFRS of the building is LRC shear walls and the building is representative of a common building type in Los Angeles required to be retrofitted per city ordinances. A wall elevation from the prototype building is shown in Figure 3-1. The highlighted 10" thick wall is flexure-dominated with an aspect ratio above 3:1 and is significantly under reinforced with no boundary elements. The typical wall reinforcing schedule for the building is also shown in Figure 3-1.

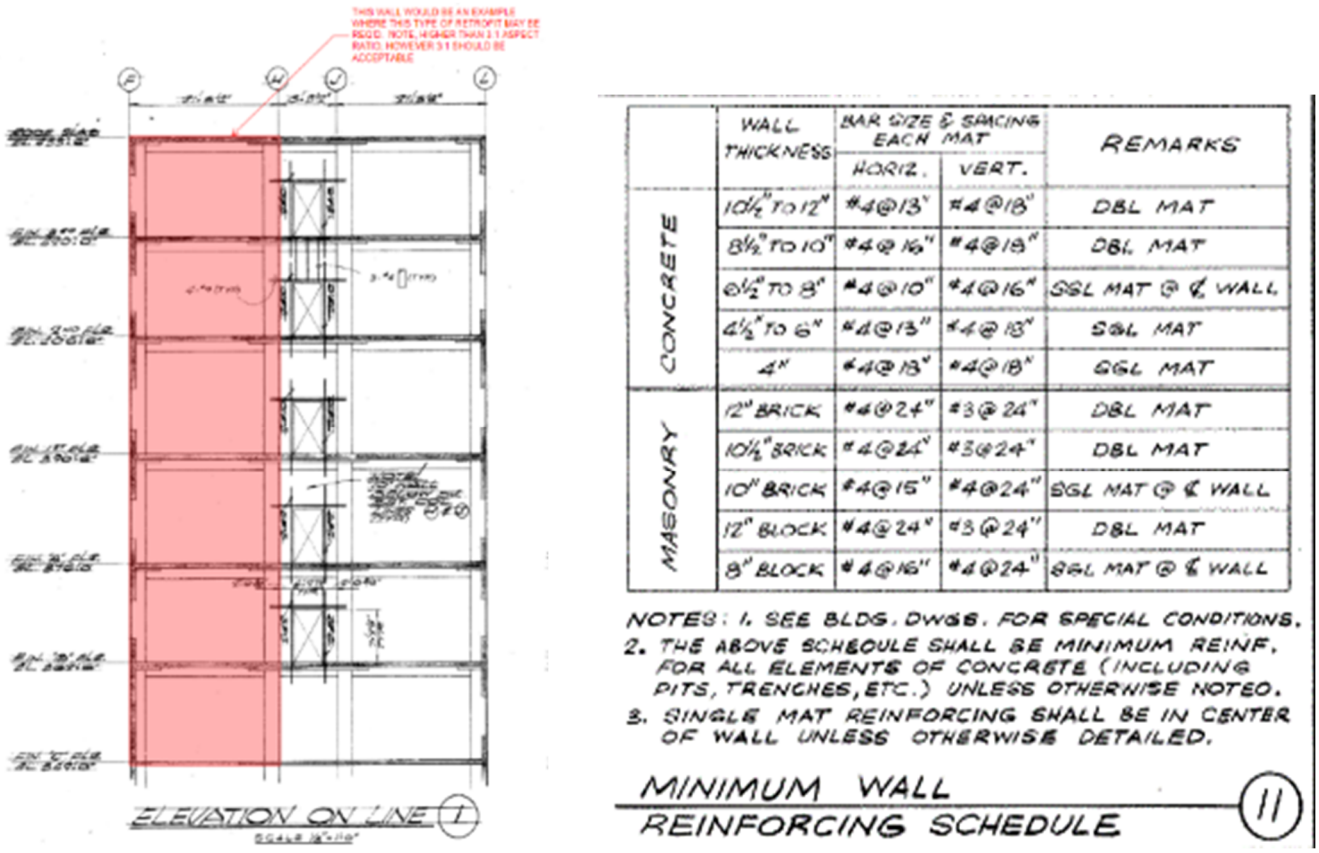

	WALL THICKNESS	BAR SIZE & SPACING EACH MAT		REMARKS
		HORIZ.	VERT.	
CONCRETE	10½" TO 12"	#4@13"	#4@18"	DBL MAT
	8½" TO 10"	#4@16"	#4@18"	DBL MAT
	6½" TO 8"	#4@10"	#4@16"	SGL MAT @ ℄ WALL
	4½" TO 6"	#4@13"	#4@18"	SGL MAT
	4"	#4@18"	#4@18"	SGL MAT
MASONRY	12" BRICK	#4@24"	#3@24"	DBL MAT
	10½" BRICK	#4@24"	#3@24"	DBL MAT
	10" BRICK	#4@15"	#4@24"	SGL MAT @ ℄ WALL
	12" BLOCK	#4@24"	#3@24"	DBL MAT
	8" BLOCK	#4@16"	#4@24"	SGL MAT @ ℄ WALL

Figure 3-1: Prototype Building Information (Hagen, 2019)
(Left) Wall elevation of a prototype building in Los Angeles and (right) wall reinforcing schedule per original structural details.

3.2. General Design Process

The prototype wall in Figure 3-1 has a longitudinal reinforcement ratio of 0.0022, axial load ratio of 1.5%, cross-sectional aspect ratio of 25.8, and shear span ratio of 3.9. Ideally, the wall specimen would have similar values for these parameters, while considering lab constraints.

3.2.1. Scale and Parametric Study

The half-scale wall test specimen represented the bottom 2 stories of the 6-story building. The exact dimensions, reinforcement layout, material properties, and axial loading of the wall were determined via a parametric study to best match the prototype wall behavior (see Table 3-1). An explanation of each wall

parameter and its constraints is described below. The final model wall specimen is shown in Figure 3-2, and the construction of the wall is discussed in Chapter 4.

- Wall Height (**h**): This parameter was constrained by the reaction frame height of 13'-0" (also, maximum height of the actuator applying lateral load to the wall).
- Wall Length ($\boldsymbol{l_w}$): This parameter was selected to achieve a minimum shear span ratio of 2.5-3.0, consistent with a flexure-dominated wall response. Given the maximum wall height of 13'-0", the upper bound for the wall length was about 5'-2". Other aspects that effected wall length were: (i) the longitudinal reinforcement spacing and (ii) the maximum shear force that could be applied by the lateral actuator to ensure wall capacity could be reached during testing.
- Wall Thickness ($\boldsymbol{t_w}$): This parameter was constrained by the target cross-sectional aspect ratio of 15-20 and by constructability concerns including bar size/spacing and cover requirements. Therefore, the wall thicknesses explored for the half-scale wall was 3" to 6", translating to 6" to 12" at full scale. Wall thickness was also dependent on the presence of one or two curtains of rebar since both were common in pre-1980's shear walls. A double curtain was chosen.
- Wall Reinforcement Ratios ($\boldsymbol{\rho_l}$ & $\boldsymbol{\rho_t}$): Both the longitudinal and transverse reinforcement ratios were informed by typical pre-1980's standards (see rebar schedule in Figure 3-1). Horizontal "U" bars at the wall ends were also implemented.
- Material Strengths ($\boldsymbol{f_y}$ & $\boldsymbol{f'_c}$): The expected steel yield stress and expected concrete compressive strength were informed by typical pre-1980's standards. Both materials were typically lower grades in vintage walls compared to current standards based on ASCE 41-17 Tables 10-3 and 10-4 (specified strengths of 40 ksi steel and 3 ksi concrete versus 60ksi and 4.5ksi, respectively).
- Shear Span ($\boldsymbol{h/l_w}$): Since this project is focused on flexure-dominated walls of mid-rise buildings, the desired shear span was 2.5-3.0 for the model wall.
- Cross Sectional Aspect Ratio ($\boldsymbol{l_w/t_w}$): This parameter was constrained by the target ratio of 15-20, representative of thin walls consistent with the vintage of the prototype building.

- Axial Load Ratio ($\mathbf{P}/(\boldsymbol{f_c}')(\boldsymbol{A_g})$): The estimated axial load ratio for the prototype wall is 1.5% and served as a target for the wall test specimen.
- Neutral Axis Depth (**c**): The neutral axis depth, in conjunction with other geometric parameters, has been coined the slenderness parameter (λ_b) and affects wall drift capacity (Abdullah & Wallace, 2019). Previous wall tests indicate λ_b may also affect whether a wall has a compression-controlled or tension-controlled failure (Hagen & Abdullah, 2019). The target neutral axis depth was based on manipulating λ_b to achieve a compression-controlled failure.

Table 3-1: Parametric Study Summary Table of Considered Wall Design Parameters (Modified from Ostrom, 2018)

	Parameter of Interest	**Desired**	**Analyzed**	**Selected**
Wall Dimension	Length (in)	48	42-62	60
	Width (in)	5-6	3-6	5
	Height (ft)	12*	11-13	12.75
Rebar Layout	Vertical Rebar (#3@ x" o.c.)	16-24	12.4-19.8	14.3
	Horizontal Rebar (#3 @ x" o.c.)	10-24	11-14.3	14.3
	Vertical Reinforcing Ratio, ρv (%)	-	0.20-0.47	0.44
Materials	Concrete Comp. Strength, f'_c (ksi)	-	3-4	3
	Rebar Yield Strength, f_y (ksi)	40	40	40
Design Parameters	Shear Span (h/l_w)	3*	2.13-3.41	2.55
	CSAR (l_w/t_w)	15-20*	7.04-20.68	12
	Axial Load Ratio (x% * f'_c*A_g)	-	1-3.1	3.1
	Neutral Axis	4.17-6.25	2.28-5.25	5.25

** Based on Lab Restrictions*

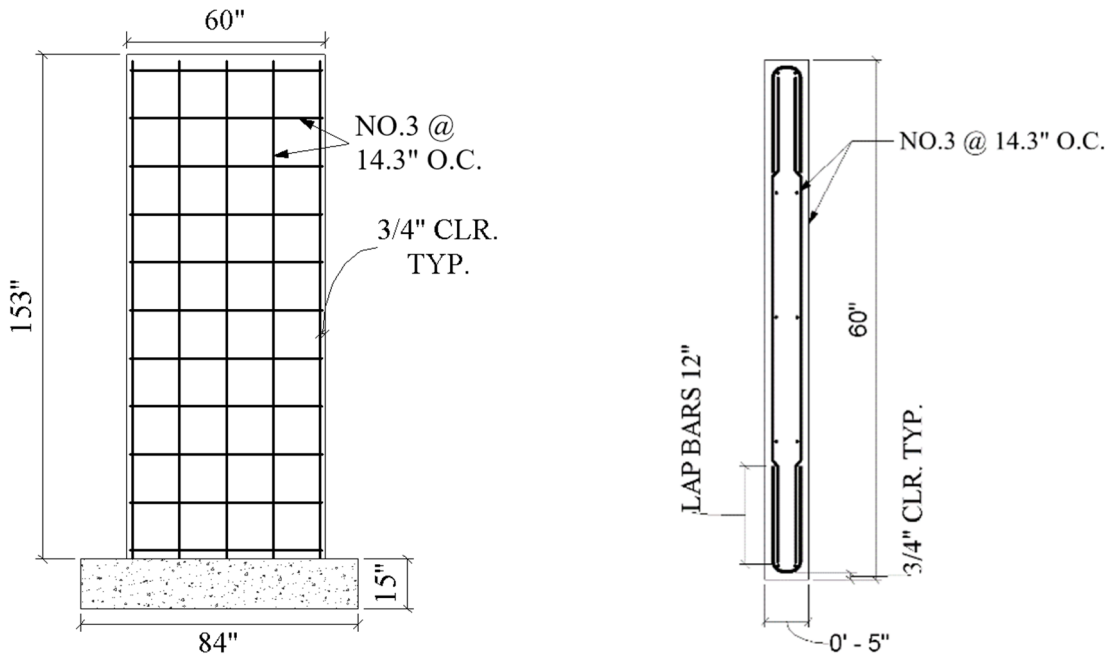

Figure 3-2: Final Half-Scale Wall Specimen Dimensions and Rebar Layout

3.3. Sectional Capacities

3.3.1. Wall Flexural Design

This section discusses the flexural design of the half-scale wall specimen given design parameter values described in Section 3.2.1. Based on the prototype wall in Figure 3-1, No. 4's at 18" on center for a double curtain 10" thick wall were specified. For the scaled wall specimen, this resulted in flexural reinforcement of No. 3's spaced at 19.8" and shear reinforcement of No. 3's spaced at 14.3" (a stricter spacing requirement). For simplicity, No. 3's spaced at 14.3" were chosen for both the shear and flexural reinforcement, compliant with the maximum bar spacing of 18" per ACI 318-19. With this rebar layout, the wall thickness and length were selected to be 5" and 60", respectively. A specified concrete compressive strength of 3000 psi was also selected.

The wall's flexural design was governed by the maximum load capacity of the lateral load actuator, capable of 110 kips (compression) and 23.6 kips (tension). The tension capacity governed the shear force that could be applied at the top of the wall at a maximum of 13 feet above the specimen's base equating to a maximum applied moment of 306.8 k-ft. A capacity-based analysis was used to verify that the wall would

fail in flexure. With the given specimen geometry and reinforcement configuration, an axial load-moment interaction diagram was created using SPColumn (StructurePoint, 2019) to estimate the flexural capacity of the wall at the given axial load ratio. A nominal moment of 223 kip-ft was predicted, well within the capacity of the actuator.

3.3.2. Wall Shear Design

This section discusses the shear design of the wall specimen per ACI 318-14. The nominal shear strength based on No 3's at 14.3" was calculated per ACI 318-14 Equation 18.10.4.1.

$$V_n = A_{cv} \left(\propto_c \lambda \sqrt{f_c'} + \rho_t f_y\right) \qquad [3-1]$$

where V_n is the nominal shear strength, A_{cv} is the gross area of concrete, $\propto_c$ is the shear-span coefficient, and ρ_t is the shear reinforcement ratio. The calculated nominal shear strength is 87.4 kips. The nominal shear strength across the assumed shear plane at the base is calculated by ACI 318-14 Equation 22.9.4.2:

$$V_{n,f} = \mu A_{vf} f_y \qquad [3-2]$$

where μ is the coefficient of friction and A_{vf} is the area of reinforcement crossing the assumed shear plane to resist shear. The longitudinal rebar from the walls provided shear friction resistance. A coefficient of friction of 1.0 is assumed because the interface between the footing and concrete shear wall was roughened. The calculated nominal shear friction strength is 60.3 kips.

3.4. Shear Wall Footing Design

The reinforced concrete footing was required to provide an adequate tie-down to the strong floor to resist loads applied to the wall specimen, be reusable for future wall tests to reduce fabrication time and cost, and weigh no more than 5000 pounds to meet the lab crane capacity. The connection of the footing to the strong floor relies on clamping and friction (not bearing) of all-thread bolts spaced on a 3'0" grid. The 48" W x 84" L x 15" H footing was cast directly on top of the existing strong floor to maximize friction between the two surfaces; six PVC tubes were cast as sleeves for the all-thread bolts. Since the intent was to use the same footing for subsequent wall tests, plans were made for each wall to be constructed in a separate pour

from the footing. The vertical rebar in the wall specimens were designed to be epoxied and embedded into the footing where the first wall specimen is offset 4”, in the long direction of the footing, from the intended location of the second wall specimen.

Figure 3-3 shows the rebar layout for the footing. 90-degree rebar was provided around the PVC sleeves to prevent side-face blowout or concrete cone failure in the footing. Connection points for the vertical actuator system applying axial load were located at the middle of the footing on both sides of the wall. These regions were assumed to be highly stressed and thus a heavily reinforced strut was designed at the bottom of the footing to prevent pullout failure. For more information on the construction of the footing refer to Section 4.2, and for footing design or capacities see Appendix Section A.

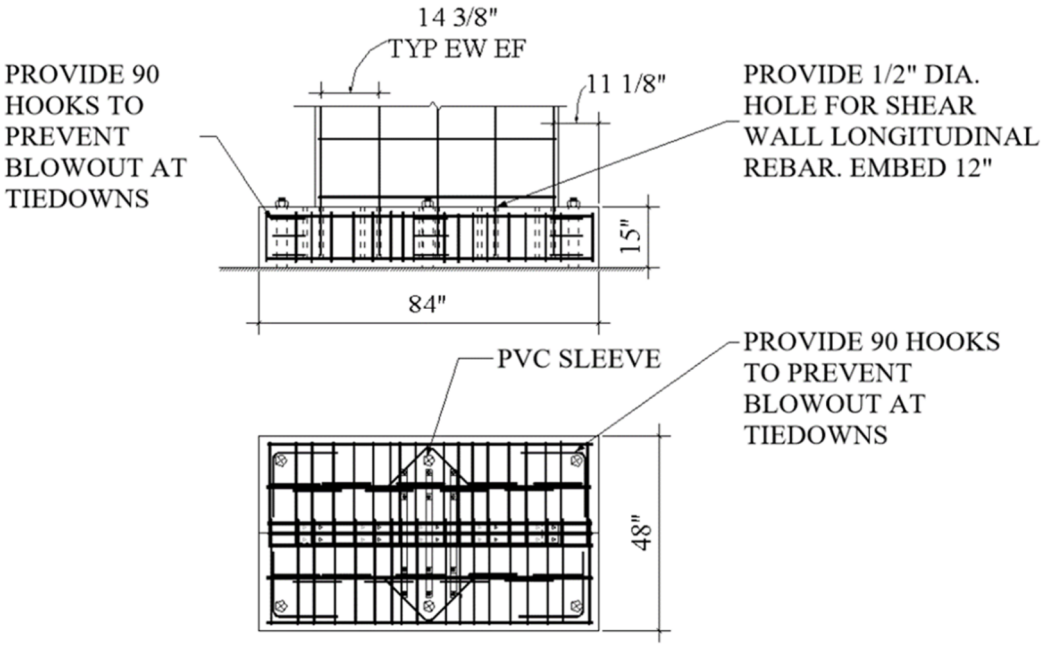

Figure 3-3: Reinforcement in Footing
(Top) Cross-section and elevation of rebar in footing and (bottom) plan view of rebar in footing.

3.5. Concrete Mix Design

The concrete mix design provided by CalPortland for the footing and wall was intended to have similar properties to that of 1980’s walls. Vintage concrete mixes typically had a nominal compression strength of 3000 psi, as opposed to the current standard of 4000 psi. For the half-scale wall specimen, the specified

mix also had a maximum aggregate diameter of 3/8” (as opposed to the typical 3/4”) to allow the concrete to pass between the rebar and formwork in the narrow wall cross-section for proper consolidation. See Table 3-2 for more information on the mix design.

Table 3-2: Concrete Mix Design

Materials	Percent Used	Absolute Volume [ft^3]	Pounds/Cubic Yard [lb/yd^3]
Cement – Type I/II/V Low Alkali	82%	0.27	462
Pozzolan – Class F: Replacement for Cement	18%	0.47	100
Water	-	4.808	300
Air (Entrapped)	1.5%	0.405	-
Garey HMS Gravel (3/8” x #8)	52.7%	9.787	1600
Garey C 33 Sand	47.3%	8.907	1434

3.5.1. Concrete Cylinder Tests for Footing

Four 6x12 concrete cylinders were prepared according to ASTM C31, and after 28 days were tested in a Test Mark Compression Testing machine according to ASTM C39 (Table 3-4 presents averaged results). Additionally, a slump test according to ASTM C143 was performed. The resulting slump was approximately 6-7” at the time of the pour.

Table 3-3: Summary of Footing Concrete Properties

	f_c’ (psi)	f_r (psi)	E_c (ksi)
Avg. of 4 Cylinders	1879	325	2471

Figure 3-4: Footing Concrete Cylinder Compression Failure

3.5.2. Concrete Cylinder Test for Wall

At various stages during the wall pour, a total of nine cylinders were prepared of sizes 6x12 and 4x8. A slump cone test was also conducted and a 5" slump was measured. After 41 days, one 6x12 and one 4x8 cylinder were tested in a Test Mark Compression Testing machine. Three days later, four more cylinders were tested. On the test day, 82 days after the wall pour, the rest of the cylinders were tested. See Table 3-4 for results. An average compression strength of 3,790 psi was obtained, including outliers. Figure 3-5 shows a typical failure obtained from two of the concrete cylinder compression tests. Appendix Sections A and B show additional documentation of each cylinder tested for both the footing and wall, respectively.

Table 3-4: Summary of Wall Concrete Properties

	f_c' (psi)	f_r (psi)	E_c (ksi)
Avg. of 9 Cylinders	3790	446	3386

Figure 3-5: Typical Concrete Cylinder Test for Wall

3.6. Reinforcing Steel Tension Testing

The rebar used for the wall tests were tested for axial tensile capacity in a Tinius Olsen machine. Figure 3-6 shows the test setup used for each rebar specimen and the stress-strain curves produced. Since grade 40 rebar was used for these tests, the expected yield stress of these bars according to ASCE 41-17, Table 10-1 was 50 ksi. The actual average yield and ultimate stresses were about 55 ksi and 83 ksi, respectively and the average ultimate fracture strain was about 19%

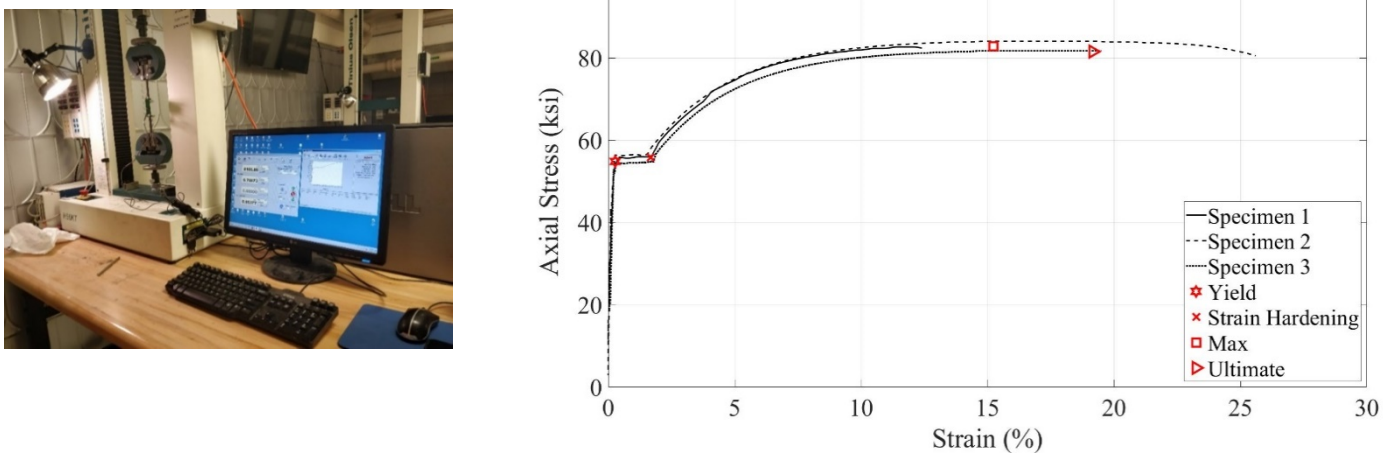

Figure 3-6: Rebar Tension Testing
(Left) Tinius Olsen test setup (Right) Rebar testing results, axial stress versus axial strain. Markers visually show averages.

Table 3-5: Average Rebar Properties

State	*Yield*		*Strain Hardening*		*Max*		*Ultimate*	
Parameter	f_y	ε_y	f_{sh}	ε_{sh}	f_{max}	ε_{max}	f_u	ε_u
Average Value	54.8	0.28	55.8	1.68	82.8	15.24	81.5	19.16

Note: Stresses in ksi, strains in %

4. TEST SETUP & WALL CONSTRUCTION

This chapter outlines the experiment setup, footing/wall construction, and instrumentation layout. Section 4.1 discusses the existing conditions of the High Bay laboratory and overview of the test setup. Section 4.2 discusses the footing and wall construction. Section 4.3 discusses the instrumentation layout for the wall.

4.1. Test Setup Overview

The LRC wall test was performed in the Cal Poly College of Architectural & Environmental Design (CAED) High Bay laboratory. As shown in Figure 4-1, many components were necessary in the test setup for this experiment including: the wall specimen, strong floor, instrumentation column, out-of-plane stability system, axial loading system, and cameras.

The reinforced concrete strong floor in the CAED High Bay laboratory provided a fixed connection for the base of the wall footing via all-thread anchors spaced at 3’-0” each way. During preparations for the LRC wall test described in this report, the CAED High Bay’s steel reaction frame was upgraded to stiffen the system to limit deflection when applying lateral loading to a reinforced concrete wall specimen.

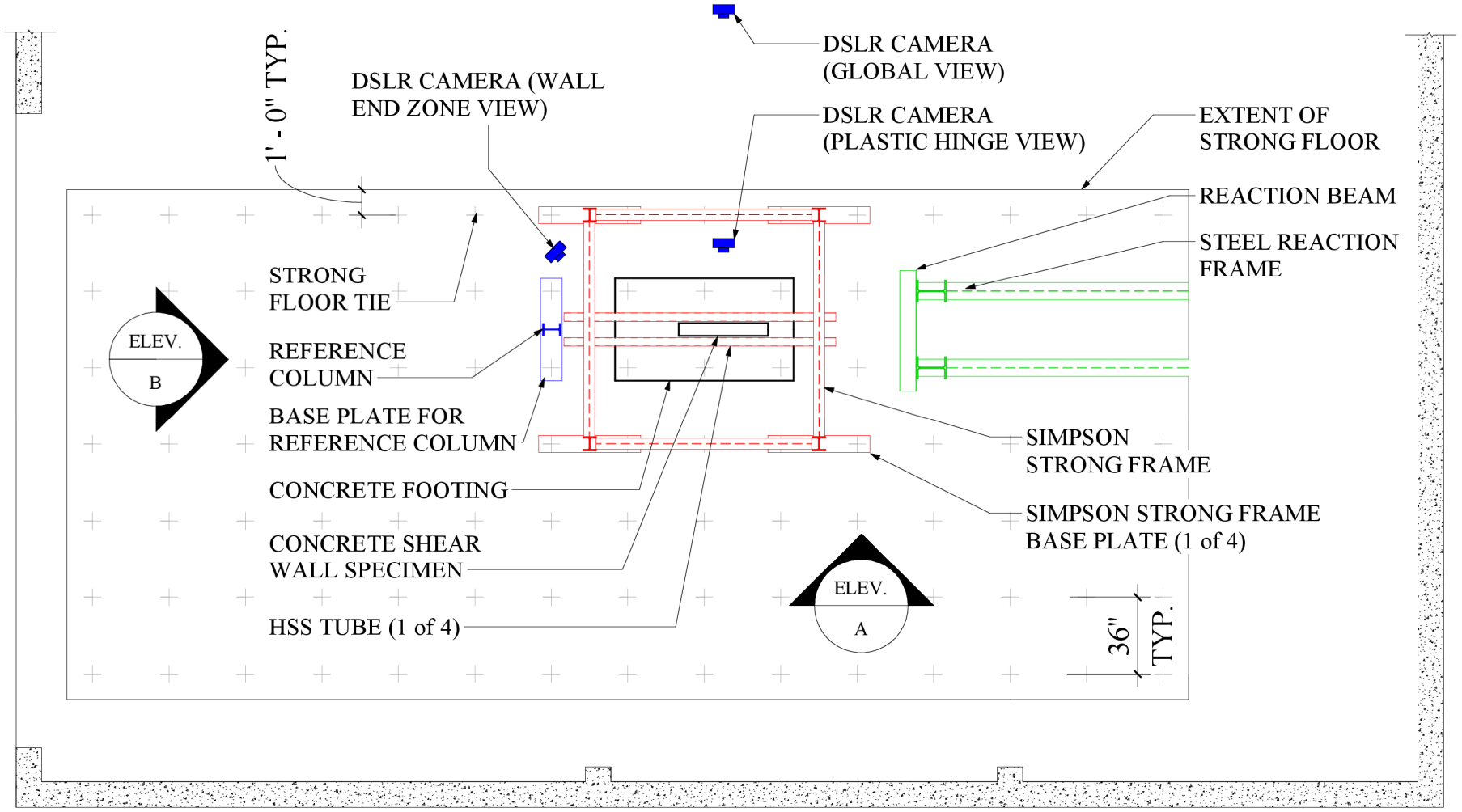

Figure 4-1: Plan View of Test Setup

(Note: Horizontal and vertical actuators not shown for clarity)

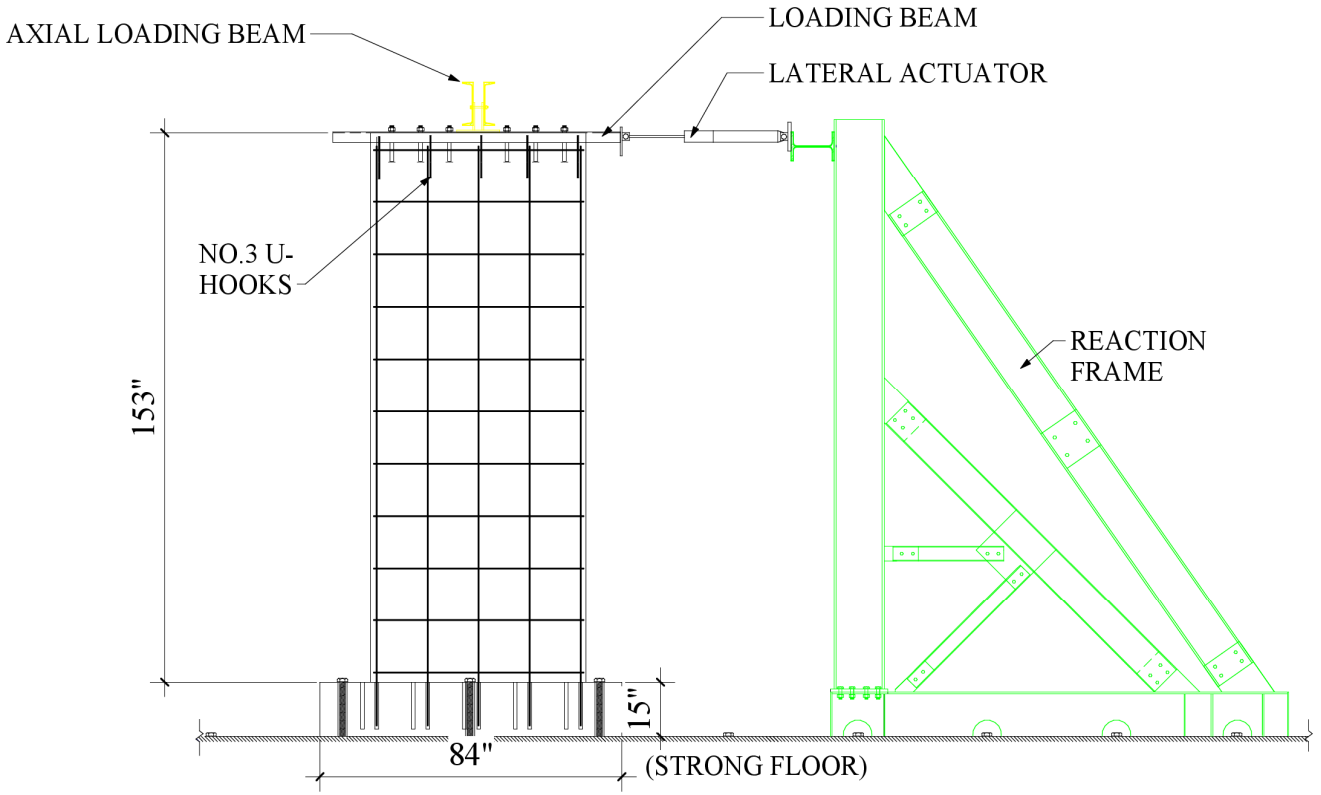

Figure 4-2: Elevation A, Test Setup (West Face of Wall)

(Note: Vertical actuator, reference column, and out-of-plane stability system not shown for clarity)

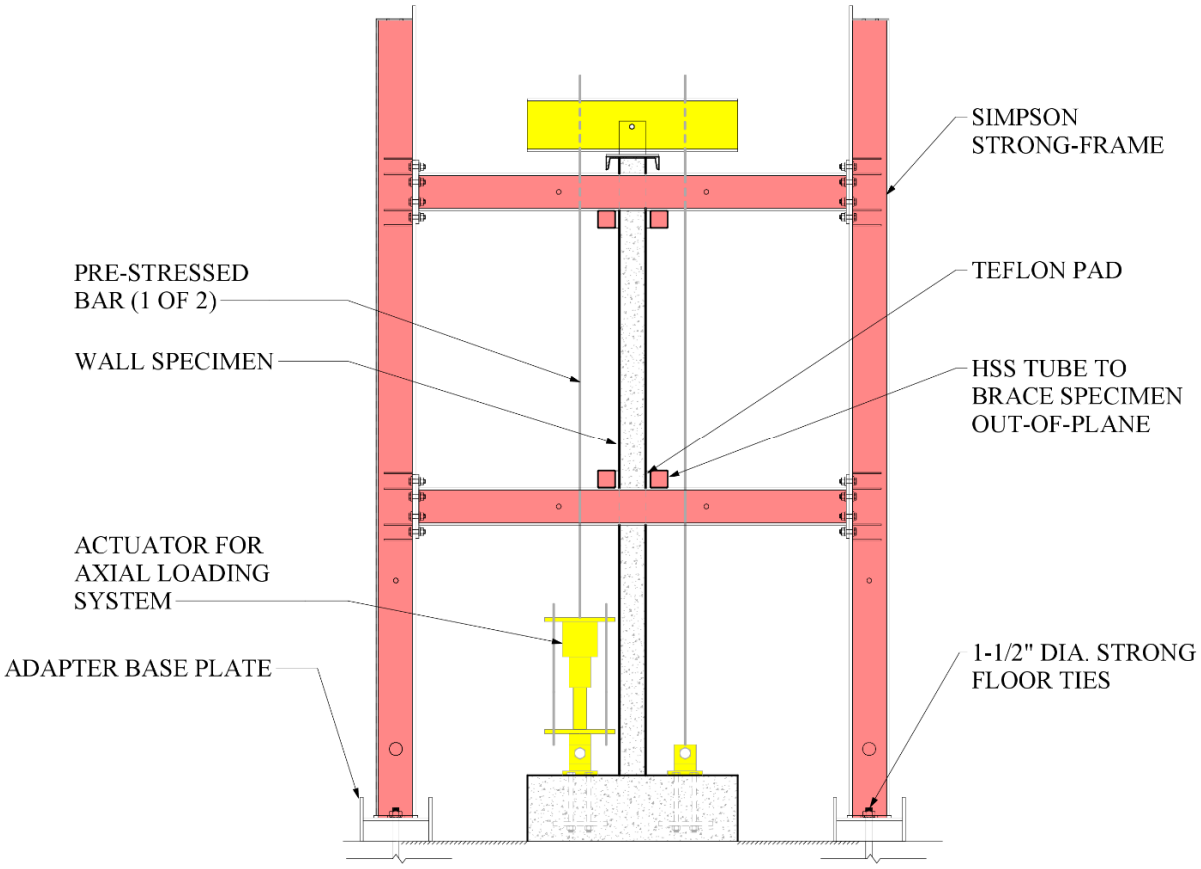

Figure 4-3: Elevation B, Out-of-Plane Support System and Axial Loading System

4.2. Out of Plane Stability System

The out-of-plane system consisted of two Simpson Strong-Frames, four HSS beams, and four Teflon pads which together provided stability for the wall during testing and added no additional in-plane stiffness. The primary component of the out-of-plane support was the donated Simpson Strong-Frame system, as shown in Figure 4-4. This custom set of two, 2-story wide-flange ordinary moment frames (OMF's) were connected by transverse beams and integrated into the existing strong floor system by bolting to wide flange section adapter base plates which were anchored to the strong floor. The construction of the out-of-plane stability frame was a major undertaking for the authors of this report and supporting CAED shop technicians, requiring complete assembly upon arrival and taking several weeks to finish.

Figure 4-4: Simpson Strong Frame for Test Setup

The secondary components of the out-of-plane support were the HSS members, which combined with the Simpson Strong-Frames, provided stability, and reduced accidental torsion on the wall specimen. The four HSS members were 5x5 sections and 9'-0" in length, running parallel to the wall as shown in Figure 4-3 and Figure 4-4. The HSS section dimensions were chosen based on a conservative calculation of an eccentric load applied to the wall and was governed by a desired stiffness rather than strength. The HSS shape was chosen because of ease of use and versatility in both loading directions as well as cost when compared to equivalently performing channel section. Each HSS was securely welded onto fabricated steel adapter plates designed to be bolted onto the Strong-Frames. This system allows for various placement configurations on the Strong-Frame and can be used for later experiments.

Teflon pads were utilized as a frictionless medium between the rough concrete wall surface and the HSS members running parallel to the wall. A total of eight Teflon pieces were drilled into wood shims which were epoxied to the ends of the walls at each HSS. To ensure a smooth surface, the holes were countersunk with a drill press ahead of time. As a result, the Teflon pads helped create a flat surface between the wall and the HSS members.

4.3. Axial Loading System

The axial loading system was designed with the ability to apply adjustable magnitudes of force to the longitudinal axis of the wall (Ridgley, 2019). The system is shown in Figure 4-3 and consisted of prestressed bars, a loading beam, an actuator, a load cell, an automatic hydraulic pump, and three pin connections. Using basic statics, the total axial load on the wall specimen is equal to twice the force recorded by the load cell on one side of the wall. The maximum force the axial loading system could safely apply to the wall was 40 kips. For this experiment, the system delivered a constant axial load of 35 kips to the wall.

4.4. Lateral Loading System

The lateral loading system consisted of a loading beam, actuator, embedded anchors into the top of the wall specimen, a manually powered hydraulic pump, and the lab reaction frame. As discussed previously in Section 3.3.1, the limiting force the actuator could exert was 23.6 kips (tension), so each component in the system had to be able to transfer this force to the wall. The load path for this system started with the actuator, which applied force to the reaction frame. The reaction frame was designed to be at least 10 times stiffer than the wall so that there were minimal deflections during testing. The lateral load is transferred to the wall through the longitudinal axis of the horizontal loading beam, applied at the channel's shear center. From the loading beam, the lateral load is transferred into the wall through shear applied to (6) 5/8" diameter anchor bolts embedded into the top of the wall.

4.5. Specimen Construction

4.5.1. Footing Construction

The design of the shear wall footing is discussed previously in Section 3.4. The formwork was built according to the drawings shown in Appendix Section D. Figure 4-5 shows the construction of the footing formwork. The footing formwork was braced to the Simpson Strong Frame footing for additional stability. The reinforcing steel for the footing was built according to Figure 3-3. A minimum cover of 1.5" was provided on all sides of the footing. A formwork release agent was applied to all surfaces to aid with the

removal of the formwork after the concrete cured. Silicone sealant was provided at all corners or edges where concrete leaking was a concern. Figure 4-6 shows the rebar cage before and during the concrete pour.

Figure 4-5: Shear Wall Footing Formwork Construction

Figure 4-6: Shear Wall Footing Reinforcement
(Left) Footing rebar cage and (right) concrete pour.

4.5.2. Shear Wall Construction

The design of the shear wall is discussed previously in Section 3.3. Construction of the wall rebar cage and formwork are shown in Figure 4-7. Before setting the wall formwork in place, 7/16” diameter holes in the footing were first drilled and vacuumed in preparation for embedding and epoxying the longitudinal reinforcing steel. Additionally, the footing surface was roughened to increase shear friction between the wall and footing. The longitudinal reinforcement for the wall was then epoxied into the footing using Simpson ‘SET-XP’ epoxy with 1’-0” of embedment. After the longitudinal bars were in place, the transverse reinforcing (straight bars and U-hooks) was tied to complete the rebar cage per the wall design in Figure 3-2. The reinforcing steel cage was completed with vertically oriented U-hooks installed at the top of the wall. After the completion of the rebar cage, the formwork was secured on each side of the cage with careful considerations to concrete cover, strain gauges and their lead wires. The schematic drawings of the wall formwork can be found in Appendix Section D. During this process, scaffolding was also designed and constructed by the project team to increase accessibility to higher portions of the wall.

Figure 4-7: Shear Wall Formwork & Rebar Cage Construction

The wall was poured in one lift through two access openings in the formwork - one at the mid height and one at the top of the wall. Pump access through these intermediately spaced openings allowed the concrete to correctly consolidiate and prevent significant honeycombing effects. After curing, the wall formwork was removed and whitewash was applied to the front (east) face of the wall to allow for ease of crack mapping and photography of damage progression during testing. The back (west) face of the wall was reserved for installation of linear potentiometers as described in Section 4.6.2.

4.6. Wall Instrumentation

This section describes the instrumentation used to measure the response of the wall and other test setup components, and the data acquisition hardware/software used to record data. Each instrument type as described in the subsequent sections were calibrated prior to use in the main experiment. The calibration process ensured proper function and data recording for each instrument.

4.6.1. Strain Gauges

Strain gauges were applied to rebar in strategic locations so that longitudinal strain values could be recorded during testing. A total of 20 gauges were used: 17 applied to longitudinal steel, and three applied to transverse steel. The location of each strain gauge is shown schematically in Figure 4-8. Most strain gauges were located near the bottom of the wall in the expected critical section. The strain gauges were named based on three parameters: location along the length of the wall (Columns A to E), height along wall (Levels 2 to 60), and row of reinforcement (Row 1 or 2). The exceptions to this nomenclature were the gauges placed on the transverse steel, which were all on level 2 and named “ST-XX” where the “XX” represented the column location.

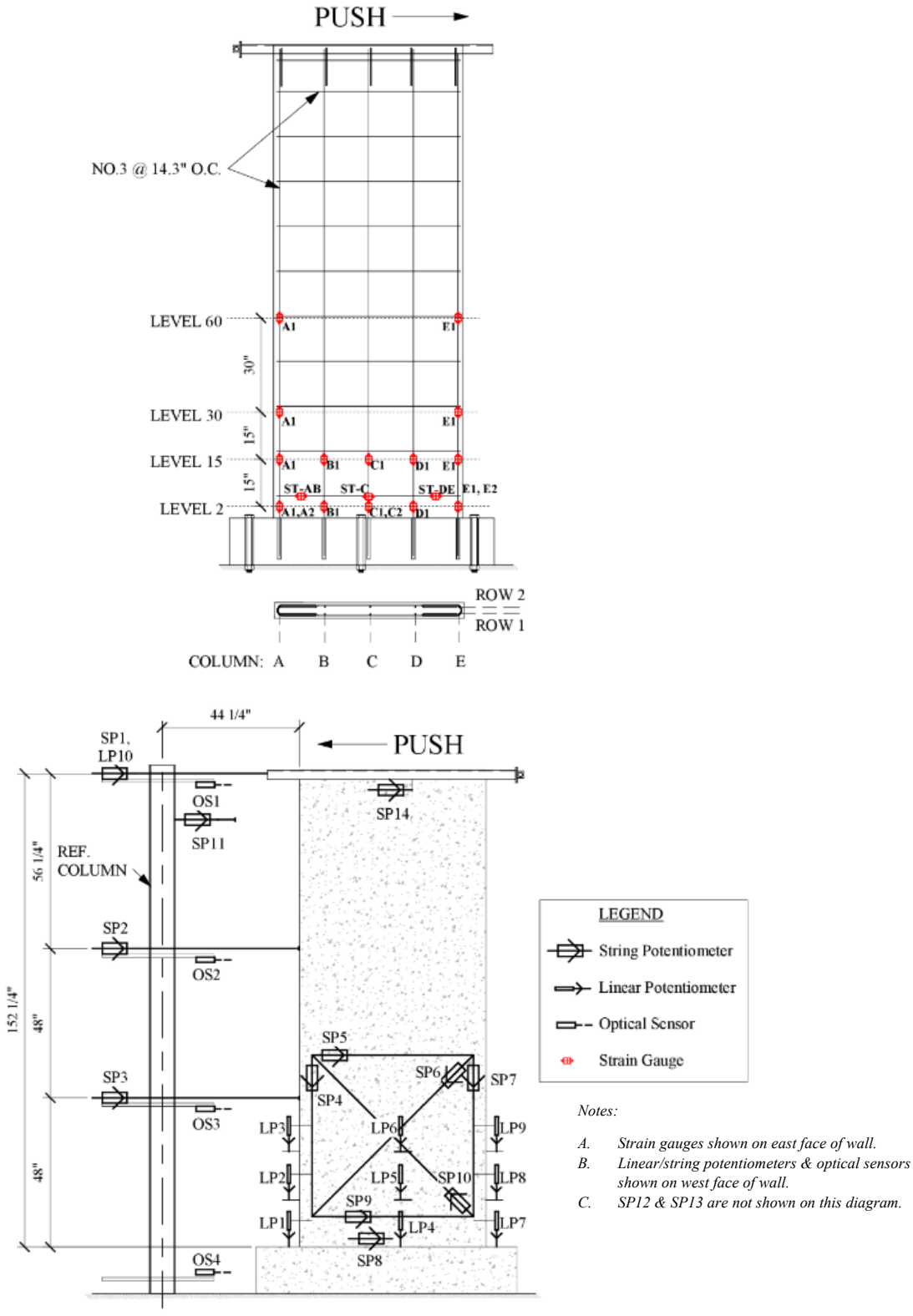

Notes:

A. Strain gauges shown on east face of wall.
B. Linear/string potentiometers & optical sensors shown on west face of wall.
C. SP12 & SP13 are not shown on this diagram.

Figure 4-8: Instrumentation Layout

4.6.2. LVDT's, Optical Sensors, and String Potentiometers

The instruments described in this section were used to measure absolute and relative displacement of the wall specimen. Linear variable differential transformers (LVDTs) were used to measure displacements especially in locations with small, expected displacements. Figure 4-8 presents the overall LVDT layout on the specimen and Figure 4-9 shows a typical LVDT applied to this project. These sensors were used to measure vertical displacements along the height of the expected critical section by stacking LVDTs in groups of three at the ends and in the middle of the wall. In post-processing the data, researchers could calculate vertical straining and base rotation at the wall-footing interface. A high-resolution LVDT was also used for accurate measurement of horizontal displacement at the top of the wall, necessary as the test was conducted via displacement-control after the initial elastic range of response.

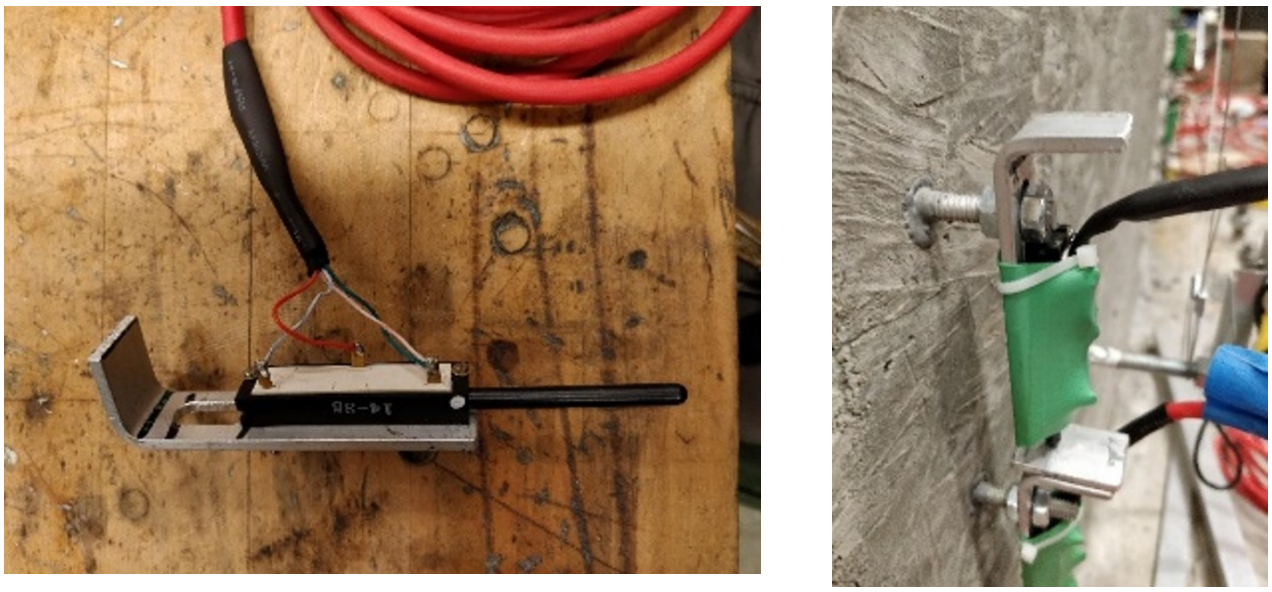

Figure 4-9: LDVT Instrumentation
(Left) LVDT connected to aluminum bracket (Right) LVDT with protective wrap attached to wall face

Optical or laser sensors were used to measure absolute displacements along the height (later converted to drifts) of the wall specimen. Figure 4-10 shows a typical optical sensor mounted to the stationary reference column using a metal extension bar as well as the location of the four optical sensors that were attached at various heights and base of the footing to measure in-plane displacement of the wall. The optical sensors provided redundancy to other instruments used to calculate drift to ensure the displacement-based loading protocol was being executed correctly and in post-processing to create drift profiles for various stages during the wall test.

Figure 4-10: Instrumentation Column
(Left) Typical optical sensor attached to a metal extension bar anchored to the instrumentation column and (Right) Instrumentation column with instruments extending out towards the wall.

String potentiometers shown in Figure 4-8 were used to measure: absolute displacement to determine drift (SP1-3); relative displacement between test setup components (SP11-14); and relative displacement to calculate wall base sliding, flexural and shear deformation (SP4-10). The SP14 string pot measuring relative displacements between the loading beam and the wall is shown in Figure 4-11. String pots are especially useful for measuring displacements along lengths which move in two planes at the same time. Like the optical sensors, the string pots measuring drift were mounted on the instrument column and attached to the wall at various points along the height.

Figure 4-11: String Potentiometers, Close-up view of a typical string pot.

4.6.3. Load Cells

Two load cells were used to measure the force applied by the lateral and axial actuators throughout the wall test. The axial and lateral load cells are shown in Figure 4-12 and Figure 4-13 respectively. The load cells were calibrated at the start of the testing to ensure the force-deformation hysteresis plot was accurate.

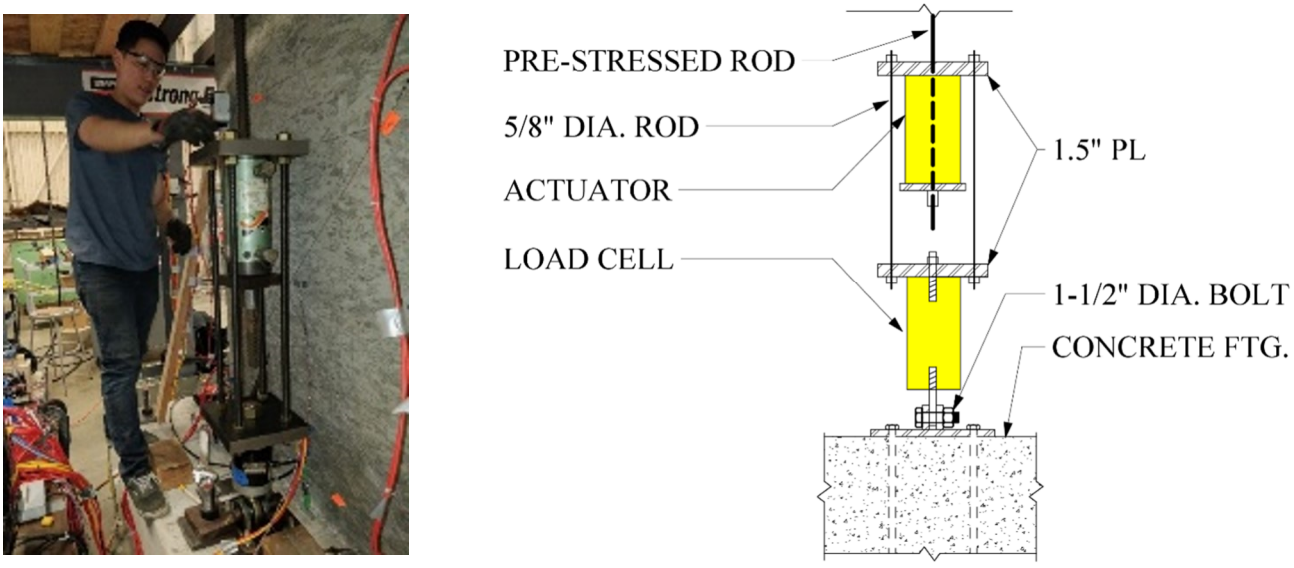

Figure 4-12: Load Cell Attached to Axial Actuator

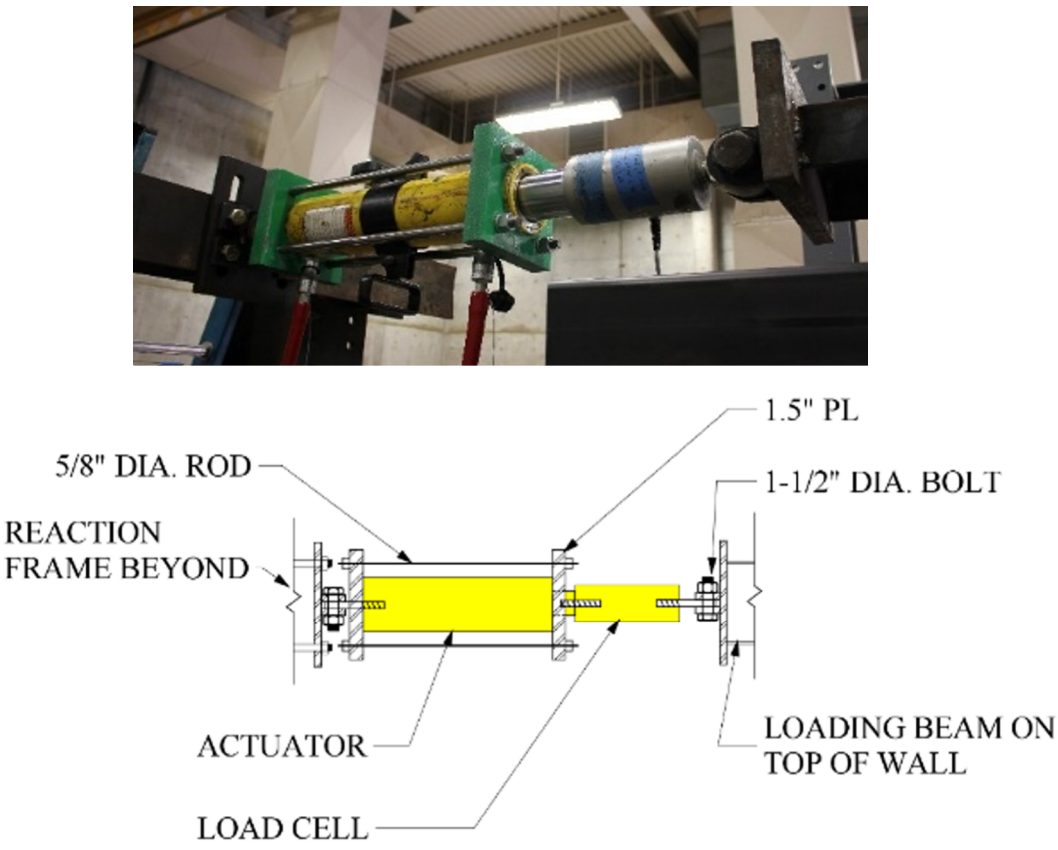

Figure 4-13: Plan View of Lateral Actuator and Load Cell

4.6.4. Data Acquisition System

The data acquisition system used an in-house MATLAB GUI script that integrated with National Instruments (NI) compact DAQ hardware/software to plot and record data in real time. The MATLAB GUI script allowed a user to select channels to use for data acquisition, plot instrument readings against time or other variables, pause or resume data acquisition, create a bias, save data to a file, and enter unique calibration factors for each instrument. Figure 4-14 shows a screenshot of the MATLAB GUI.

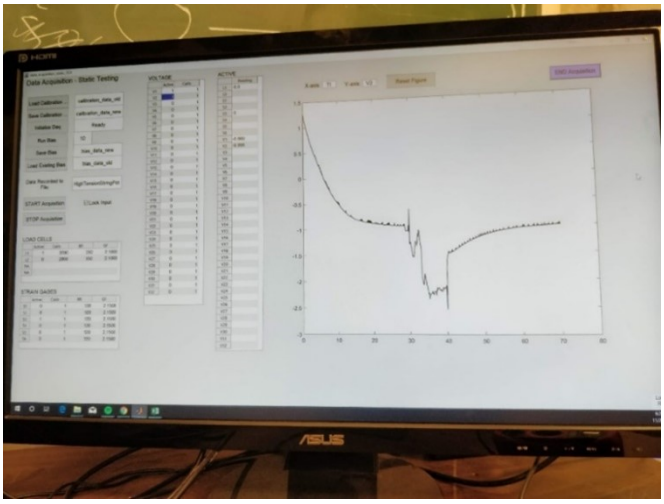

Figure 4-14: Data Acquisition GUI using MATLAB

The NI DAQ modules used for this experiment measured voltage differentials through a discrete number of inputs. To make the inputs more accessible to physical connection of instruments, each input was extended into a corresponding channel within a custom-made channel box.

5. WALL TESTING

This chapter discusses the experimental testing of the lightly reinforced concrete (LRC) wall specimen introduced in Chapter 3, henceforth named R1. Section 5.1 overviews the experimental loading protocol. Section 5.2 presents test results including damage progression and general wall performance. Section 5.3 and 5.4 describe vertical strain and curvature distributions along the height of the wall. Section 5.5 discusses contributions to global deformation. Lastly, Section 5.6 presents the drift profile at various stages of testing.

5.1. Loading Protocol

The loading protocol was informed by ASCE 41-17 and Priestly (2007) type predictions described in Chapter 6 and other cyclic tests of LRC walls summarized in Chapter 2. At low levels of drift and until global yielding of the wall (predicted to occur at about 12.5 kips of lateral force), the loading protocol was force controlled with 2-cycle sets at each force level. After global yielding of the wall, the loading protocol was changed to displacement controlled with 2-cycle sets at each drift level for the remainder of the test. Figure 5-1 and Table 5-1 summarize this loading protocol. The increase in applied drift at load step 46, or conduct of a monotonic push, was based on the belief that wall failure was imminent after the +/-1.67% drift cycles and also where the displacement capacity of the actuator in the tension (negative drift) direction had been achieved. However, the load carrying capacity during the monotonic push remained relatively constant, so after reaching about + 3.33% drift the decision was made to revert to 2-cycle sets at +2.00/-1.67%.

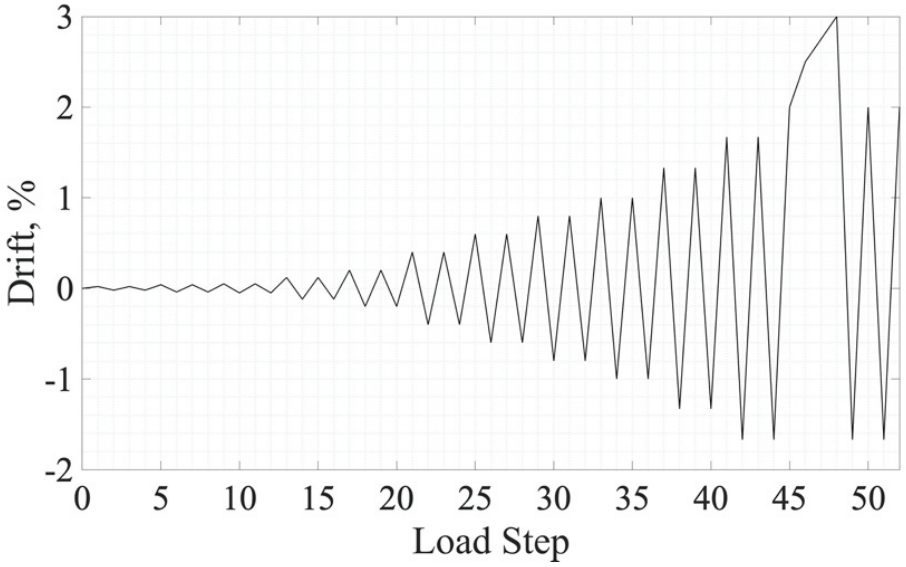

Figure 5-1: Loading Protocol of R1

Table 5-1: Loading Protocol of R1

Load Steps	Drift (%)	Force (Kips)
1-4	-	± 2.2
5-8	-	± 4.4
9-12	-	± 6.4
13-16	-	± 12.6
17-20	± 0.20	-
21-24	± 0.40	-
25-28	± 0.60	-
29-32	± 0.80	-
33-36	± 1.00	-
37-40	± 1.33	-
41-44	± 1.67	-
45	+ 2.00	-
46	+ 2.50	-
47	+ 2.75	-
48	+ 3.33	-
49-52	+2.00/-1.67	-

5.2. Wall Experimental Results

5.2.1. Global Force-Displacement

In general, the wall response is comparable to other walls mentioned in Section 2.2, with similar peak strength and hysteretic behavior, as shown in Figure 5-2. The wall is cyclically loaded to ±1.67% and then is pushed monotonically to +3.3%. After the monotonic push, the wall is cycled at +2% and -1.67%. It is determined that the wall fails during the final +2% cycle because the wall loses more than 20% of the peak strength. However, it is believed that if the wall test had continued with symmetrical loading, not including the monotonic push, the drift capacity of the wall would likely be between 2 to 3% drift, rather than the maximum 3.3% drift level. The shear capacity of the wall is approximately 20.9 kips, resulting in an ultimate moment demand of 266.5 kip-feet.

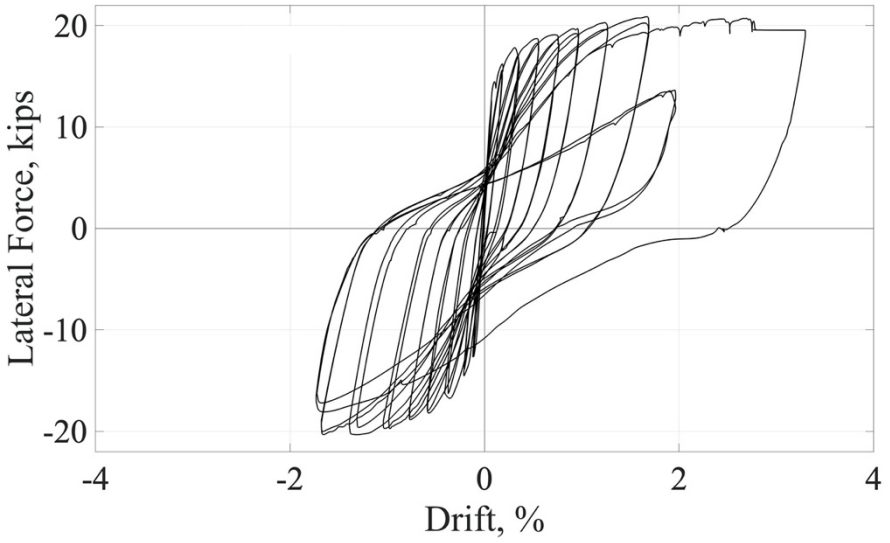

Figure 5-2: Global Force-Displacement Response

5.2.2. Damage Progression

This section will discuss the progression of damage of the wall at key stages during the experiment:

5.2.2.1. Load Step 13 (12.6 Kips)

The first yield of rebar occurred at load step 13, with an applied lateral force of 12.6 kips and approximately 0.075% global drift, which resulted in a 7” long by 0.01” wide at the wall-footing interface.

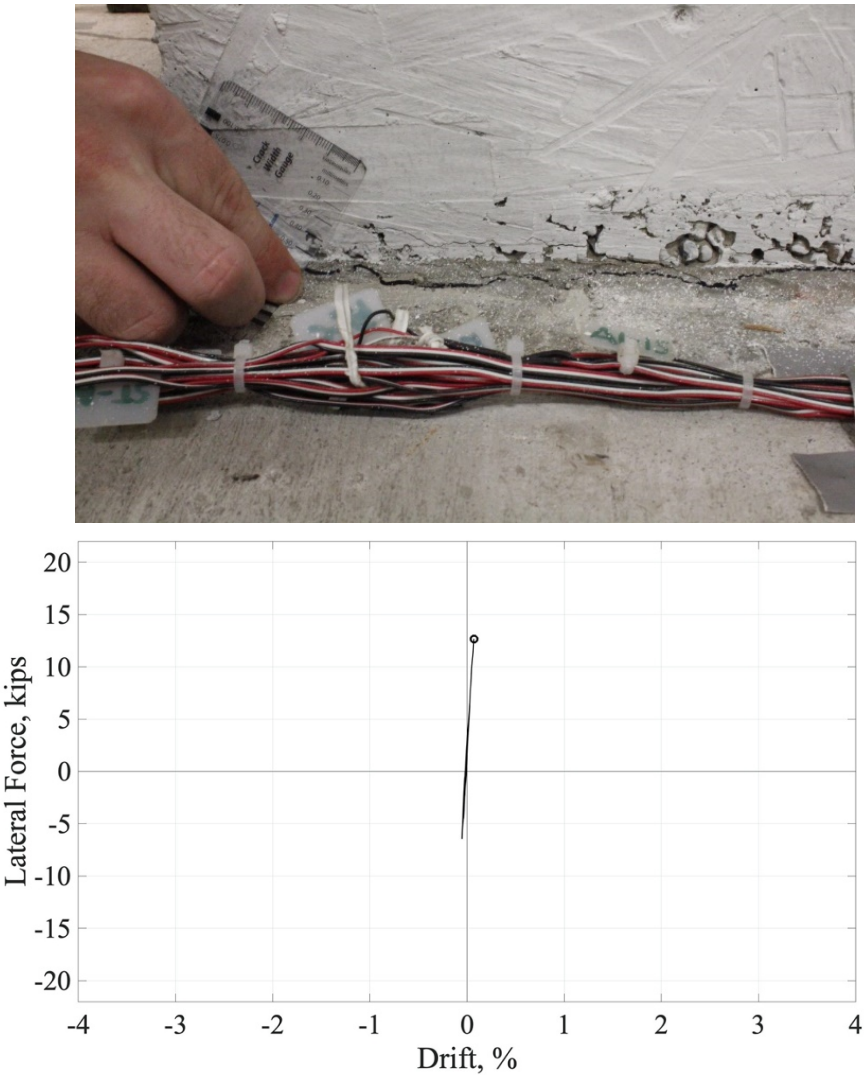

Figure 5-3: Minor Base Cracking at First Yield of Rebar

5.2.2.2. Load Step 17 (0.2% Drift)

Global yield occurred at load step 17, which was recorded at 0.2% drift and about 15 kips of lateral force. The first horizontal crack, measured at 31” long by 0.005” wide, appeared 32” above the footing and stiffness degradation is first noted.

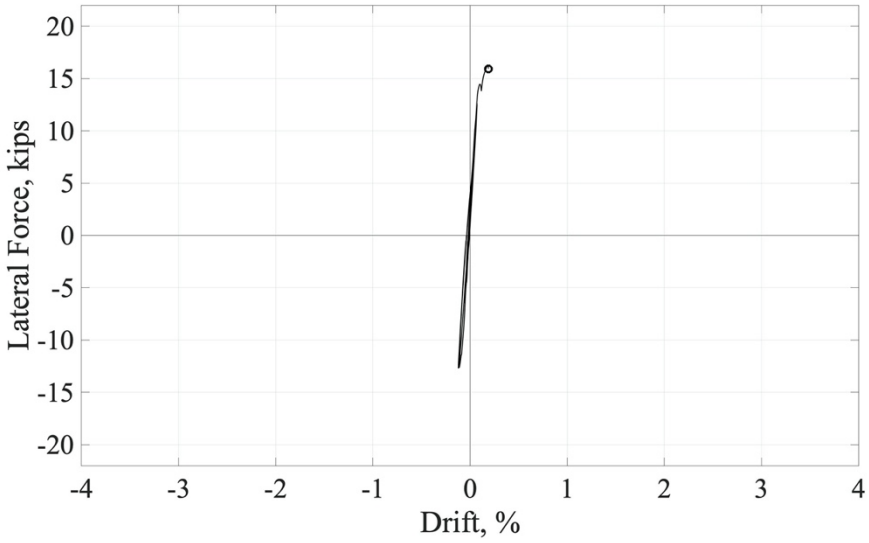

Figure 5-4: Wall Damage at 0.2% Drift

5.2.2.3. Load Step 21-24 (0.4% Drift)

At load step 21, a flexural crack formed 17” above the footing. At load step 23, a 25” long by 0.025” wide crack formed at the base. The recorded drift and lateral force applied were 0.4% and 17.2 kips, respectively.

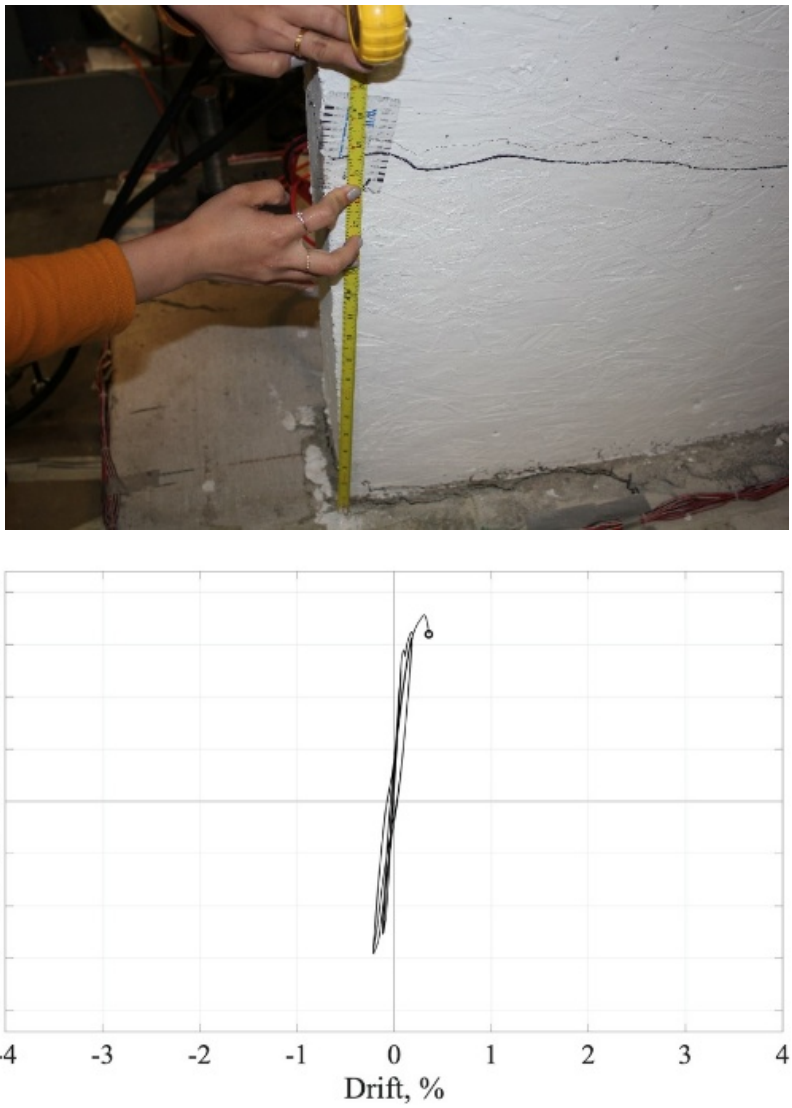

Figure 5-5: Wall Damage at 0.4% Drift

5.2.2.4. Load Step 25 (0.6% Drift)

At load step 25, the first diagonal crack appeared and was 0.005” wide. The crack formed at a height of about 16” and extended 11” inches down at a 60-degree angle. The recorded drift and lateral force were 0.6% and 18.6 kips, respectively.

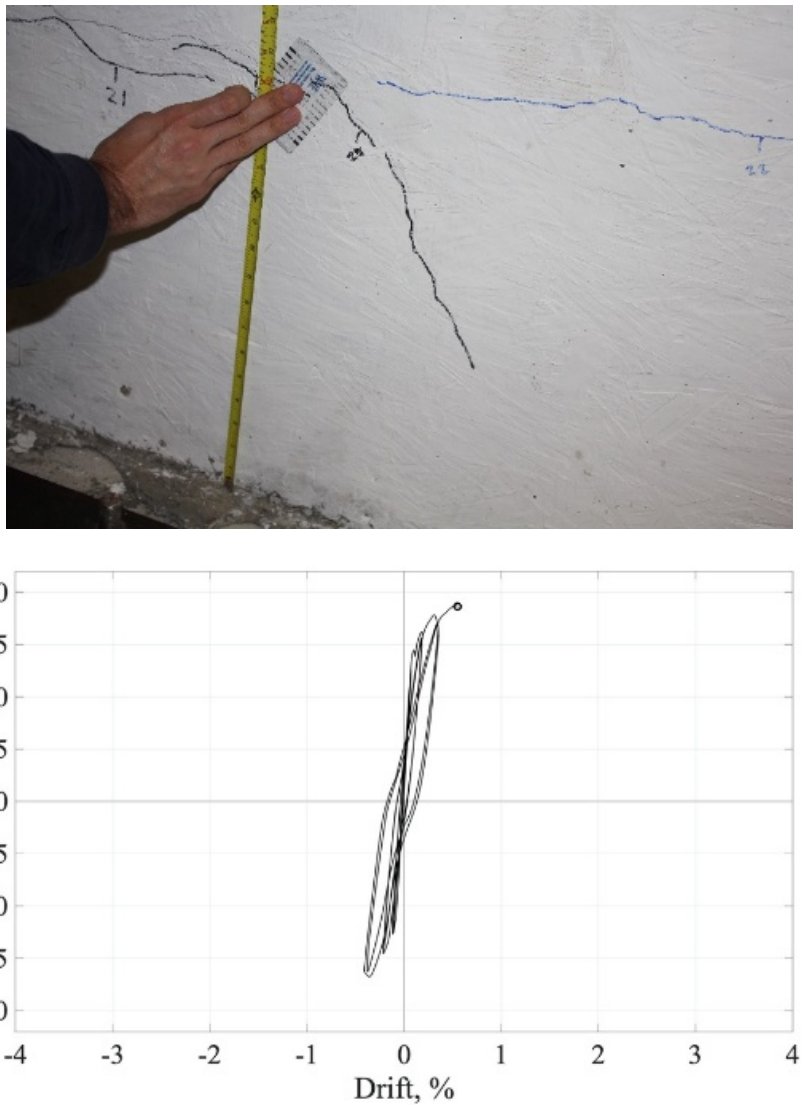

Figure 5-6: Wall Damage at 0.6% Drift

5.2.2.5. Load Step 25-32 (0.6-0.8% Drift)

Between load steps 25-32, the wall was cycled between 0.6% and 0.8% drifts, respectively. The horizontal cracks progressively widened and a residual drift of 0.39” or 0.26% drift was recorded at the unloaded state between cycles. The maximum crack width measured was 0.1875” at load step 29. The wall lateral load capacity began to plateau at this stage.

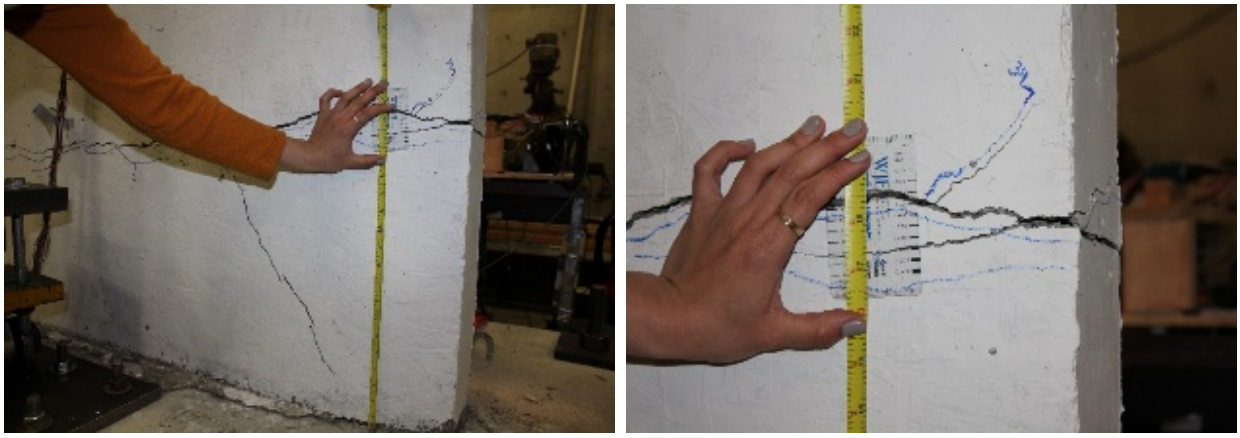

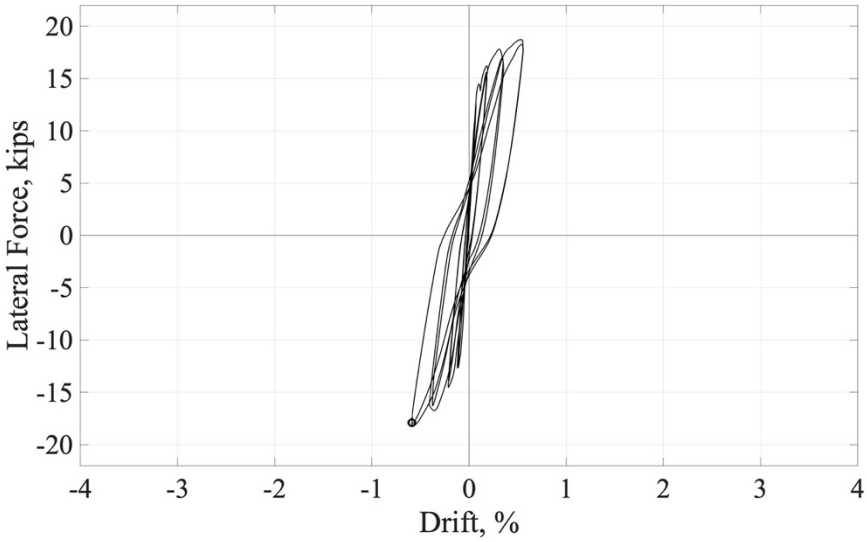

Figure 5-7: Wall Damage at 0.8% Drift

5.2.2.6. Load Step 41 (1.67% Drift)

At load step 41, new horizontal cracks continued forming and the previous horizontal cracks began to expose transverse rebar. The maximum crack width measured is 0.6875”. Additionally, vertical cracks begin to form in the concrete near the exposed rebar. The recorded drift and lateral force were 1.67% and 21.1 kips, respectively. A residual drift of about 1% remained in the wall at the unloaded state between load steps at this point (when the lateral force was zero).

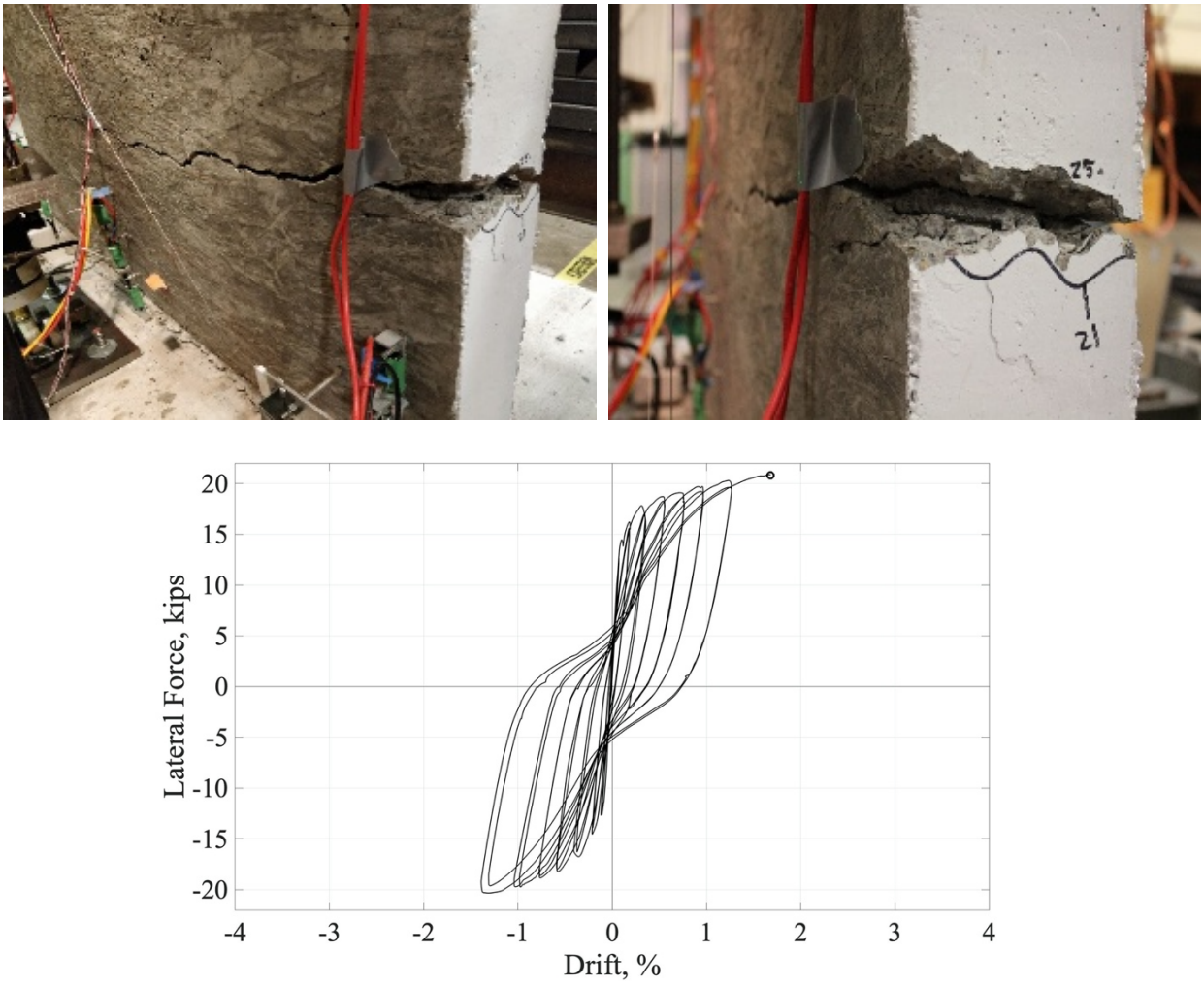

Figure 5-8: Wall Damage at 1.67% Drift

5.2.2.7. Load Step 45 (2.00% Drift)

The monotonic loading began at load step 45 and the recorded drift and lateral force were 2.00% and 20 kips, respectively. At this load step, it was noted that there was a slight decrease in the lateral capacity. There was significant base uplift at one end of the wall and minor concrete spalling on the opposite end of the wall.

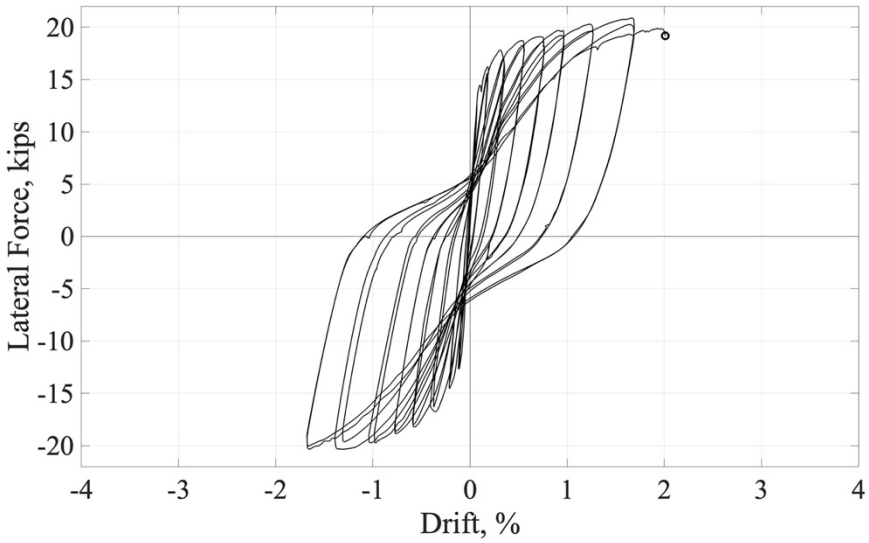

Figure 5-9: Wall Damage at 2% Drift

5.2.2.8. Load Step 48 (3.33% Drift)

Expecting imminent failure of the wall, the monotonic loading was incrementally continued to 3.33% drift. At this point, the largest horizontal crack width was measured to be 0.5” wide.

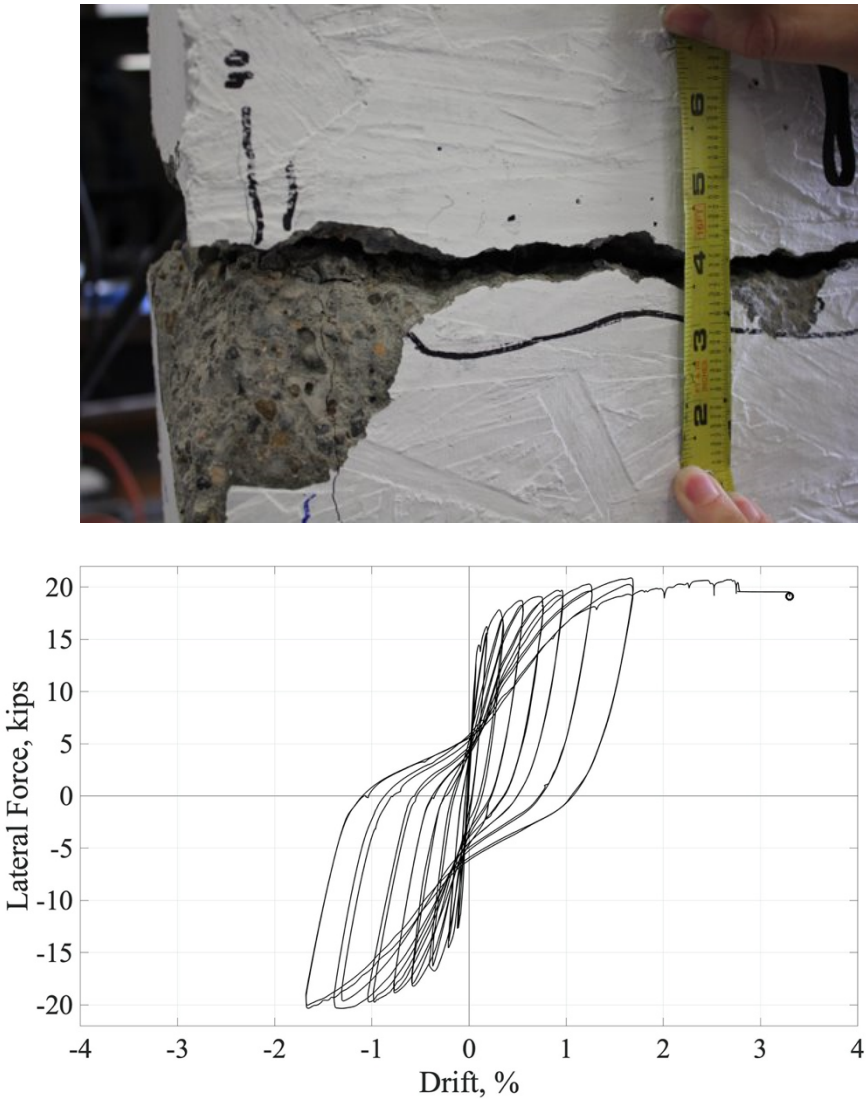

Figure 5-10: Wall Damage at 3.33% drift.

5.2.2.9. Load Step 49-52 (+2.0/-1.67% Drift)

Since the wall had little loss in strength, the wall was re-cycled at a lower level drift set of 1.67% (pull) and 2% (push) at which point the wall strength dropped by more than a 20% and failed due to fracture of longitudinal rebar due to flexure at the base crack plane. With this final stage of loading, the wall had four major horizontal crack planes and no secondary cracking. The wall also experienced significant spalling on the northern side during load step 50. A maximum out of plane wall offset of about 0.08" was also observed along the major crack planes.

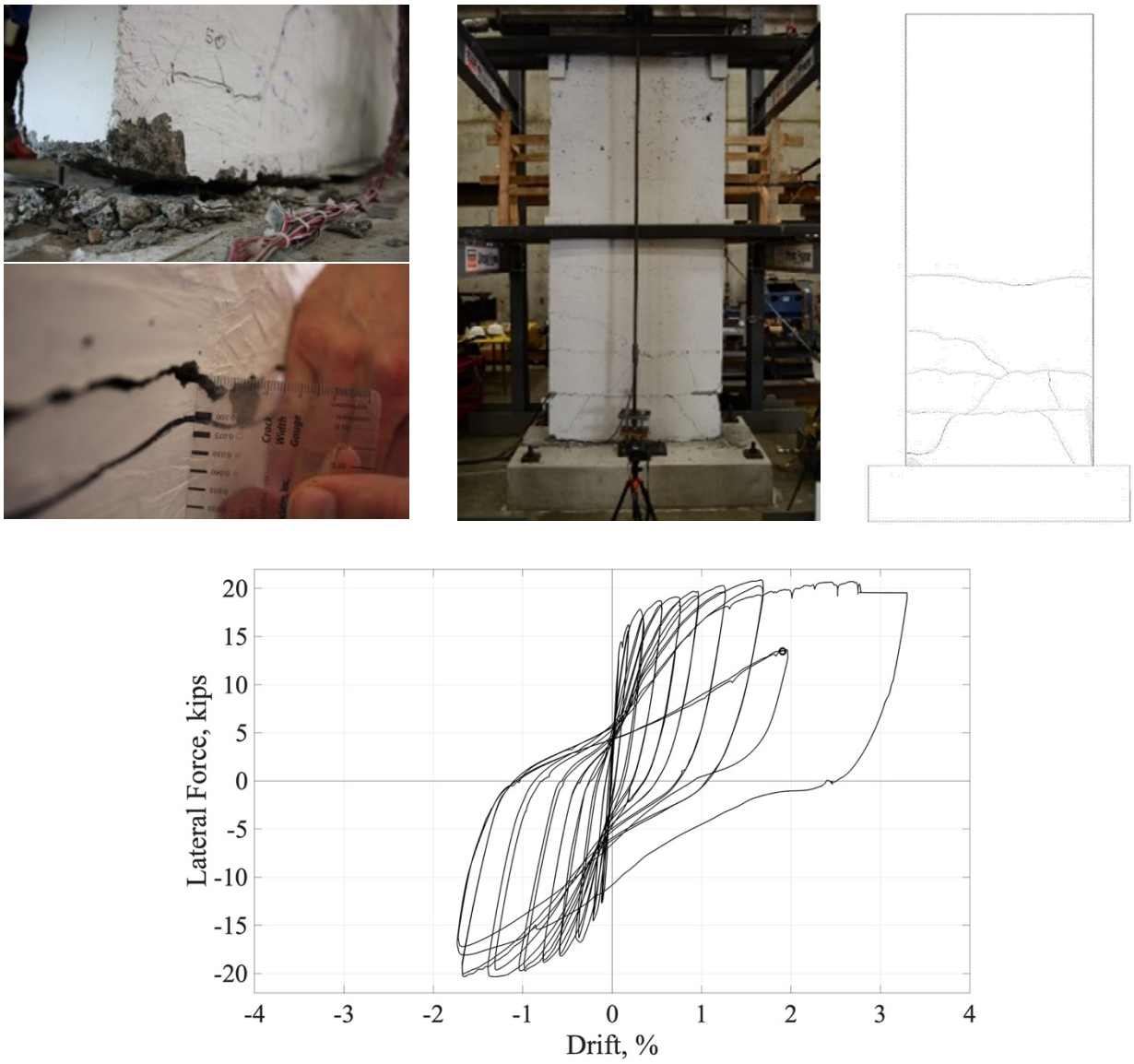

Figure 5-11: Final Damage State of Wall

Table 5-2: Summary of Observations

Load Step	Drift (%)	Force (kips)	Observations
13	0.075	12.6	Rebar begins yielding and cracking occurs at the base of the wall
17	0.2	15	First major horizontal crack appears at 32” above the base of the wall and stiffness degradation of the wall is noted
21	0.4	17.2	Second major horizontal crack appeared at 17” above the base of the wall and splitting at the base of the wall enlarges
25	0.6	18.6	First diagonal crack appears at 16” above base of the wall
25-32	0.6-0.8	18.6-19	Horizontal cracks widen as wall is cycled, measured residual drift of 0.39” (0.26% drift), and wall stiffness begins to plateau.
41	1.67	21.1	Transverse rebar is exposed and vertical cracks in concrete begin forming near exposed rebar
45	2.00	20	Slight drop in lateral resistance with monotonic loading and there is significant base uplift at the end of the wall
48	3.33	19.5	Largest crack opening of 0.50” is measured
49-52	+2.00/-1.67	13.5/17.5	Rebar fracture due to flexure and concrete spalling. Failure in wall due to lateral strength loss of more than 20%

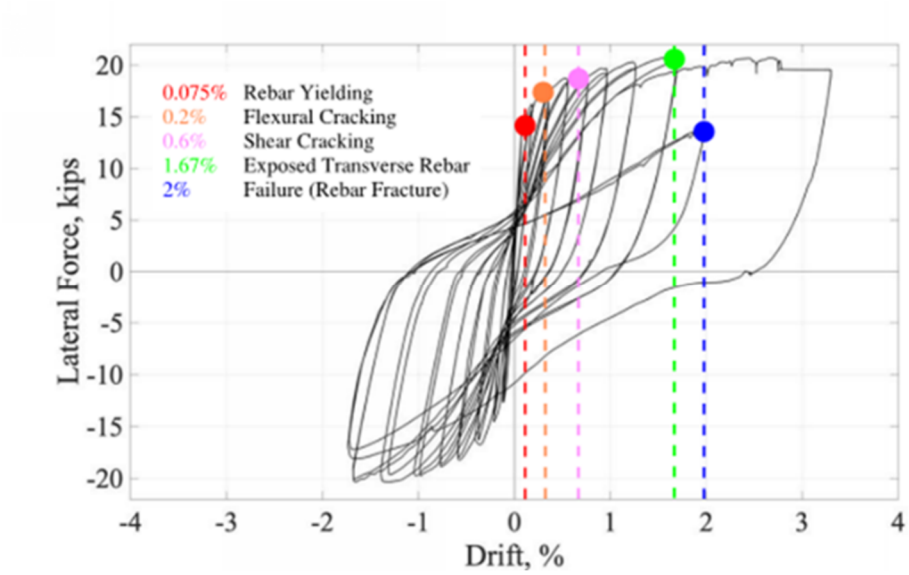

Figure 5-12: Final Hysteresis with Damage States

5.3. Vertical Reinforcement Strain

Strain gauges were installed on both horizontal and vertical reinforcing steel, as discussed in Section 4.5.2 where Figure 4-8 provides the orientation and position of the strain gauges. A hysteresis of the vertical reinforcing steel at the ends of the wall at level 2 is shown in Figure 5-13. Data is plotted up to 0.4% global drift because after this the strain gages began malfunctioning due to high strains in the rebar (nearing the strain capacity of the gauge). The magnitude of strain is visually represented by the relative size of the colored circles on the wall elevation shown.

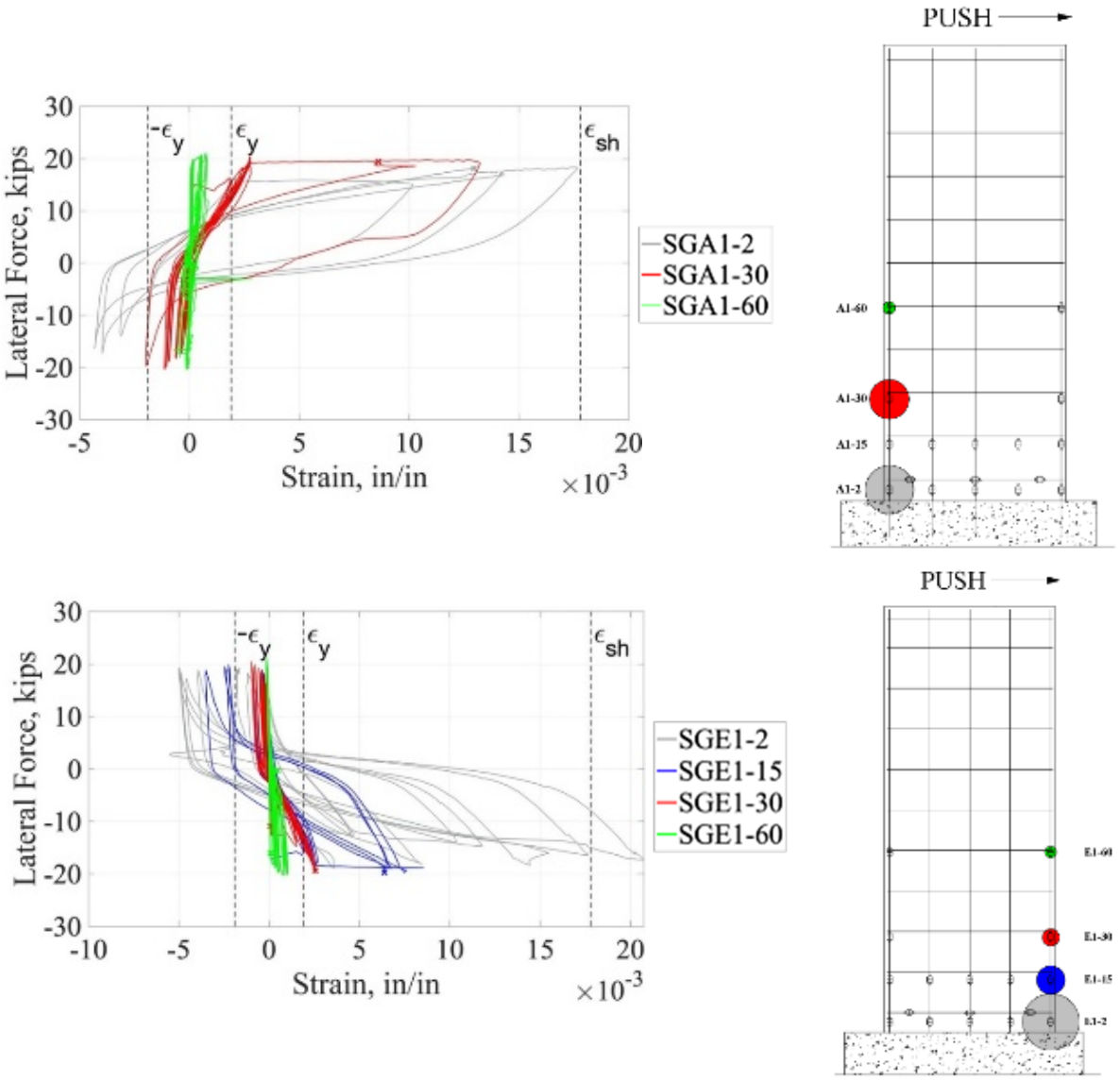

Figure 5-13: Lateral Force vs. Strain for Strain Gages in Column A (Top) and Column E (Bottom)

In Figure 5-13 the magnitude of strain varies along the height of the wall with the largest strain near the base of the wall. The strain gages inform the horizontal strain distribution, resulting curvature, and curvature distribution along the height of the wall. Note that strain data for SGA1-15 was corrupt.

5.4. Curvature Distribution

The strain distributions in Figure 5-14 are calculated as the average strain in the push direction from strain gages located in columns A1 and E1 and levels 2, 15, and 30 (see Figure 4-8). The strain was averaged at these heights because it is the region that contained most of the plastic deformation. The large shift in strain from 0.2% to 0.4% occurs because of rebar yielding when large inelastic deformations begin to occur. The strain profiles are limited to 0.4% global drift because the rebar strain gages reach their maximum capacity.

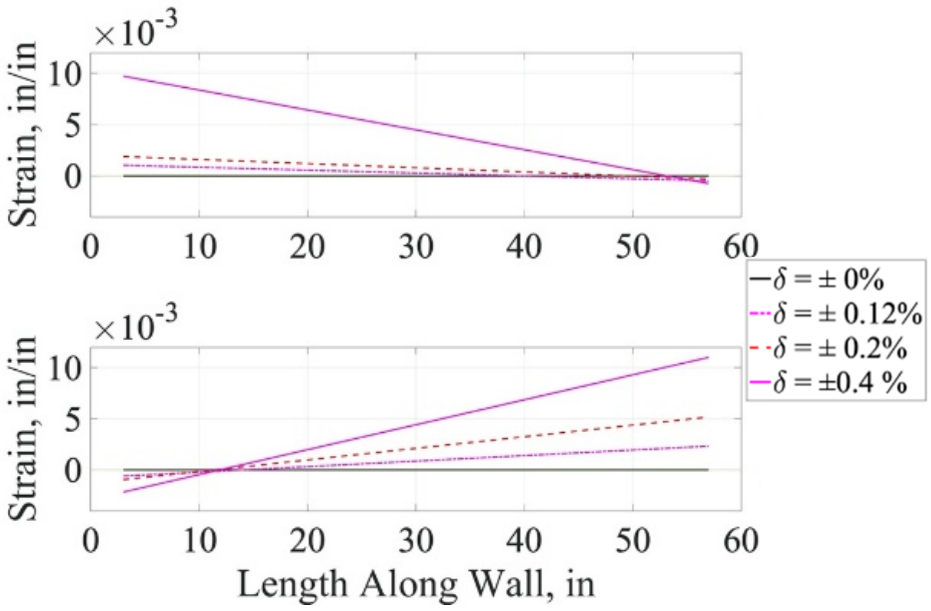

Figure 5-14: Average Strain Profile Along Length of Wall in Push (Top) and Pull Direction (Bottom)

The compression depth is calculated based on the geometry of the strain profile up to 0.4% drift, which informed the curvature profile along the height of the wall. Figure 5-15 illustrates that plastic deformation is limited to the bottom of the wall, particularly at the primary flexural cracks which corresponds to a limited distribution of plasticity. Curvature is calculated to 60” above the wall base and that curvature was assumed zero at the top of the wall due to the whole section being in compression. The non-linear distribution of curvature is expected in an idealized and well-detailed cantilever wall system.

Research by Lu et al. (2017) suggest that reversal of curvature near the base may be a result of concentrated strains at primary flexural cracks. The unsymmetrical curvature disitrribution in the push and pull directions, as shown in Figure 5-15, may be a result of asymetric formation of flexural cracking.

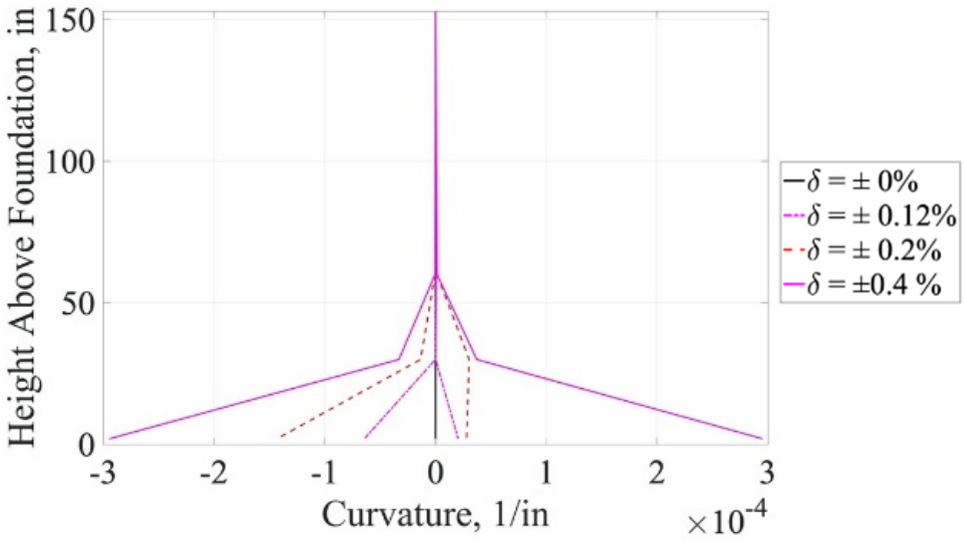

Figure 5-15:Curvature Along Height of Wall

5.5. Comparison of Contributions to Deformation

The contribution of other methods of deformation to the global deformation of the wall is minimal – less than 5%. Due to data spikes shown in the time history shown in Figure 5-16, outliers with percent errors larger than 20% were excluded.

5.6. Drift Profile

The drift profile was measured using string potentiometers placed along the height of the wall. Additionally, base slip is measured between the wall and footing interface. As shown in Figure 5-17, there is a linear drift profile at each drift level, even at significant drifts (+3.33%). This suggests that there is significant base rotation/ rocking at drifts after global yield of the wall. Figure 5-18 indicates there is a maximum of 0.05% drift due to sliding between the wall and the footing in the pull direction (final -1.67% cycle). This was determined to be insignificant, when compared to the global deformation of the wall.

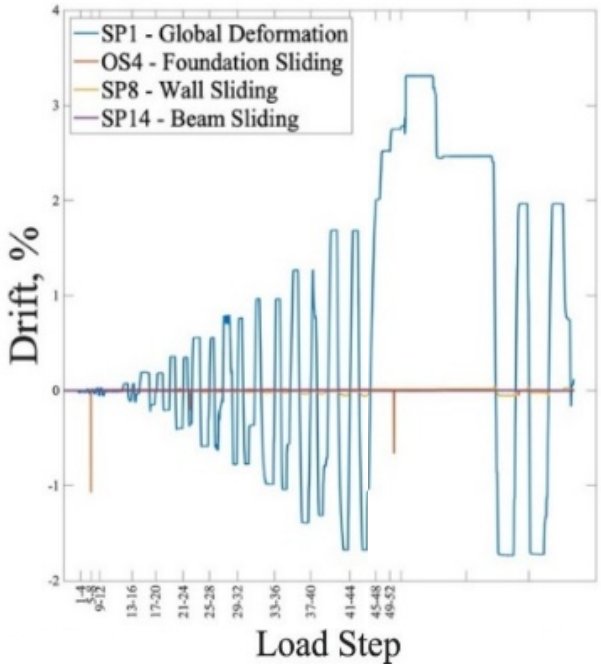

Figure 5-16: Contributions to Global Deformation

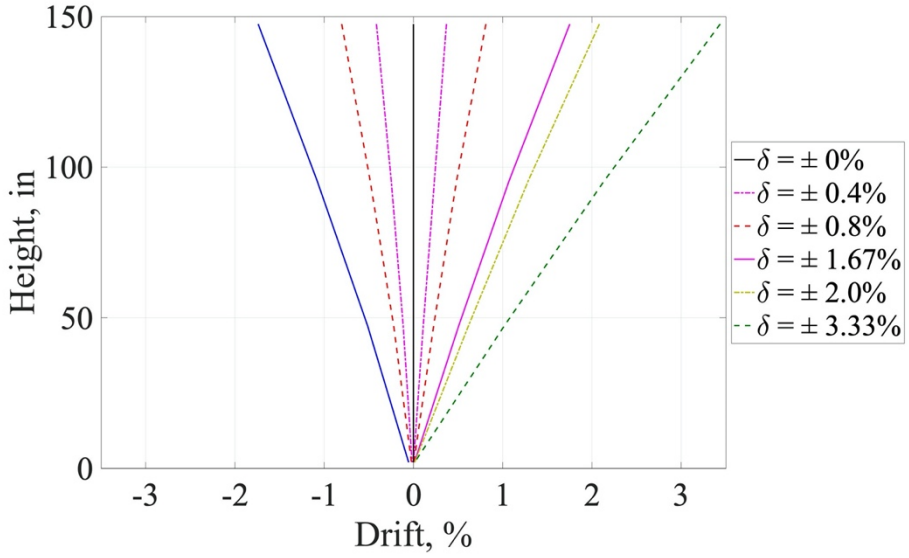

Figure 5-17: Global Drift Profile

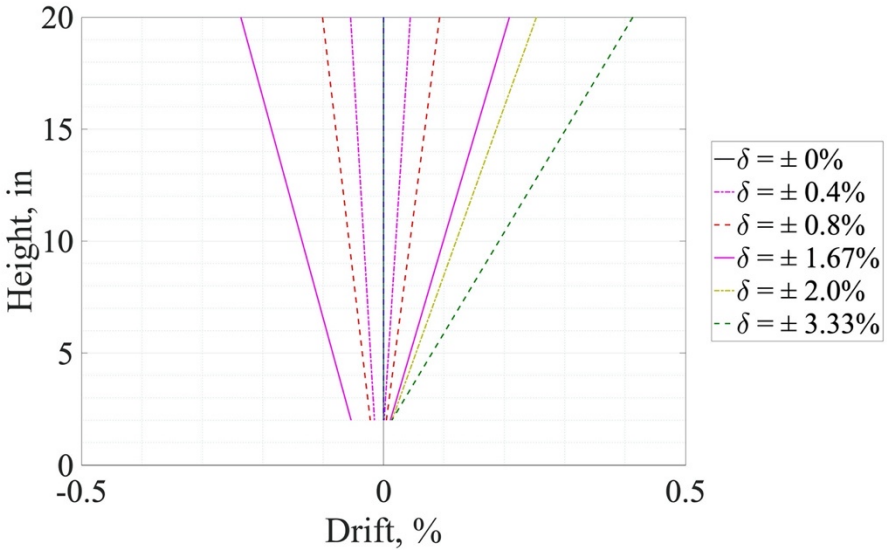

Figure 5-18: Drift Profile at Base

6. PREDICTIONS

This chapter explains the analysis procedures used to predict the global performance of the wall. These analyses were performed to inform the loading protocol and provide useful comparisons to experimental results. The analyses range from design-oriented methods using ASCE 41 to more rigorous methods using PERFORM-3D. Below is a list of assumptions made in the predictions of the wall performance: constant axial load of 35.1 kips, or N_a = 3.1%, plane sections remain plane, and small angles approximation.

6.1. ASCE 41-17 Analysis

ASCE 41-17 provides guidance for creating an action-deformation relationship for concrete members in Chapter 10, and more specifically for structural walls in Chapter 10.7. The action-deformation relationship can take various forms, including a force-displacement or moment-rotation plot. To compare to experimental results most easily from the R1 wall test, a force-displacement plot was developed. Figure 6-1 illustrates the general plot formation and includes points of interest indicated with capital letters and tabular parameters indicated by lowercase letters.

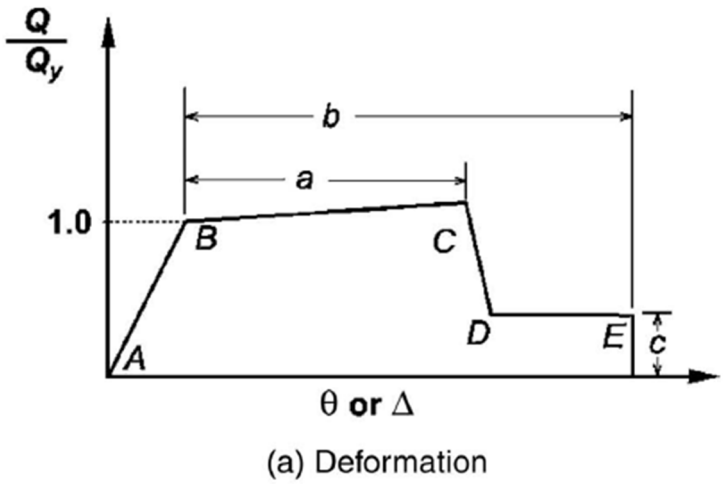

Figure 6-1: Force-Displacement Relationship for Concrete Members from ASCE 41-17 Figure 10-1(a).

To generate a simple force-displacement relationship based on Figure 6-19 for the wall specimen in this experiment, each point along the plot indicated by a capital letter can be calculated using the guidelines outlined in Section 10.3.1.2.2 of ASCE 41-17. Starting from point "A" (the unloaded state) and incrementing to point "B" (global yielding) represents an initial linear response with an effective stiffness. Point "B" to "C" represents a linear response at a reduced stiffness of between 0-10% of the initial stiffness. Point "D" represents a sudden loss of seismic resistance. The final leg to Point "E" represents a maintained low strength capacity until complete loss of capacity at point "E".

The initial portion of the force-displacement response from point "A" to point "B" requires a calculated yield force (V_y) and yield deflection (Δ_y) utilizing an effective stiffness (EI_{eff}). The relationship between these variables is shown in the equation below and assumes small angles:

$$\Delta_y = \theta_y h = \left(\frac{M_y}{EI_{eff}} l_p\right) h = \left(\frac{V_y h}{EI_{eff}} l_p\right) h \qquad [6-1]$$

where θ_y is the yield rotation of the wall per ASCE 41 equation 10-5 and l_p is defined in ASCE 41 section 10.7.2.2.2 as the plastic hinge length. The plastic hinge length is approximated as half the wall length. The yield force, V_y is already known based on the nominal flexural strength of the wall as calculated in Chapter 3 of this paper. The effective stiffness can be determined using several options, including usage of a tabular effective stiffness value from Table 10-5 in ASCE 41. For cracked wall components, the effective stiffness is equal to $0.35E_{cE}I_g$ where E_{cE} is the expected modulus of elasticity of concrete and I_g is the section moment of inertia (note that a typo exists in Table 10-5 where I_g is mistakenly replaced by A_g). With this information, the yield deflection can be calculated along with the yield force so point "B" can be plotted.

The next point of the force-displacement response, point "C", requires a new reduced stiffness as a proportion of the effective stiffness calculated previously and a plastic hinge rotation from Table 10-19 in ASCE 41. Based on the reduced stiffness, 1% of the initial stiffness was chosen. Regarding the plastic hinge rotation or "a" parameter, a rotation of 0.008 radians was obtained. Converting this plastic hinge rotation into a displacement at the top of the wall specimen is shown below:

$$\Delta_{"C"} = \Delta_y + a(h - l_p) \qquad [6-2]$$

The next point of the force-displacement response, point "D", requires only the parameter "c" from ASCE 41 table 10-19, calculated to be 0.6. The resulting shear at point "D" is 60% of the shear at point "C" at the same displacement $\Delta_{"C"}$. At this point, the wall has failed (loss of load carrying capacity by more than 20%), but the last point will be calculated for completeness. The final point "E" is found by maintaining the reduced shear at point "D" and by using the plastic hinge rotation or "b" parameter equal to 0.015 from Table 10-19. Like point "C", the new displacement can be calculated as shown below:

$$\Delta_{"E"} = \Delta_y + b(h - l_p) \qquad [6-3]$$

The resulting force-displacement plot compared to experimental results is shown below in Figure 6-2. As shown, the prediction was accurate in every respect except displacement ductility. That is, the actual wall had a larger final drift before failure compared to the prediction from ASCE 41.

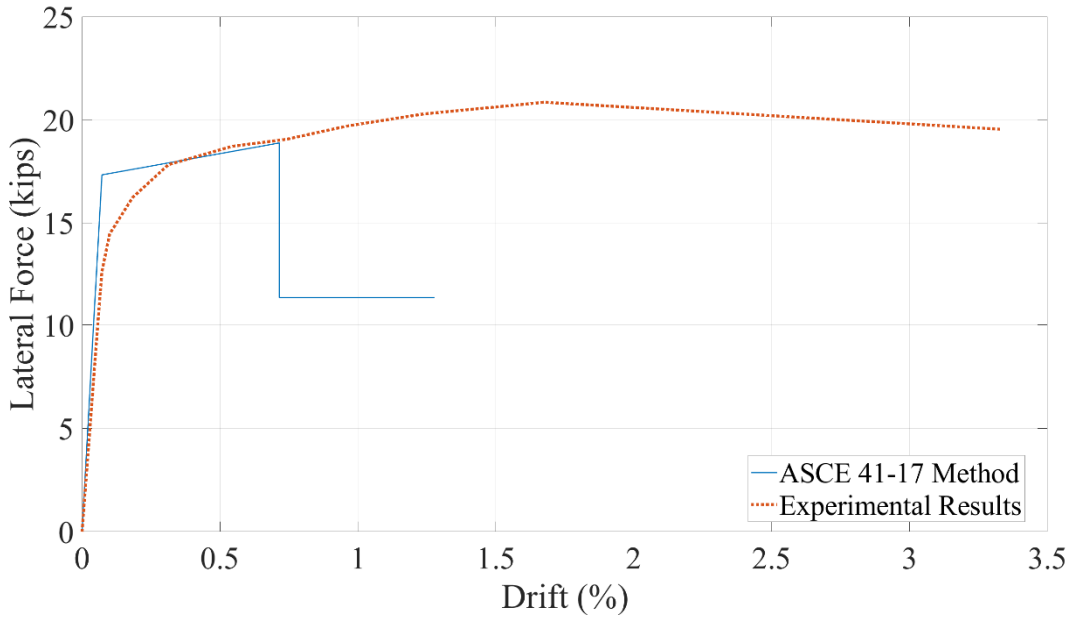

Figure 6-2: ASCE 41-17 Predictions Compared to Experimental Results

6.2. Priestley Analysis

The next analysis method used to predict wall performance is based on guidelines from *Displacement-Based Seismic Design of Structures* (Priestley et. al., 2007). From this point going forward, the methods derived from this book will be referenced as the "Priestley method" for clarity. Like the ASCE 41 method discussed previously, the Priestley method is a lumped plasticity model and utilizes various equations and previously recorded experimental findings to ultimately construct a force-displacement response approximate to the envelope of the wall's cyclic behavior.

6.2.1. Moment-Curvature Relationship

Since curvature is a better parameter than deflection for estimating nonlinear deformations in flexure-dominated shear walls, a moment-curvature analysis was performed to understand how the wall cross section responds to increasing moment demands. Given the numerical rigor of performing a moment-curvature analysis, various software has been created over the years to assist in the process such as XTRACT (Chadwell & Imbsen & Associates, 2002) and Sketchulation (Tipping Applications, 2018). Many of these programs use fiber discretization or fiber-section analysis to produce a moment-curvature response of a cross-section at a critical location, typically the base of a cantilever wall.

For this paper, Sketchulation was selected as the software to produce a moment-curvature response. The moment-curvature analysis was dependent upon user-defined constitutive models for unconfined concrete and reinforcing. Typically, the cover concrete is differentiated from the concrete within the transverse reinforced core, but since the spacing of the transverse reinforcing was so sparse (14.3 inches) there was little to no confinement and thus no justification to create a separate material model for confined concrete. The unconfined concrete model used is shown in Figure 6-3 and is based on a trilinear Mander model approximation (Elwood and Moehle, 2006) using the average concrete cylinder strength of 3.79 ksi.

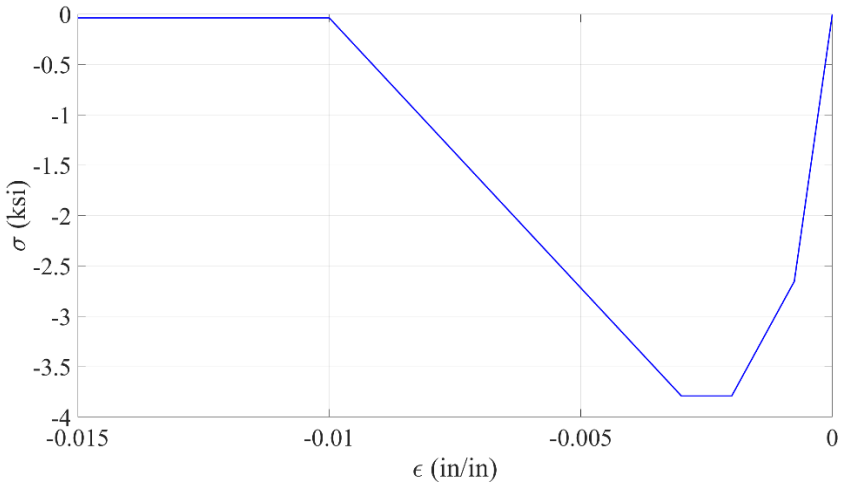

Figure 6-3: Unconfined Concrete Constitutive Model

For the reinforcement models used in Sketchulation, two versions were explored: one with only tension capacity, and one with both tension and compression capacity (symmetrical). The reason for this differentiation was to bound the actual behavior of the reinforcing steel which would have limited compression capacity due to bar buckling. The reinforcement models were based on tensile steel test values as discussed in Section 3.6 and are shown in Figure 6-4.

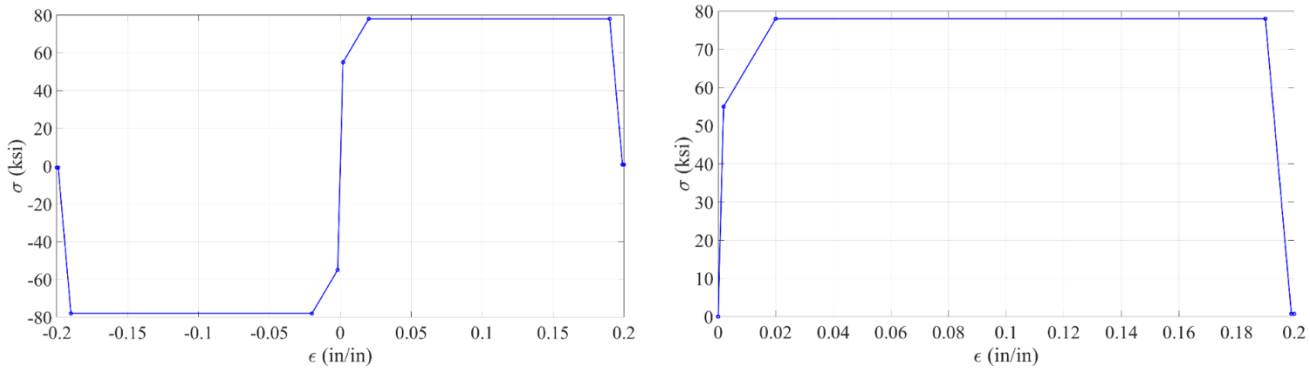

Figure 6-4: Reinforcing Steel Constitutive Model
(Right) Tension only constitutive model used for reinforcement in Sketchulation and
(Left) tension and compression constitutive model used for reinforcement in Sketchulation.

Figure 6-5 shows the complete moment-curvature response from Sketchulation after inputting the constitutive models into the program and using a constant axial load of 35.1 kips. Note that Figure 6-5 is truncated to include data up until 20% loss of strength in the test specimen. As shown, the tension-only analysis results in lower ultimate moments and curvatures due to the reduced contribution of the steel. The difference in ultimate moment magnitude is about 6%, and the difference in ultimate curvature is about 9%. The most accurate model would lie somewhere between the two analyses.

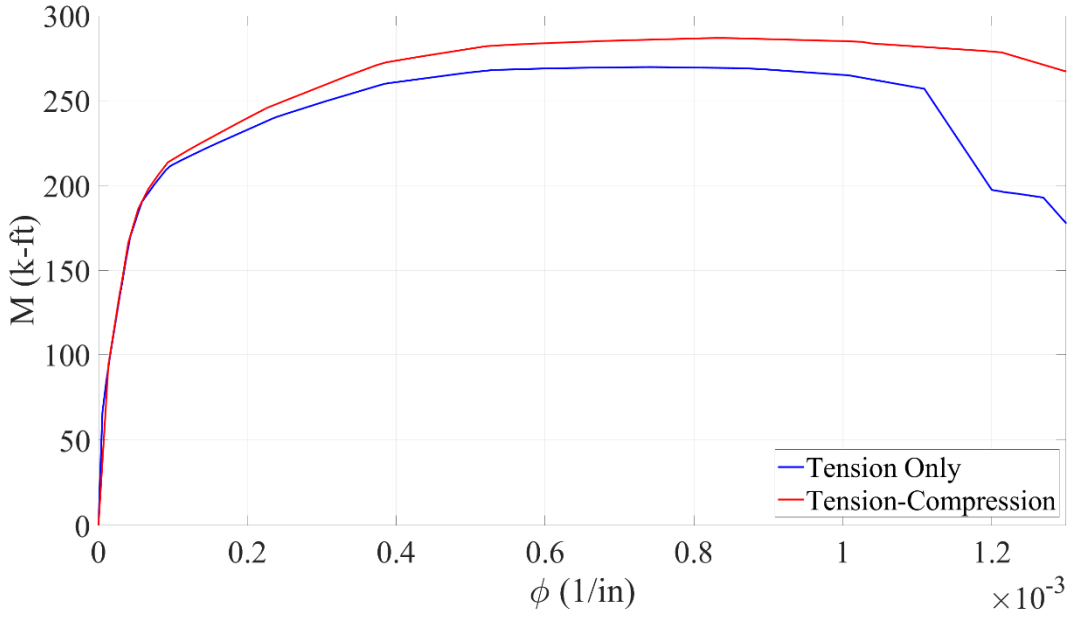

Figure 6-5: Moment Curvature Analysis of Wall Cross Section

6.2.2. Priestley Bilinearization of Moment-Curvature

With the moment-curvature response complete, it would be possible to integrate the curvatures with respect to the wall height along the entire curve to obtain a theoretical top displacement of the wall. However, as Priestley mentions, this process does not necessarily produce accurate results because it ignores tension shift, shear deformation, strain penetration into the foundation, and other considerations. Instead, a simplified approach to account for these factors is to assume a lumped plasticity model (plastic hinge) and bilinearize the moment curvature response using several key points on the curve. The bilinear moment-curvature response compared to the unaltered response from Sketchulation is shown in Figure 6-6. The major values used to bilinearize the moment-curvature response are listed below:

- The cracked moment M_{cr} is calculated per ACI 318-14 per the following equation:

$$M_{cr} = \frac{f_r I_g}{(\frac{l_w}{2})} \qquad [6-4]$$

- ϕ_{cr} is the corresponding curvature to M_{cr}
- The yield moment M_y is the moment on the Sketchulation moment-curvature curve when the extreme tension reinforcement first attains yield strain or when the extreme concrete compression fiber attains a strain of 0.002, whichever occurs first. The tension reinforcement attained a yield strain first.
- ϕ'_y is the corresponding curvature to M_y
- The nominal moment M_N is the moment on the Sketchulation moment-curvature curve when the extreme tension reinforcement attains a strain of 0.015 or when the extreme concrete compression fiber attains a strain of 0.004, whichever occurs first. The tension reinforcement attained the strain limit first.
- The nominal yield curvature ϕ_y is the projection of M_y until M_N is reached as shown in the equation:

$$\phi_y = \frac{M_N}{M_y}\phi'_y \qquad [6-5]$$

- The ultimate moment M_u is the largest moment attained by Sketchulation.
- The ultimate curvature ϕ_u is the largest curvature attained by Sketchulation and is plotted with M_u as described above.

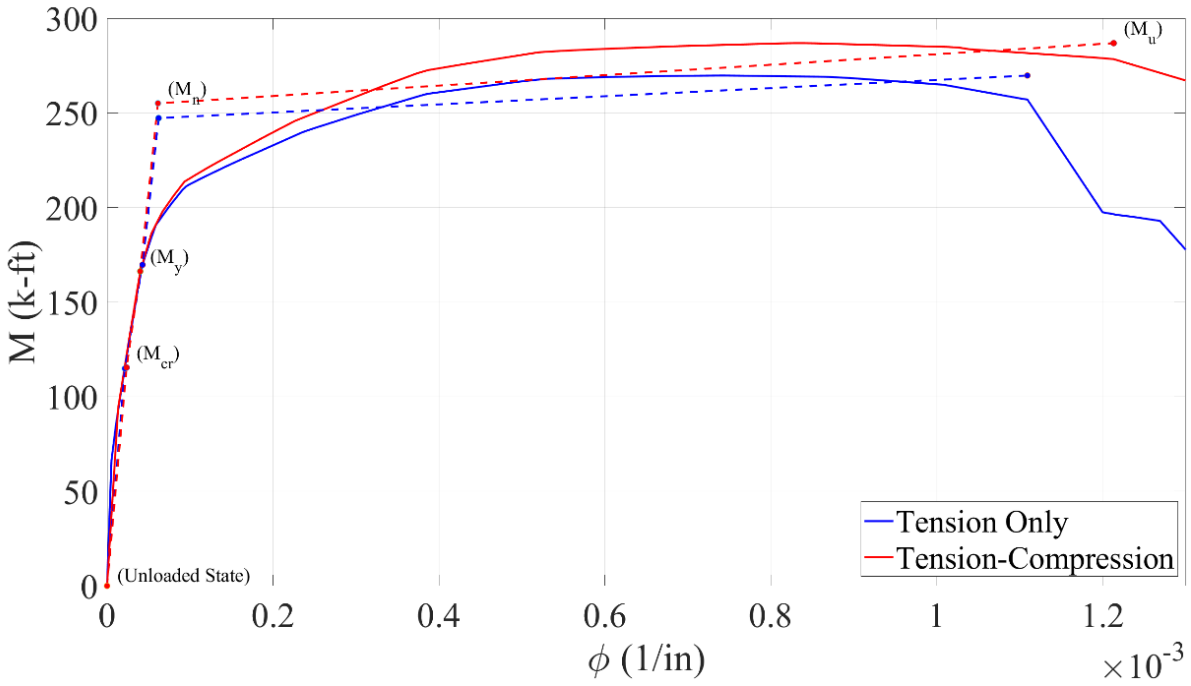

Figure 6-6: Bilinearization of Moment Curvature per the Priestley Method

6.2.3. Priestley Bilinearization of Force-Displacement

With the bilinear moment-curvature response completed, a series of equations can be used to construct a bilinear force-displacement response. In general, each moment corresponds to a force in accordance with the following equation:

$$F = \frac{M}{H_{eff}} \qquad [6-6]$$

where an effective height, strain penetration depth, and plastic hinge length are defined as follows:

$$H_{eff} = H + L_{sp} - \frac{L_p}{2} \qquad [6-7]$$

$$L_{sp} = 0.15 f_y d_{bar} \qquad [6-8]$$

$$L_p = 0.08H + 0.1 l_\omega + L_{sp} \qquad [6-9]$$

To find the associated displacements, the following equations are provided:

$$\Delta_{cr} = \emptyset_{cr} \frac{H^2}{3} \qquad [6-10]$$

$$\Delta'_y = \emptyset'_y \frac{\left(H + L_{sp}\right)^2}{3} \qquad [6-11]$$

$$\Delta_y = \emptyset_y \frac{\left(H + L_{sp}\right)^2}{3} \qquad [6-12]$$

$$\Delta_u = \Delta_y + (\emptyset_u - \emptyset_y) L_p H \qquad [6-13]$$

The equations are based on the diagram from Priestley's book shown in Figure 6-7 below. The resulting force-displacement plot is shown in Figure 6-8 and is plotted against the experimental hysteresis envelope for comparison.

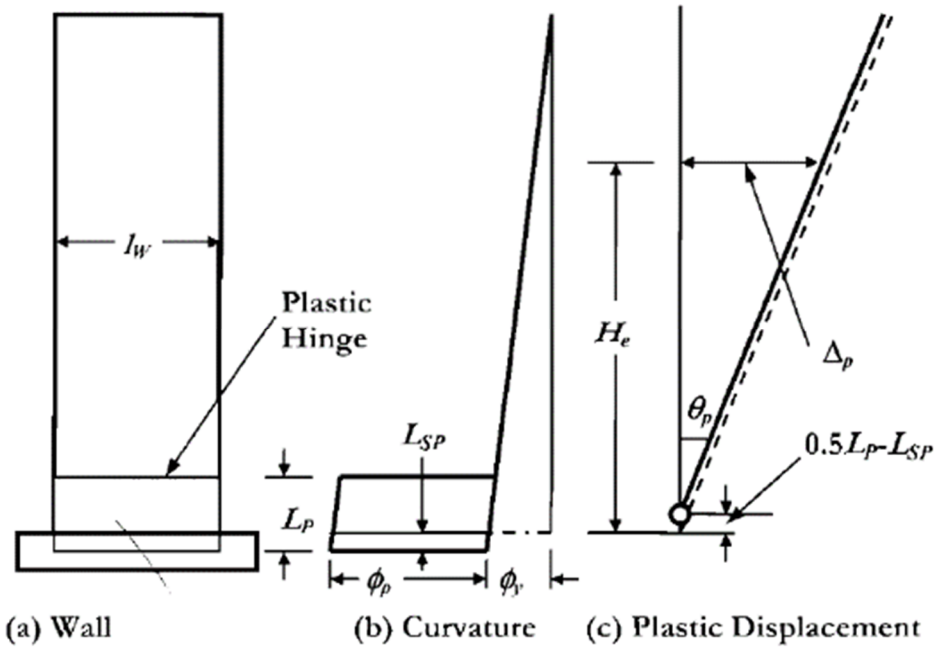

Figure 6-7: Theory for Lumped Plasticity Model Used in the Priestley Method

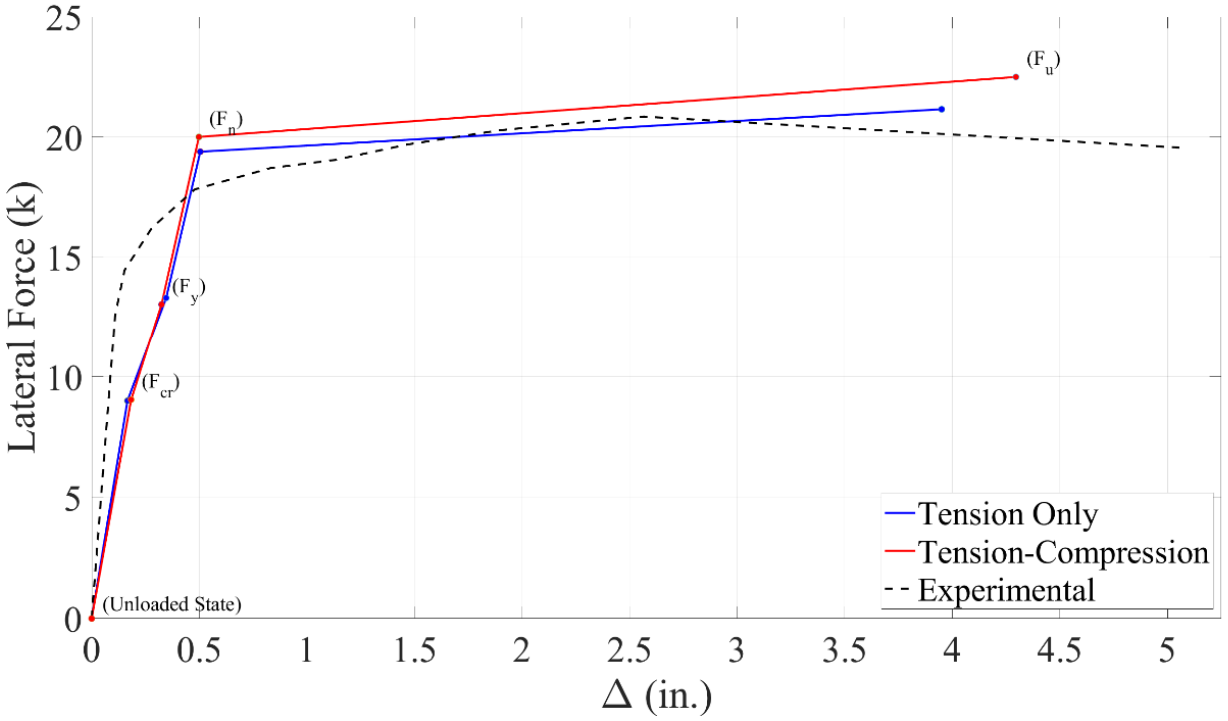

Figure 6-8: Force-Displacement Comparison between Priestley Method and Envelop of Experimental Results

Compared to the experimental results, the Priestley method provides a good approximation of wall behavior. However, the initial stiffness is not captured very well due to an overestimation of yield displacement. Corrections for this overestimated yield displacement common in lightly reinforced walls are presented elsewhere (Beyer, 2007 & Hoult et al., 2018) and are outside of the scope for this prediction.

6.3. PERFORM-3D Analysis

The final tool used for predicting wall behavior was a Computers & Structures Inc. (CSI) software called PERFORM 3D. This software is a high-end analysis tool with many sophisticated abilities not covered in the scope of this paper. The PERFORM 3D analyses for this wall test are summarized in work completed by research collaborators Doan & Williams (2020).

7. CONCLUSIONS & FUTURE WORK

7.1. Summary of Research Study

Non-ductile RC buildings with insufficient detailing are the most vulnerable concrete structures to critical earthquake damage or collapse. Many of these buildings were built before important ACI 318 updates (pre-1980's construction) and utilize RC shear walls as the seismic force resisting system. The shear walls in these buildings are typically lacking longitudinal or horizontal reinforcement, especially in the wall end-zones, and may have undesirable compression failure mechanisms such as rebar buckling or concrete crushing as noted in recent earthquake reconnaissance. Unfortunately, retrofit solutions for addressing the remaining insufficient shear walls are expensive. As a result, structural engineers are exploring why LRC walls seem to perform poorly during earthquakes and how to make retrofits more cost effective.

The primary objective of this project was to investigate the behavior of flexurally dominated LRC shear walls subjected to cyclic loading via testing of a slender LRC wall representative of pre-1980's construction at California Polytechnic State University - San Luis Obispo. This experimental investigation was performed to physically assess the behavior of the shear wall and to further enable numerical investigations to confirm the appropriateness of current computational non-linear methodologies. The continuation of this project being undertaken by Doan & Williams (2020), is to review current industry's non-linear analysis practices for LRC walls and to utilize the testing results discussed in this paper.

7.2. Comparison to Prior LRC Wall Experiments

This section will compare R1 to the most relevant test specimens discussed in other experiments from Section 2.3. Table 7-1 summarizes the parameters compared. SW-1 tested by Cardenas & Magura (1973) performed much like R1. SW-1 had a higher CSAR, lower vertical reinforcement ratio, and a higher axial load ratio. These factors are shown to influence wall ductility (Wibowo et al., 2013) and contributed to SW-1 achieving a lower ductility. Both walls experienced flexural failures due to longitudinal rebar fracture after the onset of a base crack of significant width.

The wall specimen W1 tested by Ireland et al. (2007) had a lower CSAR, nearly equivalent vertical reinforcement ratio, and a higher axial load ratio compared to R1. Although W1 had a lower ductility at failure, both walls experienced a flexural failure after the onset of a significant wall-foundation interface crack. One noticeable difference is that W1 exhibited bar buckling which is unexpected given that W1 had smaller longitudinal bars and more closely spaced horizontal reinforcement. W1 also exhibited noticeable sliding at the wall-foundation interface which was negligible for R1 at ~0.1 inch. Reinforcement type also varied between walls - W1 used smooth rebar and R1 used deformed rebar. The smooth rebar would be expected to have a lesser concrete bond which may partially explain the concentrated crack plane at the base of W1 with no other crack planes along the height.

The wall specimen C1 tested by Lu et al. (2017) performed most similarly to R1. C1 had a lower CSAR, slightly greater vertical reinforcement ratio, and slightly higher axial load ratio. These parameters alone suggest C1 would be expected to have a very comparable ultimate displacement ductility compared to R1. Both walls experienced a flexural failure after the onset of a significant wall-foundation interface crack, and both walls lost 20% of the maximum load carrying capacity due to bar rupture.

Table 7-1: Summary of Previous Experiments Compared to R1

Researcher	Specimen	ρ_l (%)	N_a (%)	f'_c (ksi)	CSAR	SS	Ductility	Failure Mode
Cardenas & Magura (1973)	SW-1	0.27	5.6	7.42	25	2.0	7.0[1]	FT
Ireland et. al. (2007)	W1	0.47	4.7	3.63	8.2	1.3	10	FC
Lu et. al. (2017)	C1	0.53	3.5	5.58	9.3	2.0	12.5	FC
	C2	0.53	3.5	5.00	9.3	4.0	12.5	FC
Luong & de Sevilla (2020)	R1	0.44	3.1	3.79	12	2.6	10-15[5]	FT

[1] *Listed value is curvature ductility.*
[2] *FT indicates flexural-tension failure (rebar fracture). FC indicates flexural-compression failure (bar buckling / concrete crushing).*
[3] *A flexural tension failure can occur after bar buckling and/or concrete crushing have occurred.*
[4] *Failure defined as 20% of maximum lateral force loss.*
[5] *Ultimate displacement ductility is bounded by the given range.*

7.3. Conclusions of Research Study

7.3.1. LRC Wall Behavior

Generally, practitioners have a perception that lightly reinforced concrete (LRC) walls are non-ductile and do not perform well in large seismic events. However, the experimental results in this paper and others examining LRC walls demonstrate that this assumption is not necessarily correct. The LRC wall specimen tested in this paper (R1) had a moderate axial load and was able to achieve ultimate drifts of about 2-3% and a corresponding displacement ductility of 10-15. When compared to other LRC experiments, and even modern wall tests, this result is on the higher end of what is expected. A major contribution to this behavior was the failure mechanism of R1, governed by several primary horizontal crack planes extending up the wall height with a flexural tension failure characterized by the rupture of longitudinal rebar at the wall-foundation interface. This failure mechanism promoted global rocking action of the wall.

If the wall was not braced out-of-plane, it may have suffered an out-of-plane failure prematurely given the significant amount of rocking. The authors suspect that the prominent rocking behavior may not be representative of actual walls in buildings braced at each story by the floor slab, leading to an overestimate to global displacement ductility, as determined in this experiment.

7.3.2. LRC Wall Analysis Methods

ASCE 41-17 underestimates LRC wall global ductility but captures initial stiffness more accurately than the Priestley method. However, this prediction method is sensitive to assumed values for post yield stiffness and code-recommended tabular values for plastic rotation. The Priestley method provides accurate results compared to experimental results in every aspect except for initial stiffness due to an overestimate of yield displacement. The prediction options offered by a calibrated Perform-3D model offer the most accurate results and provide valuable hysteretic data not obtained from lumped plasticity methods (Doan & Williams 2020). For a future LRC wall experiment, the authors of this paper would recommend a Perform-3D model for predictions as opposed to ASCE-41 and the Priestley Method.

7.4. Future Work

There is evidence in recent literature which shows the cracking behavior of LRC walls can be improved with added longitudinal reinforcement in the boundary zones (Lu, 2017; Lu et al., 2017; Lu et al., 2018; Shegay et al., 2020). If FRP could be used in a future experiment to increase the longitudinal area of resistance in the boundary zones, this could prove to be a useful retrofit strategy for existing LRC walls.

The continuation of this research investigates the non-linear modeling strategies currently used in the structural engineering profession applied to LRC walls, as discussed in Doan and Williams.

REFERENCES

Abdullah, S. A., & Wallace, J. W. (2019). Drift Capacity of Reinforced Concrete Structural Walls with Special Boundary Elements. *ACI Structural Journal*, 183-194.

American Concrete Institute. (1963). *Building Code Requirements for Structural Concrete (ACI 318-63).*

American Concrete Institute. (1971). *Building Code Requirements for Structural Concrete (ACI 318-71).*

American Concrete Institute. (2014). *Building Code Requirements for Structural Concrete (ACI 318-14) and Commentary.* Farmington Hills, MI, USA.

American Concrete Institute. (2019). *Building Code Requirements for Structural Concrete (ACI 318-19) and Commentary.*

American Concrete Institution. (2014). *Building Code Requirements for Structural Concrete (ACI 318-14) and Commentary.* American Concrete Institution.

American Society of Civil Engineers; Structural Engineering Institute. (2017). *ASCE 41-17: Seismic Evaluation and Retrofit of Existing Buildings.* Reston, Virginia: American Society of Civil Engineers.

Behrouzi, A. A. (2016). *Impact of Cross Section, Web Reinforcement, and Load History on the Seismic Peformance of Slender Concrete Walls.* PhD Dissertation, University of Illinois at Urbana-Champaign.

Bernstein, S. (2005, October 11). How Risky Are Older Concrete Buildings? *Los Angeles Times*.

Beyer, K. (2007). *Seismic Design of Torsionally Eccentric Buildings with U-Shaped RC Walls.* PhD Thesis, ROSE School.

Birely, A. (2012). *Seismic Performance of Slender Reinforced Concrete Structural Walls.* PhD Dissertation, University of Washington.

Burwell, C. M., Hooper, J. D., & Anderson, R. D. (2006). SEISMIC STRENGTHENING OF HARBORVIEW MEDICAL CENTER USING FRP REINFORCEMENT. *8th U.S. National Conference on Earthquake Engineering.* San Francisco.

Burwell, C., Hooper, J., & Anderson, R. (2006). Seismic Strengthening of Harborview Medical Center Using FRP Reinforcement. *8th U.S. National Conference on Earthquake Engineering.*

Cardenas, A., & Magura, D. (1973). *Strength of High-Rise Shear Walls - Rectangular Cross Section.* Research Paper, Portland Cement Association.

CERC. (2012). *Canterbury Earthquakes Royal Commission. Final report: volume 2. The performance of Christchurch CBD Buildings.* Wellington, NZ.

Chadwell, C., & Imbsen & Associates. (2002). XTRACT - Cross Section Analysis Software for Structural and Earthquake Engineering. Software, http://trcbridgedesignsoftware.com/software-XTRACT.html.

Comartin, C., Bonowitz, D., Greene, M., McCormick, D., May, P., & Seymour, E. (2011). *The Concrete Coalition and the California Inventory Project: An Estimate of the Number of Pre-1980 Concrete Buildings in the State.* Concrete Coalition.

Cruz-Noguez, C. A., Lau, D. T., Sherwood, E. G., Hiotakis, S., Lombard, J., Foo, S., & Cheung, M. (2015). Seismic Behavior of RC Shear Walls Strengthened for In-Plane Bending Using Externally Bonded FRP Sheets. *Journal of Composites for Construction* .

Dashti, F., & Dhakal, R. (2013). *Comparative Performance of RC Shear Walls Designed by Different Standards.* Research Paper, University of Canterbury.

Elwood, K., & Moehle, J. (2006). *Idealized Backbone Model for Existing Reinforced Concrete Columns and Comparisons with FEMA 356 Criteria.* Struct. Design Tall Spec. Build.

Endeshaw, M. A., ElGawady, M., Sack, R. L., & McLean, D. I. (2008). *RETROFIT OF RECTANGULAR BRIDGE COLUMNS USING CFRP WRAPPING.* Olympia: Washington State Department of Transportation.

Hagen, G. (2019). Discussions of Concrete Wall Building Inventory. (J. Luong, Interviewer)

Hagen, G., & Abdullah, S. (2019, March 15). Discussions of Wall Drift Capacity, Email Conversation.

Hoult, R., Goldsworthy, H., & Lumantarna, E. (2018). *Plastic Hinge Analysis for Lightly Reinforced and Unconfined Concrete Structural Walls.* Bull Earthquake Eng.

Ireland, M. (2007). *Development of a Selective Weakening Approach for the Seismic Retrofit of Reinforced Concrete Structural Walls.* PhD Dissertation, University of Canterbury.

Ireland, M. (2007). *Development of a Selective Weakening Approach for the Seismic Retrofit of Reinforced Concrete Structural Walls.* University of Canterbury.

Kam, W. Y., Pampanin, S., & Elwood, K. (2011). *Seismic Performance of Reinforced Concrete Buildings in the 22 February Chirstchurch (Lyttelton) Earthquake* . Bulletin of the New Zealand Society for Earthquake Engineering .

Kaplan, H., Yilmaz, S., Binici, H., Yazar, E., & Cetinkaya, N. (2004). May 1, 2003 Turkey - Bingol earthquake: damage in reinforced concrete structures. *Engineering Failure Analysis*, 279-291.

Khalil, A., & Ghobarah, A. (2005). Behaviour of Rehabilitated Structural Walls. *Journal of Earthquake Engineering*.

Lu, Y. (2017). *Seismic Design of Lightly Reinforced Concrete Walls.* Auckland: PhD Dissertation, Univeristy of Auckland.

Lu, Y., Henry, R., & Ma, Q. (2018). Experimental Validation of Minimum Vertical Reinforcement Requirements for Ductile Concrete Walls. *ACI Structural Journal*, 1115-1130.

Lu, Y., Henry, R., Gultom, R., & Ma, Q. (2017). Cyclic Testing of Reinforced Concrete Walls with Distributed Minimum Vertical Reinforcement. *Journal of Structural Engineering, Volume 143 Issue 5*.

Luong, J., & Brown, G. (2018, June). Structural Analysis of the High Bay Steel Reaction Frames. Senior Project, California Polytechnic State University - San Luis Obispo, California, USA.

Microsoft Corporation. (2018). Microsoft Excel.

Moehle, J. (2011). February 27, 2010 Chile Earthquake Reconnaissance Team Investigation: Reinforced Concrete Buildings.

Ostrom, L. (2018). *Improving Ductility of Slender Reinforced Concrete Shear Walls with FRP Sheets and Splay Anchors.* San Luis Obispo: Senior Project, California Polytechnic State University - San Luis Obispo.

Paterson, J., & Mitchell, D. (2003). Seismic Retrofit of Shear Walls with Headed Bars and Carbon Fiber Wrap. *Journal of Structural Engineering*.

Priestley, M., Calvi, G., & Kowalsky, M. (2007). *Displacement-Based Seismic Design of Structures.* Fondazione Eucentre, Pavia: IUSS Press.

R., P. (1989). Evaluation of Ductility of Structures and Structural Assemblages from Laboratory Testing. *Bull. N.Z. Nat. Soc. Earthquake Eng., 22(3)*, 155-166.

Realfonzo, R., & Napoli, A. (2009). Cyclic Behavior of RC Columns Strengthened by FRP and Steel Devices. *Journal of Structural Engineering*.

Ridgley, C. (2019). *Steel Test Set-Up for Non-Ductile Concrete Shear Walls.* San Luis Obispo: Senior Project, California Polytechnic State University - San Luis Obispo.

Schotanus, M., & Maffei, J. (2008). Computer Modeling and Effective Stiffness of Concrete Wall Buildings.

Segura, C. (2017). *Seismic Performance Limitation of Slender Reinforced Concrete Structural Walls.* Los Angeles: PhD Dissertation, University of California at Los Angeles.

Shegay, A., Dashti, F., Hogan, L., Lu, Y., Niroomandi, A., Seifi, P., . . . Pampanin, S. (2020). Research Programme on Seismic Performance of Reinforced Concrete Walls: Key Recommendations. *Bulletin of the New Zealand Society for Earthquake Engineering, Vol. 53, No. 2*, 54-69.

Sheikh, S. A., & Yau, G. (2003). Seismic Behavior of Concrete Columns Confined with Steel and Fiber-Reinforced Polymers. *ACI Structural Journal*.

Sheikh, S. A., Iacobucci, R. D., & Bayrak, O. (2003). Retrofit of Square Concrete Columns with Carbon Fiber-Reinforced Polymer for Seismic Resistance. *ACI Structural Journal*.

STRUCTUREPOINT LLC. (2019). spColumn.

STRUCTUREPOINT LLC. (2019). spColumn.

The MathWorks Inc. (2019). MATLAB . *Version 9.5.0.944444 (R2018b)*. Natick, Massachussets.

Tipping Applications. (2018). Sketchulation User Guide.

Wermiel, S. E. (2009). California Concrete, 1876-1906: Jackson, Percy, and the Beginnings ofReinforced Concrete Construction in the United States. *Third International Congress on Construction History.* Cottbus.

Wibowo, A., Wilson, J., Lam, N., & Gad, E. (2013). *Seismic Performance of Lightly Reinforced Structural Walls for Design Purposes.* Institution of Civil Engineers.

Williams, J., & Doan, T. (2020). *Investigation of Modeling Strategies for Lightly Reinforced Concrete Shear Walls.* San Luis Obispo: Masters Thesis, California Polytechnic State University - San Luis Obispo.

Wood, S., Wight, J., & Moehle, J. (1987). *The 1985 Chile earthquake observations on earthquake-resistant construction in Vina del Mar.* University of Illinois at Urbana-Champaign: Techincal Report.

APPENDIX

A. Footing Documentation

A.1 Material Properties

Table A-1: Footing concrete cylinder test results.

	Cylinder 1	Cylinder 2	Cylinder 3	Cylinder 4	Average
Concrete compressive strength, f_c'	1.932	2.016	1.621	1.975	1.886

A.2 Rebar Layout and Dimensions

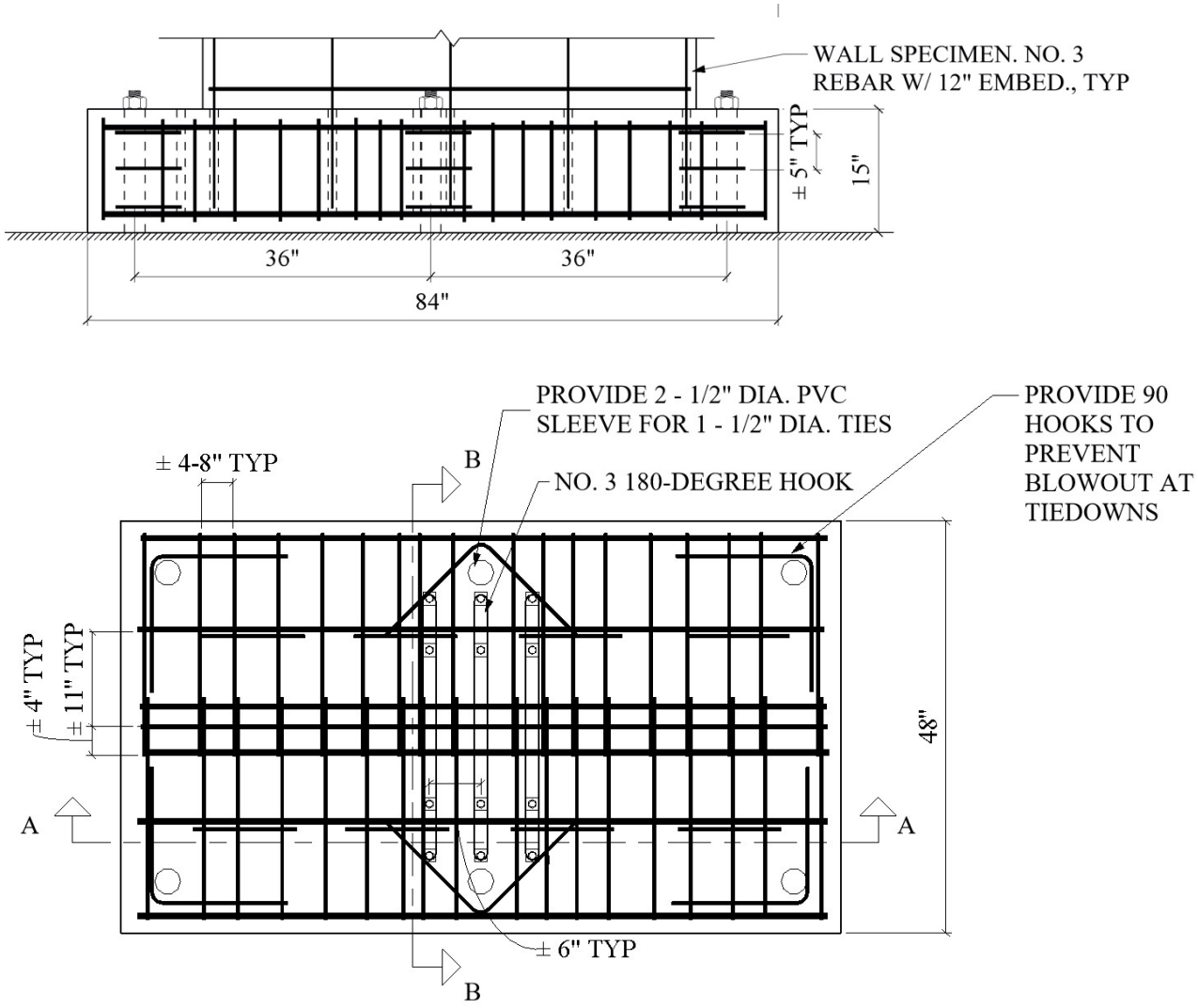

Figure A-1: Rebar layout and dimensions of wall footing.

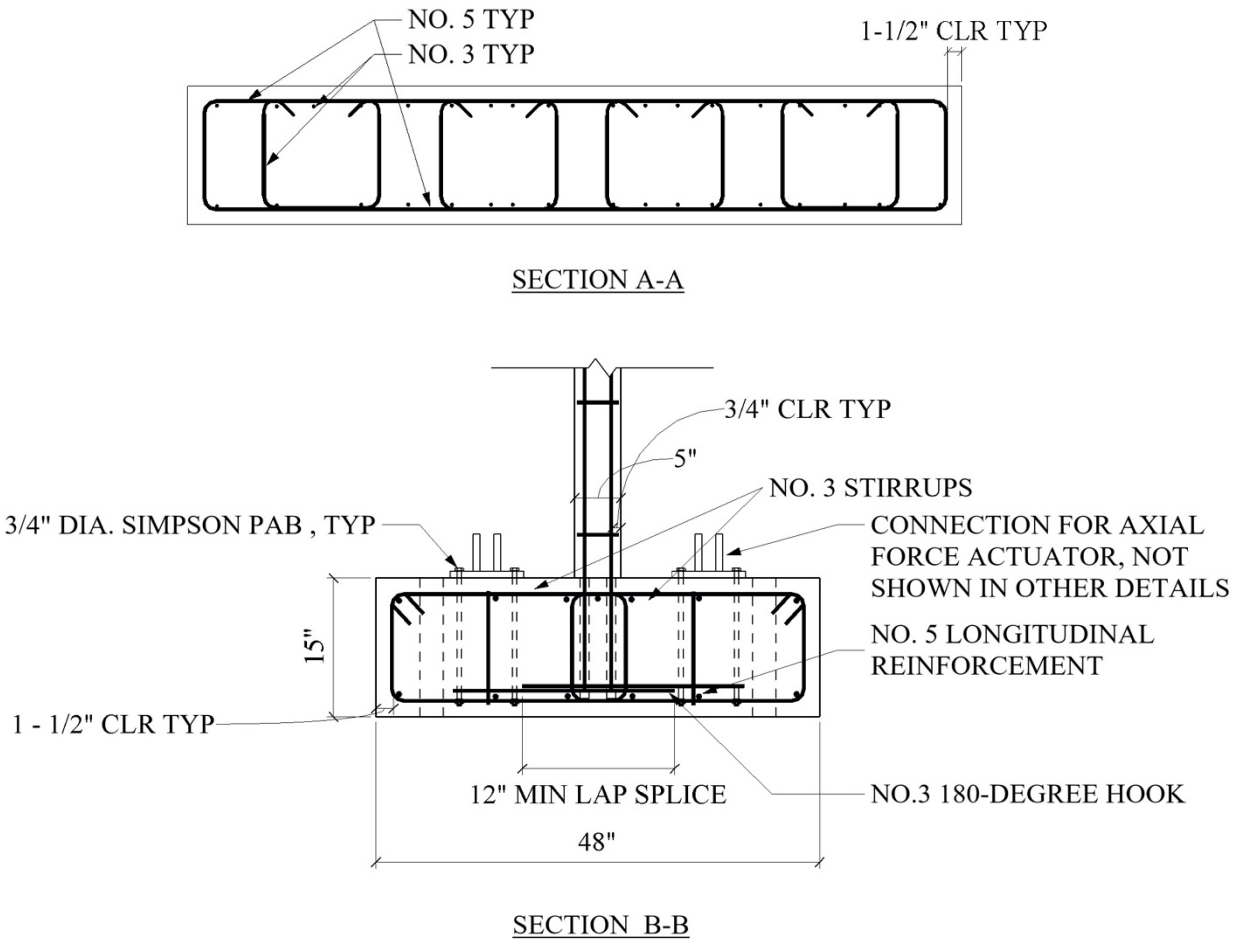

Figure A-2: Additional rebar layout and dimensions of wall footing.

A.3 Nominal Shear Capacity of Footing in Transverse Direction (Per ACI 318-14)

Concrete Strength (ACI 318-14 Eqn. 22.5.5.1)

$\lambda := 1.0$

$f'_c := 1879\ psi$ compressive strength of concrete

$V_c := 2 \cdot \lambda \cdot \sqrt{f'_c \cdot \frac{1}{psi}} \cdot psi \cdot b_w \cdot d$ nominal shear strength from concrete

$V_c = 53.317\ kip$

Steel Strength (ACI 318-14 Eqn. 22.5.10.5.3)

$n := 4$ number of legs

$A_v := 0.11\ in^2$ area per single leg of shear reinforcement

$f_y := 60\ ksi$ yield strength of steel reinforcement

$s := 6\ in$ spacing of shear reinforcement

$V_s := \frac{(n \cdot A_v \cdot f_y \cdot d)}{s}$

$V_s = 56.375\ kip$

Nominal Shear Strength (ACI 318-14 Eqn. 22.5.1.1)

$V_n := V_c + V_s$

$V_n = 109.7\ kip$ total nominal shear strength

$V_{max} := 10 \cdot \sqrt{f'_c \cdot \frac{1}{psi}} \cdot psi \cdot b_w \cdot d$ limit on shear strength (ACI 318-14 Eqn. 22.5.1.2)

$V_{max} = 266.6\ kip$

$V_{n1} := min(V_n, V_{max}) = 109.7\ kip$

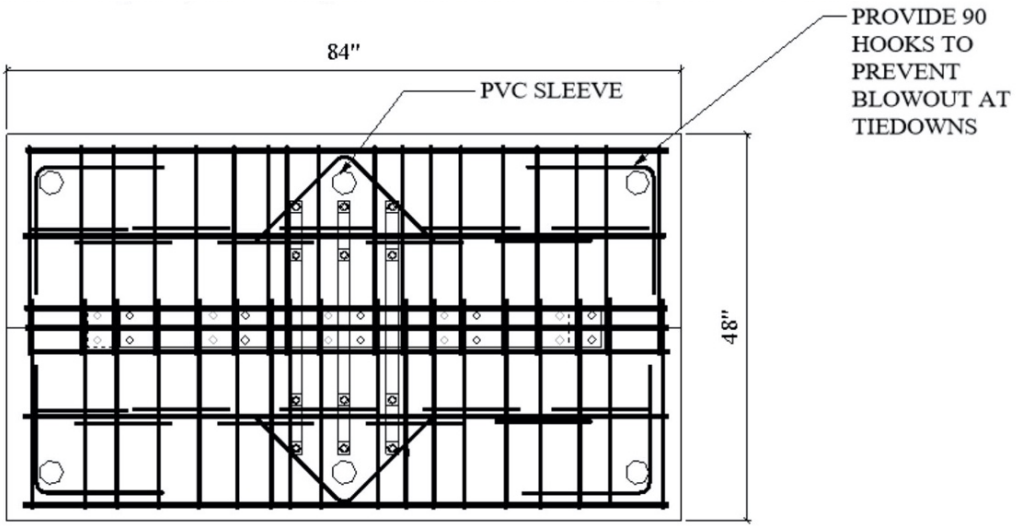

Plan View of Rebar Layout

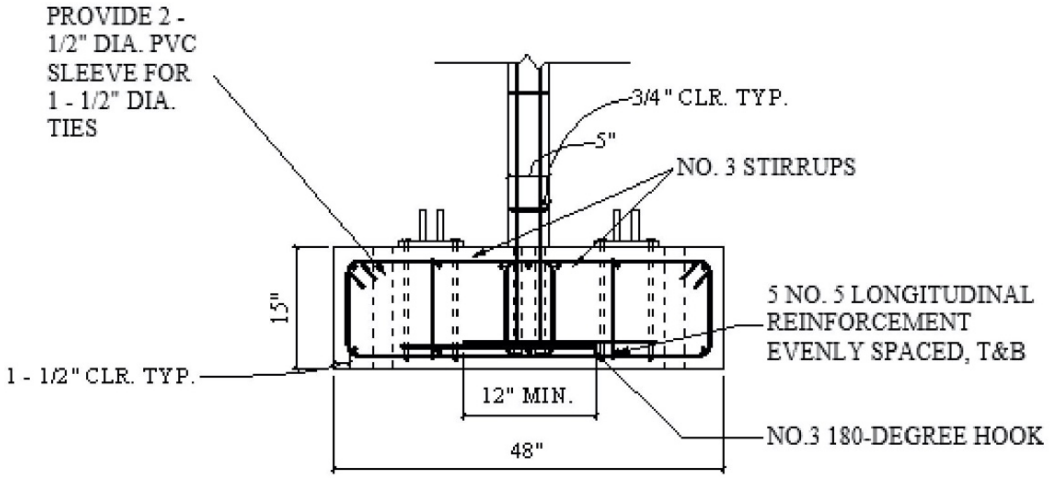

Transverse Section of Footing

$b_w := 48\ in$ width of footing

$h := 15\ in$ height of footing

$c := 1.5\ in$ clear cover

$d_s := 0.375\ in$ diameter of shear reinforcement

$d_b := 0.625\ in$ diameter of flexural reinforcement

$d := h - c - d_s - \frac{d_b}{2} = 12.813\ in$ depth to centroid of steel group

A.4 Nominal Shear Capacity of Footing in Longitudinal Direction (Per ACI 318-14)

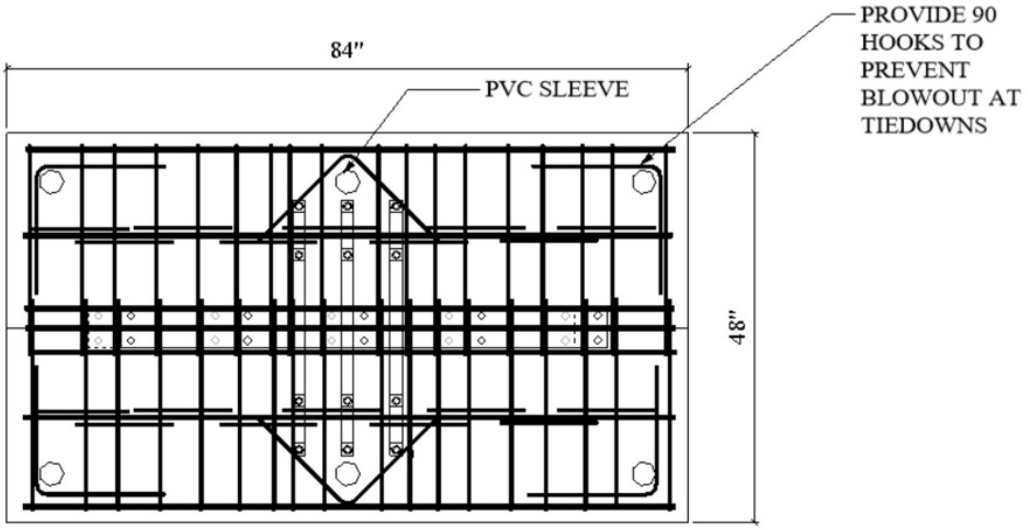

Plan View of Rebar Layout

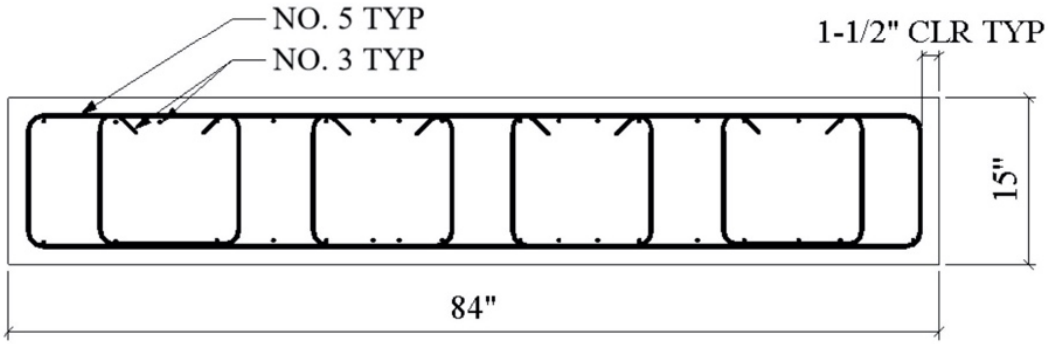

Longitudinal Section of Footing

$b_w := 84\ in$	width of footing
$h := 15\ in$	height of footing
$c := 1.5\ in$	clear cover
$d_s := 0.375\ in$	diameter of shear reinforcement
$d_b := 0.625\ in$	diameter of flexural reinforcement
$d := h - c - d_s - \frac{d_b}{2} = 12.813\ in$	depth to centroid of steel group

Concrete Strength (ACI 318-14 Eqn. 22.5.5.1)

$\lambda := 1.0$

$f'_c := 1879\ psi$ compressive strength of concrete

$V_c := 2 \cdot \lambda \cdot \sqrt{f'_c \cdot \frac{1}{psi}} \cdot psi \cdot b_w \cdot d$ nominal shear strength from concrete

$V_c = 93.3\ kip$

Steel Strength (ACI 318-14 Eqn. 22.5.10.5.3)

$n := 10$ number of legs

$A_v := 0.11\ in^2$ area per single leg of shear reinforcement

$f_y := 60\ ksi$ yield strength of steel reinforcement

$s := 6\ in$ spacing of shear reinforcement

$V_s := \frac{(n \cdot A_v \cdot f_y \cdot d)}{s}$ nominal shear strength from steel

$V_s = 140.9\ kip$

Nominal Shear Strength (ACI 318-14 Eqn. 22.5.1.1)

$V_n := V_c + V_s$

$V_n = 234.2\ kip$ total nominal shear strength

$V_{max} := 10 \cdot \sqrt{f'_c \cdot \frac{1}{psi}} \cdot psi \cdot b_w \cdot d$ limit on shear strength (ACI 318-14 Eqn. 22.5.1.2)

$V_{max} = 466.5\ kip$

$V_{n1} := min(V_n, V_{max}) = 234.2\ kip$

A.5 Flexural Capacity of Footing with All-Thread Bolts

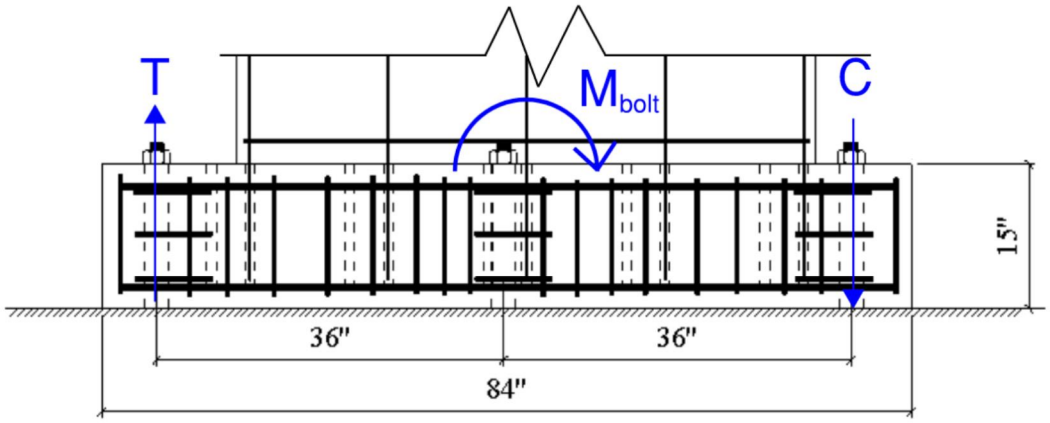

Longitudinal Section of Footing

Assumptions:

1. A36 grade bolts (there is a mix of A36 and A354 Gr. BD threaded rods used)
2. Ignore contribution from middle bolt

Longitudinal Direction

$L := 72\ in$	moment arm
$F_y := 36\ ksi$	yield stress of bolt
$d_b := 1.5\ in$	diameter of bolt
$A_b := \pi \cdot \frac{d_b^{\,2}}{4} = 1.767\ in^2$	area of all-thread bolt
$TC := F_y \cdot A_b = 63.617\ kip$	force couple
$M_{bolt} := TC \cdot L$	flexural capacity of bolt group
$M_{bolt} = 381.7\ kip \cdot ft$	(note this is conservative)

Similarly in the Transverse Direction

$L := 36\ in$	moment arm
$M_{bolt} := TC \cdot L$	flexural capacity of bolt group
$M_{bolt} = 190.9\ kip \cdot ft$	(note this is conservative)

spColumn (TM)

spColumn v6.00
Computer program for the Strength Design of Reinforced Concrete Sections

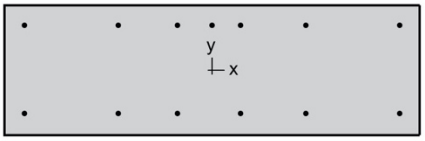

Contents

List of Figures

1. General Information

File Name	untitled.col
Project	---
Column	---
Engineer	---
Code	ACI 318-14
Bar Set	ASTM A615
Units	English
Run Option	Investigation
Run Axis	X - axis
Slenderness	Not Considered
Column Type	Structural

2. Material Properties

2.1. Concrete

Type	Standard	
f'_c	2	ksi
E_c	2549.12	ksi
f_c	1.7	ksi
ε_u	0.003	in/in
β_1	0.85	

2.2. Steel

Type	Standard	
f_y	60	ksi
E_s	29000	ksi
ε_{yt}	0.00206897	in/in

3. Section

3.1. Shape and Properties

Type	Irregular	
A_g	720	in^2
I_x	13500	in^4
I_y	138240	in^4
r_x	4.33013	in
r_y	13.8564	in
X_o	0	in
Y_o	0	in

3.2. Section Figure

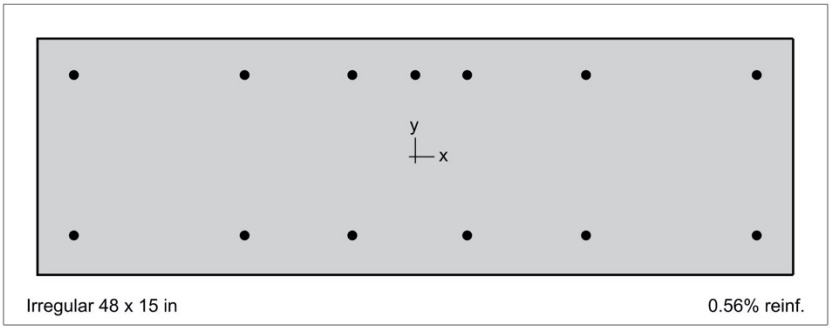

Figure 1: Column section

3.3. Exterior Points

Points	X	Y	Points	X	Y	Points	X	Y
	in	in		in	in		in	in
1	-24.0	-7.5	2	24.0	-7.5	3	24.0	7.5
4	-24.0	7.5						

4. Reinforcement

4.1. Bar Set: ASTM A615

Bar	Diameter	Area	Bar	Diameter	Area	Bar	Diameter	Area
	in	in^2		in	in^2		in	in^2
#3	0.38	0.11	#4	0.50	0.20	#5	0.63	0.31
#6	0.75	0.44	#7	0.88	0.60	#8	1.00	0.79
#9	1.13	1.00	#10	1.27	1.27	#11	1.41	1.56
#14	1.69	2.25	#18	2.26	4.00			

4.2. Confinement and Factors

Confinement type	Other
For #10 bars or less	#3 ties
For larger bars	#4 ties
Capacity Reduction Factors	
Axial compression, (a)	1
Tension controlled ϕ, (b)	1
Compression controlled ϕ, (c)	1

4.3. Arrangement

Pattern	Irregular
Bar layout	---
Cover to	---
Clear cover	---
Bars	---
Total steel area, A_s	4.03 in^2
Rho	0.56 %
Minimum clear spacing	2.67 in

(Note: Rho < 1.0%)

4.4. Bars Provided

Area	X	Y	Area	X	Y	Area	X	Y
in^2	in	in	in^2	in	in	in^2	in	in
0.31	-21.7	5.2	0.31	-10.8	5.2	0.31	0.0	5.2
0.31	10.8	5.2	0.31	21.7	5.2	0.31	-4.0	5.2
0.31	3.3	5.2	0.31	-21.7	-5.0	0.31	-10.8	-5.0
0.31	-4.0	-5.0	0.31	3.3	-5.0	0.31	10.8	-5.0
0.31	21.7	-5.0						

5. Factored Loads and Moments with Corresponding Capacities

No	P_u	M_{ux}	ϕM_{nx}	$\phi M_n/M_u$	NA Depth	d_t Depth	ε_t	ϕ
	kip	k-ft	k-ft		in	in		
1	0.00	1.00	130.44	130.438	2.20	12.50	0.01430	1.000
2	0.00	-1.00	-111.66	111.658	2.01	12.50	0.01562	1.000

spColumn v6.00
Computer program for the Strength Design of Reinforced Concrete Sections

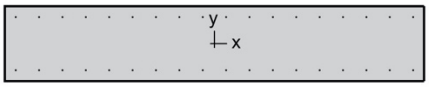

Contents

List of Figures

1. General Information

File Name	H:\THESIS\longitudinal.col
Project	---
Column	---
Engineer	---
Code	ACI 318-14
Bar Set	ASTM A615
Units	English
Run Option	Investigation
Run Axis	X - axis
Slenderness	Not Considered
Column Type	Structural

2. Material Properties

2.1. Concrete

Type	Standard	
f'_c	2	ksi
E_c	2549.12	ksi
f_c	1.7	ksi
ε_u	0.003	in/in
β_1	0.85	

2.2. Steel

Type	Standard	
f_y	60	ksi
E_s	29000	ksi
ε_{yt}	0.00206897	in/in

3. Section

3.1. Shape and Properties

Type	Irregular	
A_g	1260	in^2
I_x	23625	in^4
I_y	740880	in^4
r_x	4.33013	in
r_y	24.2487	in
X_o	0	in
Y_o	0	in

3.2. Section Figure

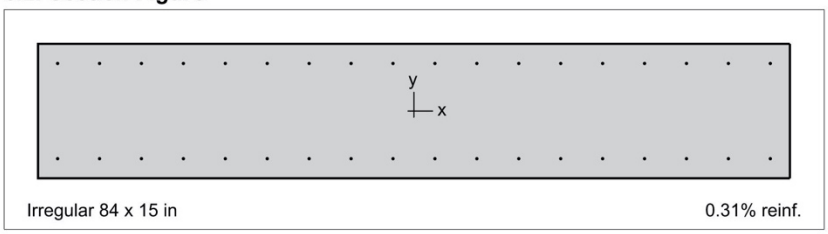

Figure 1: Column section

3.3. Exterior Points

Points	X	Y	Points	X	Y	Points	X	Y
	in	in		in	in		in	in
1	-42.0	-7.5	2	42.0	-7.5	3	42.0	7.5
4	-42.0	7.5						

4. Reinforcement

4.1. Bar Set: ASTM A615

Bar	Diameter	Area	Bar	Diameter	Area	Bar	Diameter	Area
	in	in^2		in	in^2		in	in^2
#3	0.38	0.11	#4	0.50	0.20	#5	0.63	0.31
#6	0.75	0.44	#7	0.88	0.60	#8	1.00	0.79
#9	1.13	1.00	#10	1.27	1.27	#11	1.41	1.56
#14	1.69	2.25	#18	2.26	4.00			

4.2. Confinement and Factors

Confinement type	Other
For #10 bars or less	#3 ties
For larger bars	#4 ties
Capacity Reduction Factors	
Axial compression, (a)	1
Tension controlled ϕ, (b)	1
Compression controlled ϕ, (c)	1

4.3. Arrangement

Pattern	Irregular
Bar layout	---
Cover to	---
Clear cover	---
Bars	---
Total steel area, A_s	3.96 in^2
Rho	0.31 %
Minimum clear spacing	4.31 in

(Note: Rho < 0.50%)

4.4. Bars Provided

Area	X	Y	Area	X	Y	Area	X	Y
in^2	in	in	in^2	in	in	in^2	in	in
0.11	-39.8	5.3	0.11	-35.1	5.3	0.11	-30.4	5.3
0.11	-25.8	5.3	0.11	-21.1	5.3	0.11	-16.4	5.3
0.11	-11.7	5.3	0.11	-7.0	5.3	0.11	-2.3	5.3
0.11	2.3	5.3	0.11	7.0	5.3	0.11	11.7	5.3
0.11	16.4	5.3	0.11	21.1	5.3	0.11	25.8	5.3
0.11	30.4	5.3	0.11	35.1	5.3	0.11	39.8	5.3
0.11	-39.8	-5.3	0.11	-35.1	-5.3	0.11	-30.4	-5.3
0.11	-25.8	-5.3	0.11	-21.1	-5.3	0.11	-16.4	-5.3
0.11	-11.7	-5.3	0.11	-7.0	-5.3	0.11	-2.3	-5.3
0.11	2.3	-5.3	0.11	7.0	-5.3	0.11	11.7	-5.3
0.11	16.4	-5.3	0.11	21.1	-5.3	0.11	25.8	-5.3
0.11	30.4	-5.3	0.11	35.1	-5.3	0.11	39.8	-5.3

5. Factored Loads and Moments with Corresponding Capacities

No	P_u	M_{ux}	ϕM_{nx}	$\phi M_n/M_u$	NA Depth	d_t Depth	ε_t	ϕ
	kip	k-ft	k-ft		in	in		
1	0.00	1.00	129.19	129.193	1.56	12.81	0.02171	1.000
2	0.00	-1.00	-129.19	129.193	1.56	12.81	0.02171	1.000

B. Wall Documentation

B.1 Material Properties

Due to the unexpectedly low strengths derived from the concrete cylinder tests for the footing, a higher strength concrete was specified for the wall than originally planned to avoid the same problem from occurring. As the pour commenced, a 5” slump was measured and recorded. Compared to the slump from the footing pour, this was intentionally specified lower since the previous concrete cylinder tests seemed to have moisture issues. As a precaution, extra cylinders were taken during the pour, including both sizes of cylinders (6x12 and 4x8).

The cylinders were taken at three different times during the pour: at the beginning, in the middle, and at the end. This procedure was utilized to determine if there was significant variance in the concrete strength during the pour. After the pour, half of the cylinders were placed in a moisture bath to cure while the other half were left to cure in the same environment as the wall. This procedure was utilized to determine if there was significant variance in the concrete strength due to curing conditions.

After 41 days, one 6x12 and one 4x8 cylinder were tested in a Test Mark Compression Testing machine. Three days later, four more cylinders were tested. On the test day, 82 days later, the rest of the cylinders were tested. An average compression strength of 3.79 ksi was obtained including outliers. Excluding the lowest compressive strength, the adjusted average was 4.05 ksi.

It should be noted that all the cylinders taken at the beginning of the concrete pour had significantly lower compressive strengths than those taken later in the pour. One reason for this discrepancy could be due to extra water added to the initial concrete (to ensure proper flow of concrete and to initialize the pump). The extent of this lower concrete strength is unknown except that it increased throughout the pour, reaching compressive strengths of 6ksi once the midpoint of the wall had been reached. Each cylinder failure mode was categorized according to ASTM C39/39M-18 as shown below.

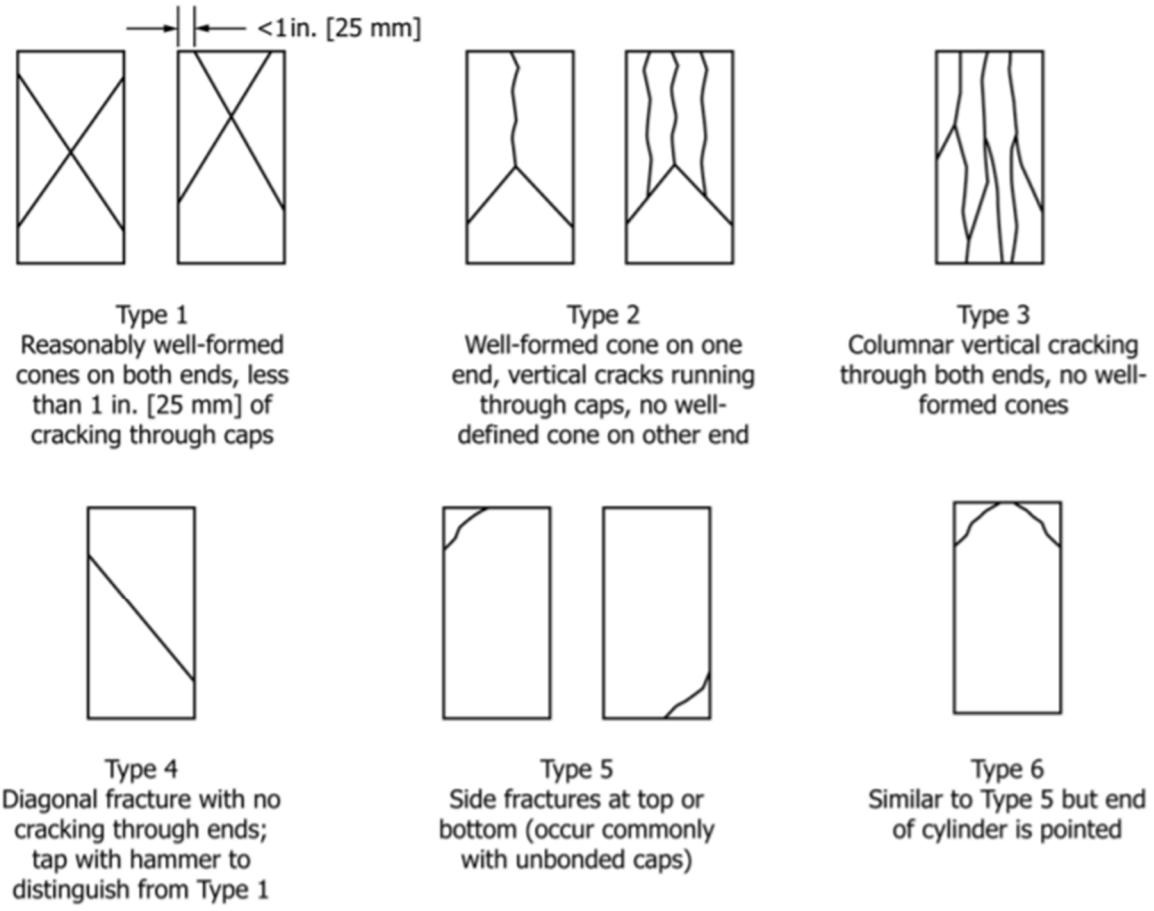

Figure B-1: Failure modes of concrete cylinders. Figure adapted from ASTM C39/C39M-18

Table B-1: Summary of Concrete Cylinder Tests for Wall Specimen

Cylinder Parameter	**1**	**2**	**3**	**4**	**5**	**6**	**7**	**8**	**9**
Curing Environment	By Wall	By Wall	Bath	Bath	Bath	By Wall	By Wall	Bath	Bath
Pour Sequence	Bottom	Bottom	Bottom	Bottom	Bottom	Bottom	Middle	Top	Middle
Date Tested	4/18	4/18	4/21	4/21	4/21	4/21	5/29	5/29	5/29
Cylinder Size	6x12	4x8	6x12	4x8	4x8	4x8	4x8	4x8	6x12
Max Comp. Force (kips)	79.03	23.87	77.64	34.37	27.10	21.81	75.90	89.40	194.98
Comp. Strength, f'_c (ksi)	2.80	1.90	2.75	2.74	2.16	1.74	6.04	7.11	6.90
Failure Type	4	5	2	3	5	5	3	5	5

B.2 Nominal Capacities of Wall

spColumn v6.00
Computer program for the Strength Design of Reinforced Concrete Sections

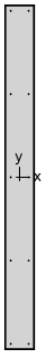

Contents

List of Figures

1. General Information

File Name	untitled.col
Project	---
Column	---
Engineer	---
Code	ACI 318-14
Bar Set	ASTM A615
Units	English
Run Option	Investigation
Run Axis	X - axis
Slenderness	Not Considered
Column Type	Structural

2. Material Properties

2.1. Concrete

Type	Standard	
f'_c	3.791	ksi
E_c	3509.56	ksi
f_c	3.22235	ksi
ε_u	0.003	in/in
β_1	0.85	

2.2. Steel

Type	Standard	
f_y	54.8	ksi
E_s	29000	ksi
ε_{yt}	0.00188966	in/in

3. Section

3.1. Shape and Properties

Type	Irregular	
A_g	300	in^2
I_x	90000	in^4
I_y	625	in^4
r_x	17.3205	in
r_y	1.44338	in
X_o	0	in
Y_o	0	in

3.2. Section Figure

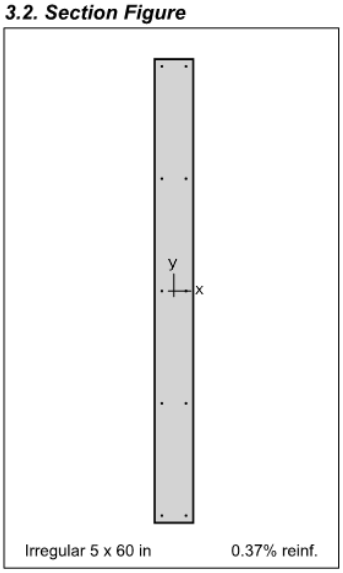

Figure 1: Column section

3.3. Exterior Points

Points	X	Y	Points	X	Y	Points	X	Y
	in	in		in	in		in	in
1	-2.5	-30.0	2	2.5	-30.0	3	2.5	30.0
4	-2.5	30.0						

4. Reinforcement

4.1. Bar Set: ASTM A615

Bar	Diameter	Area	Bar	Diameter	Area	Bar	Diameter	Area
	in	in²		in	in²		in	in²
#3	0.38	0.11	#4	0.50	0.20	#5	0.63	0.31
#6	0.75	0.44	#7	0.88	0.60	#8	1.00	0.79
#9	1.13	1.00	#10	1.27	1.27	#11	1.41	1.56
#14	1.69	2.25	#18	2.26	4.00			

4.2. Confinement and Factors

Confinement type	Other
For #10 bars or less	#3 ties
For larger bars	#4 ties
Capacity Reduction Factors	
Axial compression, (a)	1
Tension controlled ϕ, (b)	1
Compression controlled ϕ, (c)	1

4.3. Arrangement

Pattern	Irregular
Bar layout	---
Cover to	---
Clear cover	---
Bars	---
Total steel area, A_s	1.10 in^2
Rho	0.37 %
Minimum clear spacing	2.75 in

(Note: Rho < 0.50%)

4.4. Bars Provided

Area	X	Y	Area	X	Y	Area	X	Y
in^2	in	in	in^2	in	in	in^2	in	in
0.11	-1.6	-29.1	0.11	-1.6	-14.5	0.11	-1.6	0.0
0.11	-1.6	14.5	0.11	-1.6	29.1	0.11	1.6	-29.1
0.11	1.6	-14.5	0.11	1.6	0.0	0.11	1.6	14.5
0.11	1.6	29.1						

5. Axial Loads and Moments with Corresponding Capacities

No	ϕP_n	ϕM_{nx}	NA Depth	d_t Depth	ε_t	ϕ
	kip	k-ft	in	in		
1	35.0	222.95	5.246	59.063	0.03077	1.000
2	35.0	-222.95	5.246	59.063	0.03077	1.000

C. Existing Conditions

The existing conditions of the College of Architectural & Environmental Design (CAED) High Bay laboratory on Cal Poly's campus affected the design and orientation of the footing and wall specimen. This section discusses the existing strong floor and reaction frame as they relate to this project.

C.1 Strong Floor

The reinforced concrete strong floor in the High Bay laboratory provided a fixed connection for the base of the concrete footing in this project. The strong floor consists of all-thread anchors that are embedded at three feet on center, each way. Figure C-1 shows a dimensioned detail of the existing connection at each all-thread anchor.

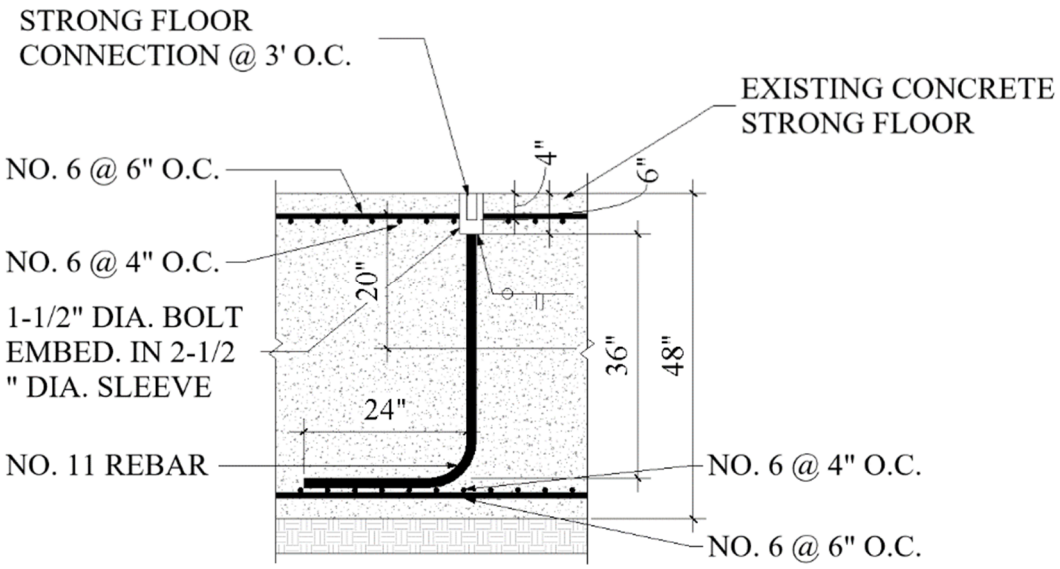

Figure C-1: Detail of Existing Connection to Strong Floor

C.2 Reaction Frame

For lateral support during testing, the High Bay's reaction frame was upgraded and utilized. Before testing, the reaction frame required stiffening to prevent inaccuracies in testing and data acquisition. The upgraded reaction frame is shown in Figure C-2.

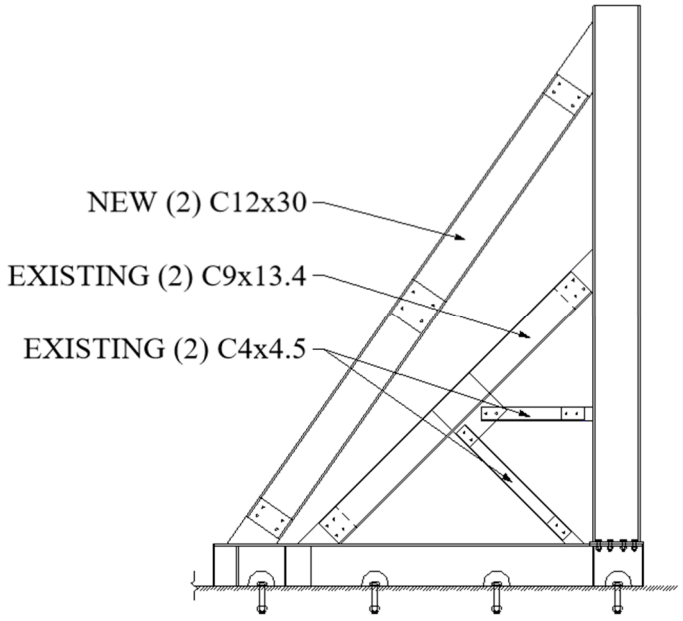

Figure C-2: Upgraded Reaction Frame in the High Bay Laboratory.

D. Wall Construction and Instrumentation

D.1 Wall Construction Details

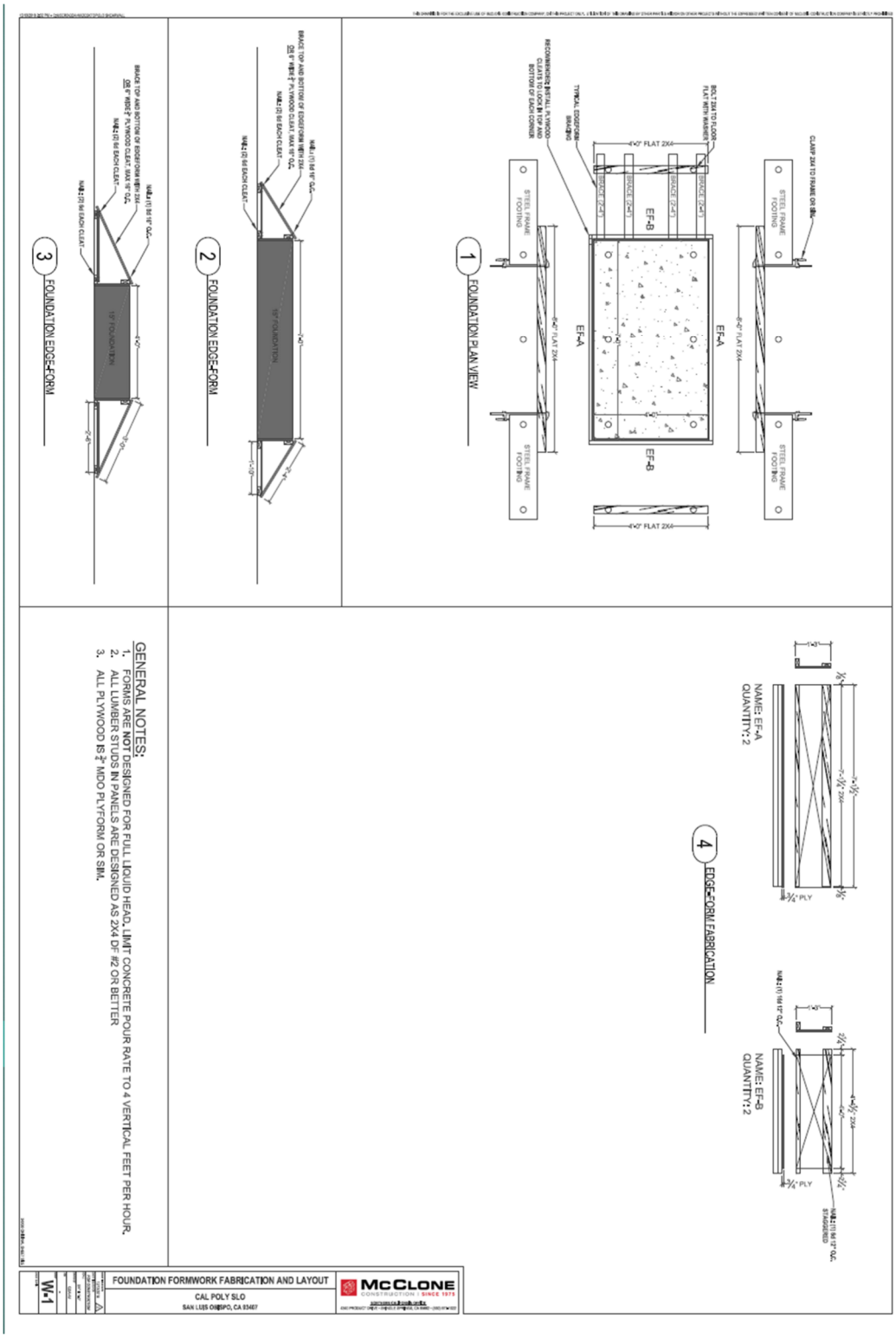

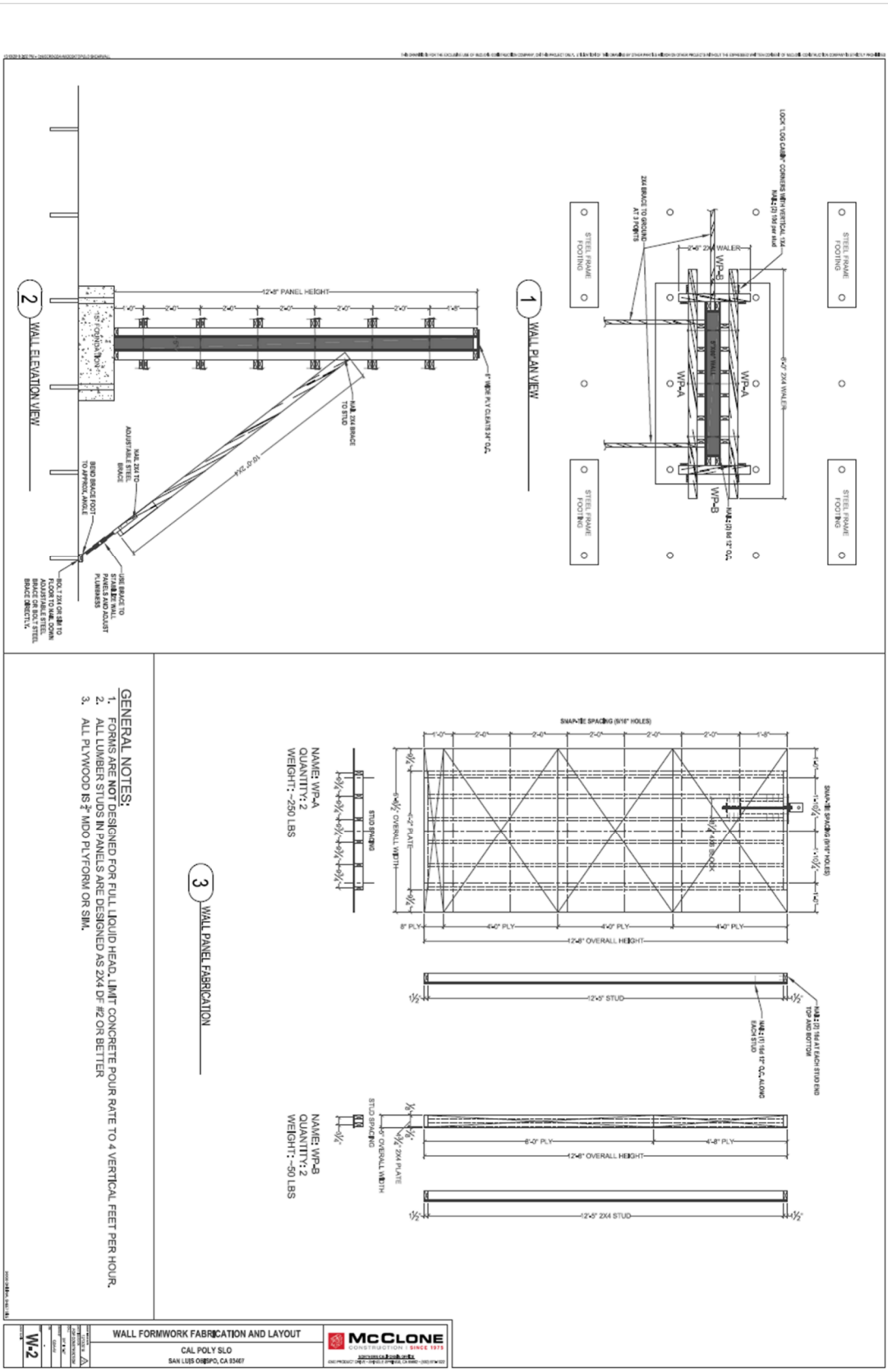
1 WALL PLAN VIEW
STEEL FRAME FOOTING
2X4 BRACE TO GROUND AT 4'-0" PORTS
2'-6" 2X4 WALER
WP-B
WP-A
4'-0" 2X4 WALER
2 WALL ELEVATION VIEW
12'-8" PANEL HEIGHT
2'-0" FOOTING TYP.
3 WALL PANEL FABRICATION
SNAP-TIE SPACING (5/16" HOLES)
NAME: WP-A
QUANTITY: 2
WEIGHT: ~250 LBS
8' PLY
4'-0" PLY
12'-8" OVERALL HEIGHT
12'-5" STUD
NAME: WP-B
QUANTITY: 2
WEIGHT: ~50 LBS
8'-0" PLY
4'-8" PLY
12'-5" 2X4 STUD
GENERAL NOTES:
1. FORMS ARE NOT DESIGNED FOR FULL LIQUID HEAD, LIMIT CONCRETE POUR RATE TO 4 VERTICAL FEET PER HOUR.
2. ALL LUMBER STUDS IN PANELS ARE DESIGNED AS 2X4 DF #2 OR BETTER
3. ALL PLYWOOD IS ¾" MDO PLYFORM OR SIM.
W-2
WALL FORMWORK FABRICATION AND LAYOUT
CAL POLY SLO
SAN LUIS OBISPO, CA 93407
McCLONE
CONSTRUCTION | SINCE 1975

D.2 Instrumentation and Calibrations

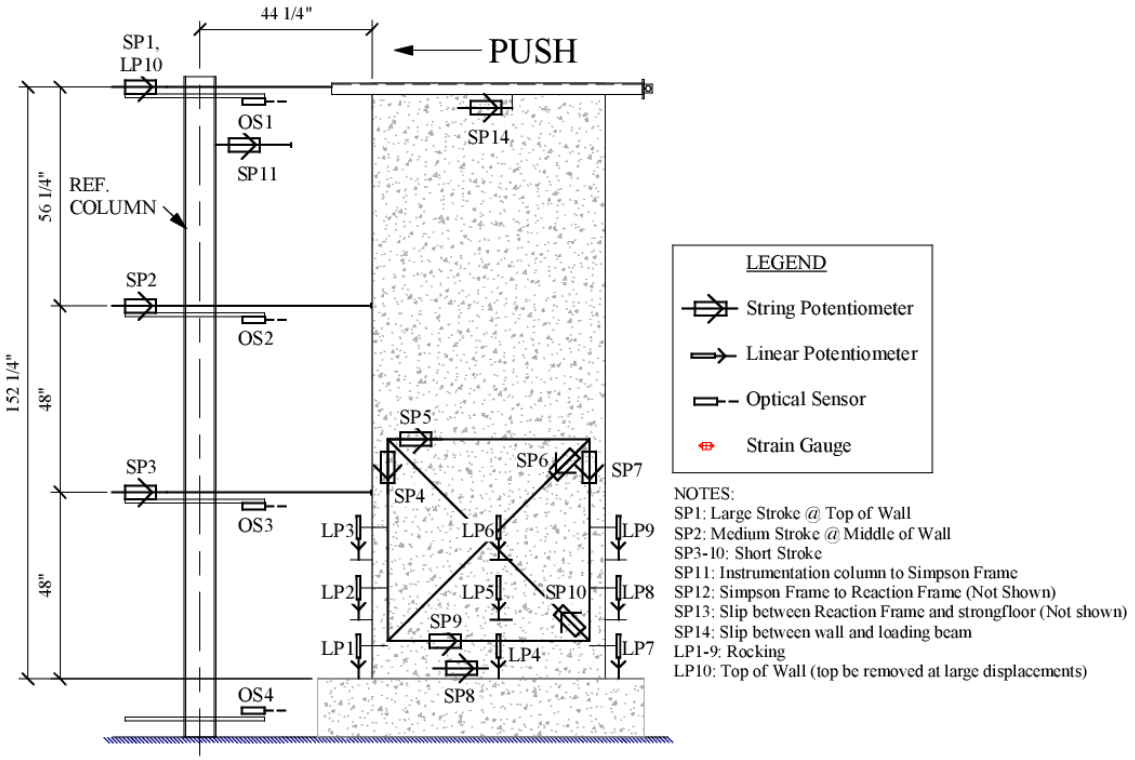

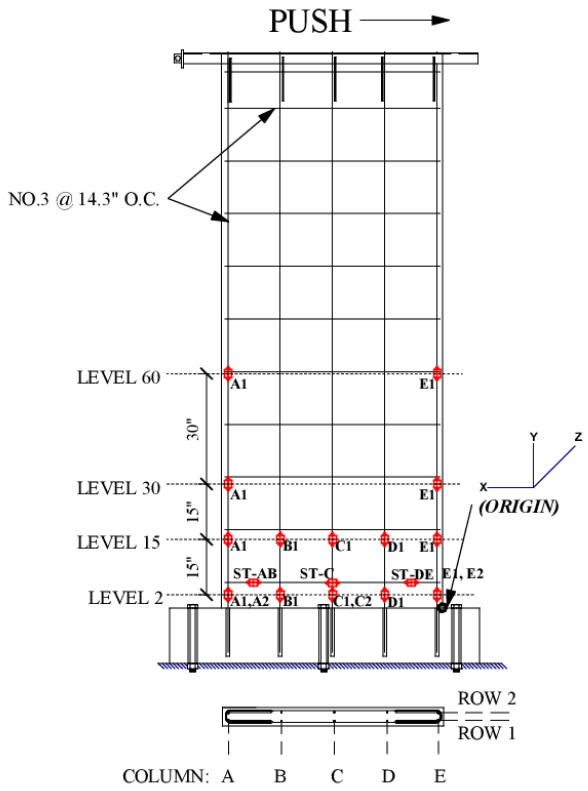

NOTES:

Strain Gages Used: 20/24

Gage Nomenclature:

SG( )( )-( )

LEVEL
ROW
COLUMN

Level 2 Gages:	(X,	Y,	Z
SGA1-2	(56,	2,	-3.5)
SGA2-2	(56,	2,	0)
SGB1-2	(45,	2,	0)
SGC1-2	(29.5,	2,	0)
SGC2-2	(29.5,	2,	-3.5)
SGD1-2	(15,	2,	0)
SGE1-2	(4,	2,	0)
SGE2-2	(4,	2,	-3.5)
ST-AB	(50,	7,	0)
ST-C	(30,	7,	0)
ST-DE	(10,	7,	0)
Level 15 Gages:			
SGA1-15	(56,	17,	0)
SGB1-15	(45,	17,	0)
SGC1-15	(29.5,	17,	0)
SGD1-15	(15	17,	0)
SGE1-15	(4,	17,	0)
Level 30 Gages:			
SGA1-30	(56,	32,	0)
SGE1-30	(4,	32,	0)
Level 60 Gages:			
SGA1-60	(56,	62,	0)
SGE1-60	(4,	62,	0)

% Quick Label	Instrument Type	Front or Back	Level	Gauge/ Calib Factor	X Location (Start)	Y Location (Start)	Z Location (Start)	X Location (End)	Y Location (End)	Z Location (End)	Manufacture	Model No.	Serial No.
% Strain Gages													
SGA1-2	SG	Front	Lvl2	2.125	56	2	-3.5	-	-	-	MicroMeasurements/Vishay	C2A-06-250LW-120	-
SGC2-2	SG	Back	Lvl2	2.125	29.5	2	-1.5	-	-	-	MicroMeasurements/Vishay	C2A-06-250LW-120	-
SGA2-2	SG	Back	Lvl2	2.125	56	2	-1.5	-	-	-	MicroMeasurements/Vishay	C2A-06-250LW-120	-
SGD1-2	SG	Front	Lvl2	2.125	15	2	-3.5	-	-	-	MicroMeasurements/Vishay	C2A-06-250LW-120	-
SGB1-2	SG	Front	Lvl2	2.125	45	2	-3.5	-	-	-	MicroMeasurements/Vishay	C2A-06-250LW-120	-
SGE1-2	SG	Front	Lvl2	2.125	4	2	-3.5	-	-	-	MicroMeasurements/Vishay	C2A-06-250LW-120	-
SGC1-2	SG	Front	Lvl2	2.125	29.5	2	-3.5	-	-	-	MicroMeasurements/Vishay	C2A-06-250LW-120	-
SGE2-2	SG	Back	Lvl2	2.125	4	2	-1.5	-	-	-	MicroMeasurements/Vishay	C2A-06-250LW-120	-
ST-AB	SGH	Front	Lvl2	2.125	50	7	-1.5	-	-	-	MicroMeasurements/Vishay	C2A-06-250LW-120	-
SGB1-15	SG	Front	Lvl15	2.125	45	17	-3.5	-	-	-	MicroMeasurements/Vishay	C2A-06-250LW-120	-
ST-C	SGH	Front	Lvl2	2.125	30	7	-1.5	-	-	-	MicroMeasurements/Vishay	C2A-06-250LW-120	-
SGC1-15	SG	Front	Lvl15	2.125	29.5	17	-3.5	-	-	-	MicroMeasurements/Vishay	C2A-06-250LW-120	-
ST-DE	SGH	Front	Lvl2	2.125	10	7	-1.5	-	-	-	MicroMeasurements/Vishay	C2A-06-250LW-120	-
SGD1-15	SG	Front	Lvl15	2.125	15	17	-3.5	-	-	-	MicroMeasurements/Vishay	C2A-06-250LW-120	-
SGA1-15	SG	Front	Lvl15	2.125	56	17	-3.5	-	-	-	MicroMeasurements/Vishay	C2A-06-250LW-120	-
SGE1-15	SG	Front	Lvl15	2.125	4	17	-3.5	-	-	-	MicroMeasurements/Vishay	C2A-06-250LW-120	-
SGA1-30	SG	Front	Lvl30	2.125	56	32	-3.5	-	-	-	MicroMeasurements/Vishay	C2A-06-250LW-120	-
SGE1-30	SG	Front	Lvl30	2.125	4	32	-3.5	-	-	-	MicroMeasurements/Vishay	C2A-06-250LW-120	-
SGA1-60	SG	Front	Lvl60	2.125	56	62	-3.5	-	-	-	MicroMeasurements/Vishay	C2A-06-250LW-120	-
SGE1-60	SG	Front	Lvl60	2.125	4	62	-3.5	-	-	-	MicroMeasurements/Vishay	C2A-06-250LW-120	-
% String Potentiometers													
SP1	SP		Top	-11.299	-36	147.5	-2.5	0	147.5	-2.5	-	P-20B	9712--4479
SP2	SP		Mid	-1.152	-36	95.5	-2.5	0	95.5	-2.5	-	1850-10	4131-003
SP3	SP		Bottom	-0.571	-36	47.375	-2.5	0	47.375	-2.5	-	PT101-0005-111-4110	G0959642
SP4	SP		Bottom	-0.578	6	55.5	0	6	7.5	0	-	PT101-0005-111-4110	G0959632
SP5	SP		Bottom	-0.579	6	55.5	0	54	55.5	0	-	PT101-0005-111-4110	G0959634
SP6	SP		Bottom	-0.574	54	55.5	0	6	7.5	0	-	PT101-0005-111-4110	G0959635
SP7	SP		Bottom	-0.572	54	55.5	0	54	7.5	0	-	PT101-0005-111-4110	G0959625
SP8	SP		Bottom	-0.573	11	2	0	19.5	2	0	-	PT101-0005-111-4110	G0959640
SP9	SP		Bottom	-0.338	6	7.5	0	54	7.5	0	-	173-0241-L1N	021858S05344
SP10	SP		Bottom	-0.334	54	7.5	0	6	55.5	0	-	173-0241-L1N	10195
SP11	SP		Top	-2.282	-36	142	-2.5	-30	142	-2.5	-	1850-020B	131586-002
SP12	SP		Top	-6.158	127	142	-2.5	80	142	-2.5	-	P-10B	9902-8090
SP13	SP		Ground	-2.325	134	-13	-2.5	143	-13	-2.5	-	N/A	N/A
SP14	SP		Top	-0.583	19	149.5	0	23	149.5	0	-	PT101-0005-111-4110	G059641

% Quick Label	Instrument Type	Front or Back	Level	Gauge/ Calib Factor	X Location (Start)	Y Location (Start)	Z Location (Start)	X Location (End)	Y Location (End)	Z Location (End)	Manufacture	Model No.	Serial No.
% Linear Potentiometers													
LP1	LP	-	Bottom	0.163	3	0	0	3	4.125	0	-	N/A	N/A
LP2	LP	-	Bottom	0.167	3	5.125	0	3	7.875	0	-	N/A	N/A
LP3	LP	-	Bottom	0.174	3	9.125	0	3	11.875	0	-	N/A	N/A
LP4	LP	-	Bottom	0.169	30	0	0	30	3.625	0	-	N/A	N/A
LP5	LP	-	Bottom	0.165	30	4.875	0	30	7.875	0	-	N/A	N/A
LP6	LP	-	Bottom	0.165	30	8.875	0	30	12.125	0	-	N/A	N/A
LP7	LP	-	Bottom	0.171	57	0	0	57	4.375	0	-	N/A	N/A
LP8	LP	-	Bottom	0.167	57	5	0	57	8.25	0	-	N/A	N/A
LP9	LP	-	Bottom	0.166	57	8.625	0	57	11.625	0	-	N/A	N/A
LP10	LP	-	Top	-0.562	-3.75	153	-2.5	-8.75	153	-2.5	-	N/A	N/A
% Optical Sensors													
OS1	OS	-	Top	-0.702	-7	151.5	-2.5	0	151.5	-2.5	-	Q50BEU	N/A
OS2	OS	-	Mid	-0.787	-5	95.5	-2.5	0	95.5	-2.5	-	Q50BEU	N/A
OS3	OS	-	Bottom	-0.946	-7	47.375	-2.5	0	47.375	-2.5	-	Q50BEU	N/A
OS4	OS	-	Ground	-0.548	-21.5	-3.5	-2.5	-14.5	-3.5	-2.5	-	Q50BEU	N/A

Box	Input	Channel	Name	Calib. Factor	Modified C. Factor	Direction Positive	X (Start)	Y (Start)	X (End)	Y (End)	Description	Comments
1	1	1	SP1	11.2994	-11.2994	0	-36	147.5	0	147.5	Top Drift	
1	2	2	SP2	1.1521	-1.1521	0	-36	95.5	0	95.5	Mid Drift	0.5% error
1	3	3	SP3	0.5706	-0.5706	0	-36	47.375	0	47.375	Bott Drift	backwards, starts at -5 inches (OK - switched box)
1	4	4	SP4	0.5782	-0.5782	-90	6	55.5	6	7.5	Top Left Shear (Looking Down)	0.6% error
1	5	5	SP5	0.5786	-0.5786	0	6	55.5	54	55.5	Top Left Shear (Looking Right)	3.6% error
1	6	6	SP6	0.5742	-0.5742	-135	54	55.5	6	7.5	Top Right Shear (Looking Down/Left)	1% error
1	7	7	SP7	0.5720	-0.5720	-90	54	55.5	54	7.5	Top Right Shear (Looking Down)	coupled with 8 if 8 is null. 0.1% error but bottom is finicky (OK)
1	8	8	SP8	0.5727	-0.5727	0	11	2	19.5	2	Wall/Footing Slip	1% error
1	9	9	SP9	0.3379	-0.3379	0	6	7.5	54	7.5	Bottom Left Shear (Looking Right)	2.5% error
1	10	10	SP10	0.3344	-0.3344	135	54	7.5	6	55.5	Bottom Right Shear (Looking Up/Left)	0.07%
1	11	11	LP1	0.1633	0.1633	90	3	0	3	4.125	Left/Bottom	offset -0.05 inches every time, even calibrated twice same problem
1	12	12	LP2	0.1668	0.1668	90	3	5.125	3	7.875	Left/Middle	1% error
4	13	13	OS1	-0.7020	-0.7020	180	-7	151.5	0	151.5	Top Drift	
4	14	14	OS2	-0.7871	-0.7871	180	-5	95.5	0	95.5	Mid Drift	
4	15	15	OS3	-0.9460	-0.9460	180	-7	47.375	0	47.375	Bott Drift	
4	16	16	OS4	-0.5478	-0.5478	180	-21.5	-3.5	-14.5	-3.5	Footing Slip	
2	1	17	LP3	0.1738	0.1738	90	3	9.125	3	11.875	Left/Top	3% error
2	2	18	LP4	0.1692	0.1692	90	30	0	30	3.625	Mid/Bottom	within 1% error
2	3	19	LP5	0.1655	0.1655	90	30	4.875	30	7.875	Mid/Mid	5.5% error, Offest by 0.04 volts
2	4	20	LP6	0.1653	0.1653	90	30	8.875	30	12.125	Mid/Top	4% error
2	5	21	LP7	0.1711	0.1711	90	57	0	57	4.375	Right/Bottom	
2	6	22	LP8	0.1674	0.1674	90	57	5	57	8.25	Right/Mid	1.5% error
3	1	23	LP9	0.1660	0.1660	90	57	8.625	57	11.625	Right/Top	within 1% error
3	2	24	LP10	-0.5620	-0.5620	180	-3.75	153	-8.75	153	Top Drift (Fine)	
3	3	25	SP11	2.2815	-2.2815	0	-36	142	-30	142	Instru. Column TO Simpson	
3	4	26	SP12	6.1576	-6.1576	180	127	142	80	142	Simpson TO Reaction Frame	
3	5	27	SP13	2.3250	-2.3250	0	134	-13	143	-13	Reaction Frame/Floor Slip	
3	6	28	SP14	0.5831	-0.5831	0	19	149.5	23	149.5	Loading Beam/Wall Slip	

E. Literature Review of FRP Tests on Walls and Columns for Ductility Improvements

The wall specimen R1 tested in this report was designed to model the cyclic behavior of slender pre-1980's lightly reinforced concrete (LRC) shear walls which are believed to display non-ductile failure modes during large earthquakes. Although understanding the LRC failure mode was the primary objective of this report, the secondary objective focused on how to retrofit such walls. A fiber reinforced polymer (FRP) retrofit scheme with FRP wrapped wall endzones and splay anchors was preliminarily proposed and investigated by performing a literature review on the previous use of FRP to retrofit columns and walls.

The following section contains literature review of FRP retrofit schemes to improve deficient wall behavior, a review of current practice modeling techniques used to analyze concrete shear walls, and a review of other retrofit methods applicable to concrete shear walls. The following is an overview of the observations made:

1. The use of FRP to retrofit reinforced concrete columns is widely accepted and successful for increasing the seismic performance of deficient columns.
2. The use of FRP and steel rods to retrofit reinforced concrete walls has developed recently but is not fully investigated regarding improving displacement ductility without also improving strength.
3. The method used to model walls is important in capturing the nonlinear effects of RC shear walls.
4. FRP retrofit schemes have worked well for in-field applications on deficient existing buildings, especially when combined with experimental testing to calibrate analysis models.
5. Selective weakening methods for RC shear walls, such as targeted saw cutting, can control the inelastic failure mechanism.

E.1 Testing of Reinforced Concrete Columns Using FRP

This section provides an overview of experimental tests on concrete columns with FRP retrofit schemes. The parameters of interest are like those for lightly reinforced walls. The purpose of this section is to confirm the effectiveness of using FRP as a ductility enhancing agent.

E.1.1 Sheikh & Yau (2002)

This paper reports the results from an experimental program which involved cyclic testing on 12 circular concrete columns. The researchers were interested in using FRP to improve the seismic performance of deficient columns to match or exceed columns designed with the provisions of the 1999 ACI-318 Code. Both glass and carbon fiber products were used and shown to enhance the strength, ductility, and energy absorption capacity of the tested columns.

Per the structure of the test program, the 12 columns were divided into three groups: the first group, Series S, acted as a control and consisted of four conventionally reinforced concrete (RC) columns utilizing longitudinal and spiral steel; the second group, Series ST, consisted of six RC columns that were strengthened with FRP; the third group, Series R, consisted of two RC columns that were intentionally damaged and subsequently repaired with FRP. Figure E-1(a) shows the rebar layout and dimensions of each specimen. The design of the specimens was meant to force the failure into the potential plastic hinge region near the face of the footing.

For ease of testing, the experiment setup was designed horizontally as shown in Figure E-1(b). A constant axial load was applied by a hydraulic jack under the column footing, and a cyclic lateral load was applied by an actuator running vertically. The loading protocol was displacement controlled for the entire test, incremented in proportions of a deflection corresponding to the initial stiffness of the specimens. Each specimen had 18 strain gauges installed on the longitudinal reinforcement, 18 LVDT’s to measure core deformations, and six LVDT’s to measure transverse deformations.

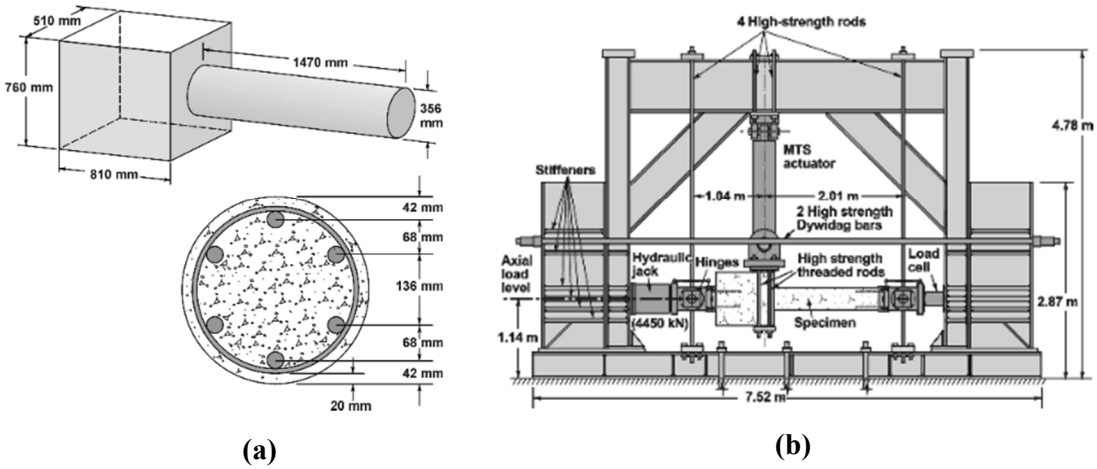

Figure E-1: Specimen dimensions and test setup
Left (a) Specimen Rebar Layout and Dimensions. Right (b) Cyclic loading test setup for each specimen, Sheikh and Yau (2002).

Most of the test data was compiled into moment-curvature plots for each specimen with labels indicating key observations made during testing (see Figure E-2 for two specimens). The researchers analyzed the data by comparing column ductility parameters, axial load levels, spiral reinforcement spacing/ area, and FRP effectiveness. In general, column ductility was decreased as axial load was added and increased as spiral reinforcement pitches were made tighter. Moreover, the FRP was effective at increasing the energy absorption capacity of the columns by several orders of magnitude. The researchers note how the FRP confines the entire column compared to the spirals which only confine the core.

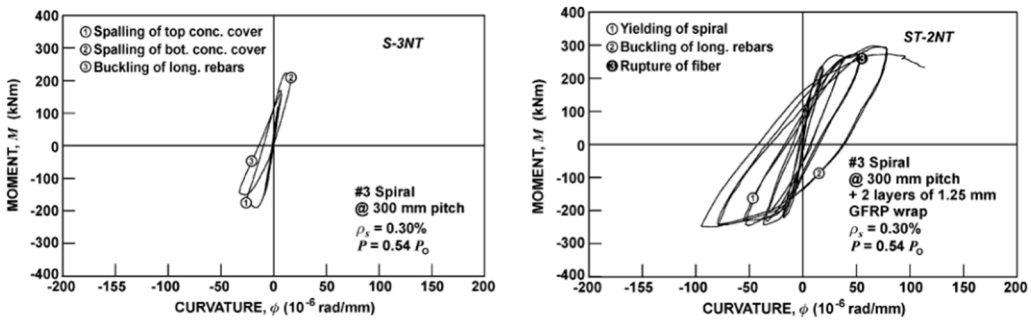

Figure E-2: Moment versus curvature plots for test specimens S-3NT and ST-2NT, Sheikh and Yau (2002).

E.1.2 Iacobucci et al. (2003)

This paper reports the results from an experimental program which involved cyclic testing on eight square concrete columns. The researchers were interested in using CFRP (carbon fiber reinforced polymer) to improve the seismic performance of deficient columns. The results showed that appropriately utilized carbon fiber products enhance the strength, ductility, and energy absorption capacity of columns and can exceed the performance of comparable columns with adequate seismic lateral reinforcement.

The test program consisted of eight columns with varying transverse steel configurations, axial loads, and layers of FRP. Each specimen had a rectangular foundation to represent a footing or frame joint. The rebar layouts were based on typical pre-1971 column details. Like Sheikh et. al., the specimens were tested in a horizontal orientation and utilized the equipment shown in Figure E-3(b). The loading protocol was displacement controlled for the entire test, incremented in proportions of a deflection corresponding to the initial stiffness of the specimens. Each specimen had 20 strain gauges installed on the longitudinal reinforcement, 18 LVDT's to measure core deformations, six LVDT's to measure transverse deformations, and eight surface strain gauges oriented in the direction of the fibers to measure strains in the CFRP where applicable.

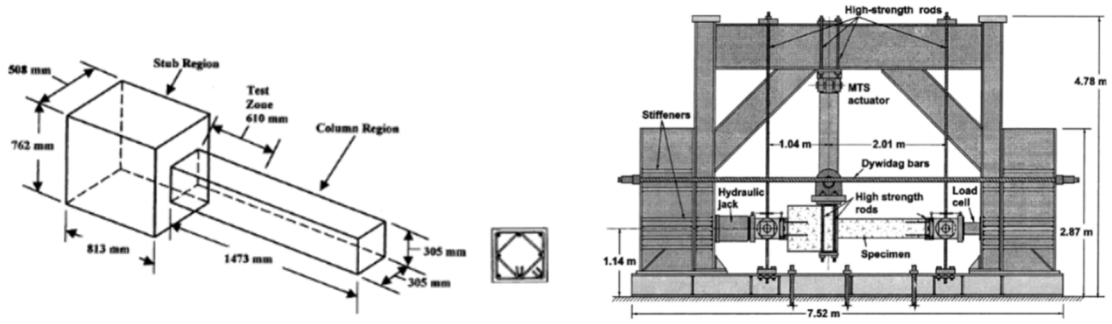

Figure E-3: Specimen dimensions and test setup
Left (a) Specimen Dimensions and Cross Section Rebar Layout. Right (b) Test Setup, Iacobucci et. al. (2003)

Most of the test data was compiled into moment-curvature plots for each specimen with labels indicating key observations made during testing (see Figure E-4 for two specimens). The researchers analyzed the data by comparing column ductility parameters, axial load levels, number of CFRP layers

used, and FRP effectiveness. In general, column ductility was decreased as axial load was added and increased as more layers of CFRP were used. Moreover, the CFRP confined the critical sections effectively enough to completely eliminate the need for additional steel ties to provide confinement. The CFRP was also successful at improving the cyclic response of previously damaged specimens.

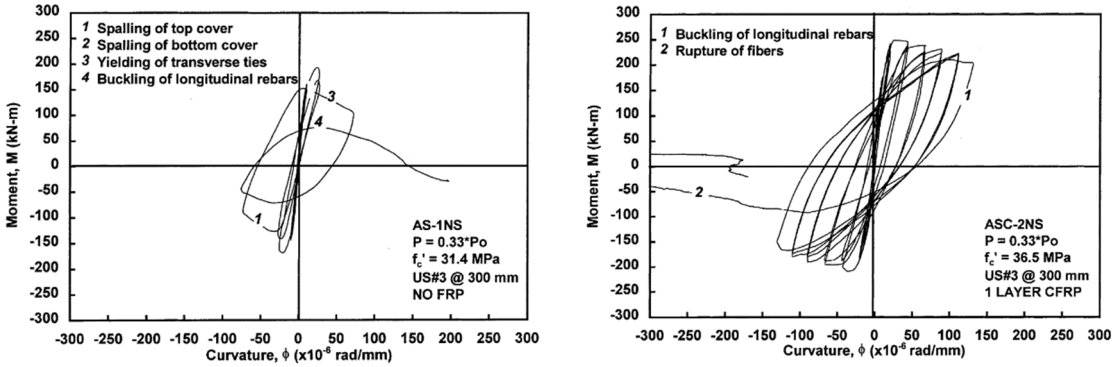

Figure E-4: Moment versus curvature plots for test specimens AS-1NS and ASC-2NS, Iacobucci et. al. (2003).

E.1.3 Endeshaw et al. (2008)

This paper investigates retrofit concepts to improve the seismic behavior of deficient rectangular concrete bridge columns. A total of eight columns designed at 40% scale and representative of Washington State's deficient interstate column inventory were tested via reverse-cyclic lateral loading under constant axial load. Failure mode, displacement ductility, and hysteretic behavior were the parameters of interest for each specimen. Columns retrofitted with steel jackets and CFRP wrapping both performed similarly, producing satisfactorily ductile response with failure due to flexural hinging and low-cycle fatigue fracture of the longitudinal reinforcement.

The column specimens were split into three distinct groups. The first group of two were un-retrofitted control specimens meant to establish the as-built behavior of the deficient columns, incorporating lap slices at the base of the columns and sparse transverse reinforcement. The second group of five columns were retrofitted with the CFRP composite wrapping. The third group of one was retrofitted with a steel jacket. The researchers note the FRP wrapping has several advantages over steel and concrete wrapping,

including low weight-to-strength ratios, high elastic moduli, resistance to corrosion, ease of application, and little stiffness amplification.

Endeshaw et. al. gives detailed guidelines for FRP application and design equations based on ACI 440-02 and the Advanced Composites Technology Transfer Consortium Report No. ACTT-95/08. Oval-shaped FRP jackets are recommended over rectangular shaped jackets when possible and are required if controlled debonding at the longitudinal reinforcing lap splice is not permissible. CFRP is also compared to other FRP products including AFRP and GFRP. Regarding modulus of elasticity, tensile strength, and weather durability, the CFRP outperforms the other options, except on cost.

The rebar layout and dimensions of the column specimens are shown in Figure E-5 below. The footings were overdesigned to force failure into the column plastic hinge region. The testing setup is shown in Figure E-6 below. A constant axial load was applied throughout the testing with lateral load delivered using a horizontally aligned actuator in a quasi-static manner under a displacement-controlled loading

protocol. Each load step consisted of three cycles at a proportion of the calculated theoretical yield displacement, and failure was defined as a 20% decrease in peak lateral load.

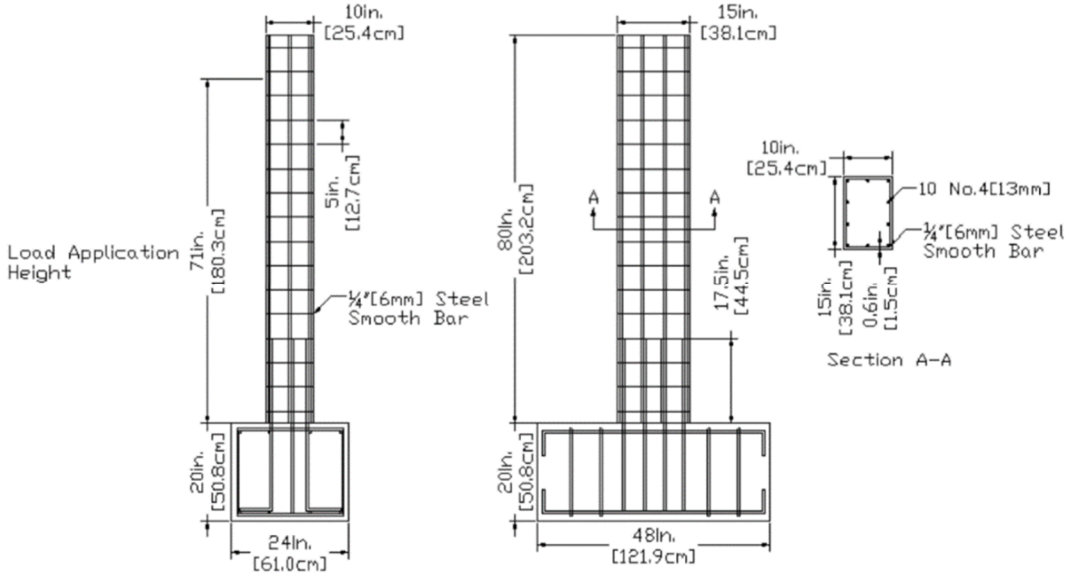

Figure E-5: Specimen Rebar Layout, Endeshaw et. al, (2008).

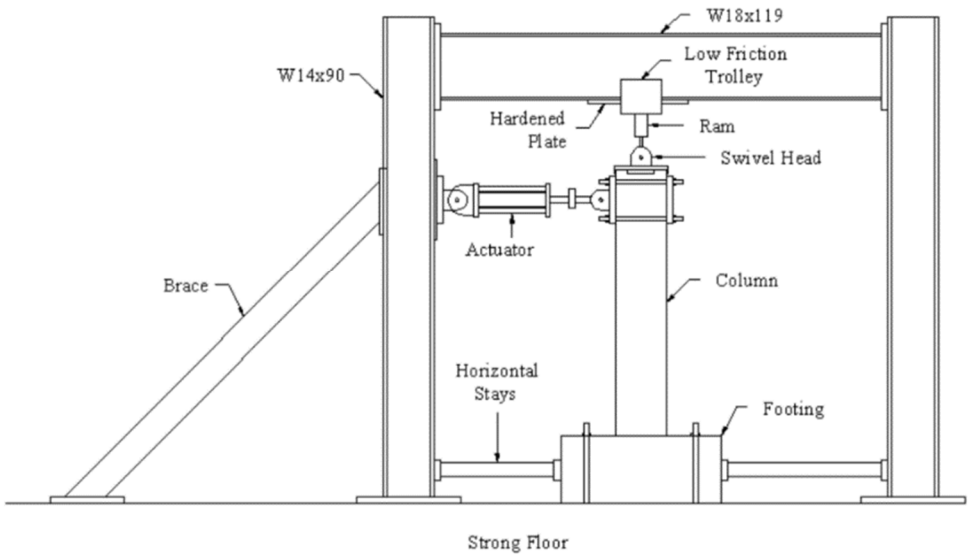

Figure E-6: Test setup for cyclic loading of concrete column, Endeshaw et. al, (2008).

The remainder of this section will focus on two specimens, AB-1 and FRP-4 for comparison reasons. Specimen AB-1 was an un-retrofitted control column and performed better than expected with a reasonable displacement ductility of 6.4. The researchers attribute this unexpected behavior to the relatively long lap

slice used (35 bar diameters), a low axial load level of 7%, and a low longitudinal reinforcement ratio of 1.2%. This column failed due to buckling of longitudinal rebar and subsequent low-cycle rebar fracture. Specimen FRP-4 was the retrofitted version of AB-1 with four layers of unidirectional CFRP impregnated with laminating resin. FRP-4 had a displacement ductility of 7.4, slightly more than AB-1, and failed after longitudinal bars began to fracture due to low-cycle fatigue fracture (see

for more information).

E.1.4 Realfonzo & Napoli (2009)

This paper discusses results of an experimental program testing the seismic performance of RC columns retrofitted with external steel devices and FRP. The 24 specimens were representative of columns designed only for gravity load, where deformation compatibility was not a concern, and were tested under cyclic lateral load. The testing consisted of columns with either deformed or smooth rebar. Additionally, the columns were further divided into two groups with non-dimensional axial loads of 14 and 40%. The literature review in this section focuses on the columns with deformed bars as shown in Table E-.

Table E-1: Column Specimens with Deformed Bars. Table Modified from Realfonzo & Napoli (2009).

Test	Steel rebars	Fibers	Number of layers	f_{cm} (MPa)	N (kN)	ν	F^{+}_{max} (kN)	F^{-}_{max} (kN)	δ_{max} (%)	Failure mode
C9-D	Deformed	—	—	31.8	365	0.13	71.08	66.32	3.51	Concrete spalling, bar buckling
C7-D-C		Carbon	2	26.1	330	0.14	65.33	69.10	6.99	FRP fracture, bar buckling, failure of a bar in tension
C8-D-C		Carbon	2	26.5	335	0.14	69.74	63.51	6.44	FRP fracture, bar buckling, failure of bar in tension
C14-D-C		Carbon	2	35.3	380	0.12	62.87	58.65	6.46	FRP fracture
C15-D-A1		Carbon	2	22.0	278	0.14	110.74	110.81	5.00	Slippage of the steel connector
C21-D		—	—	11.7	420	0.40	52.83	47.05	2.79	Concrete spalling
C22-D-C		Carbon	2	11.7	420	0.40	55.74	59.54	5.59	Local FRP fracture
C23-D-C		Carbon	4	12.5	450	0.40	72.94	69.03	8.24	FRP fracture, concrete crushing
C24-D-A1		Carbon	2	15.0	540	0.40	119.82	112.35	4.23	Slippage of the steel connector

Note: Values of ν slightly lower than 14% were applied in the case of Tests C9, C11, and C14; $\delta_{max}=s_{max}/H_{col}$; $f_{cm}=0.83\ R_{cm}$ (R_{cm} was estimated by compression tests on cubic 150-mm side specimens, taken during casting of each column and cured under the same environmental conditions).

One retrofit scheme tested both unidirectional glass and carbon fiber wrap, which were used to continuously confine the region that would experience flexural hinging. Furthermore, FRP strips were used to confine the rest of the column. Another retrofit scheme tested steel angles epoxied to the corners of the columns, with two anchoring scenarios. Figure E-7 shows type A1 specimens and the two anchoring systems. Option (a) was designed to only transfer tension forces, whereas option (b) transfers both tension and compression forces to the foundation.

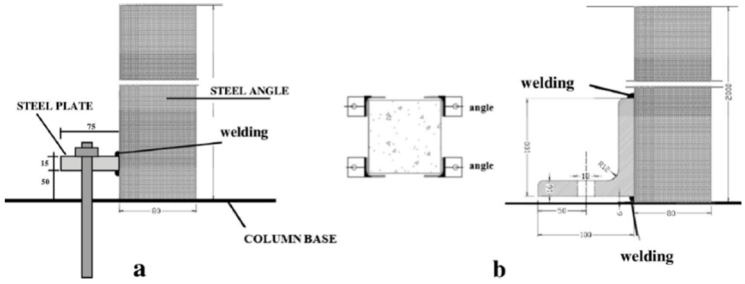

Figure E-7: Anchoring Systems for Steel Angle Retrofit, Realfonzo & Napoli (2009).

Columns subjected to axial loads of 14% experienced the most concentrated damage slightly above the column-foundation interface, with the flexural cracks distributed at the position of the steel stirrups. As testing progressed, the width of the flexural cracks increased slightly. Prior to collapse, concrete crushing occurred at the base of the column. Conversely, CFRP confined columns experienced flexural cracking at the column-foundation interface and outside the wrapped regions. These columns were governed by concrete spalling and buckling of rebar. Similarly, unconfined columns subject to 40% axial loads were governed by rebar buckling or concrete spalling. Horizontal cracks occurred at the stirrups and vertical cracks developed prior to the onset of rebar buckling. Confined columns were governed by concrete crushing or fracture of the FRP.

Axial loads did not dictate the performance of the steel devices. A1(a) anchorages were governed by either failure of the weld or pullout of the anchor rod and had sudden loss of strength contribution from the steel. A1(b) devices had a more progressive failure transition. Regardless of the axial loads, FRP provided significant increases to deformation ductility in the columns. Under high axial loads (40%), the FRP passive confinement resulted in noticeable strength increase. The ultimate FRP tensile strain at

collapse was approximately 1/5 of the maximum design tensile strain. Anchored steel anchors also provided increased flexural capacity. It was noted that columns wrapped with FRP had no increase in stiffness.

E.1.5 Summary of Experimental Testing of Concrete Columns Using FRP

This section reviewed several experimental tests of concrete columns with FRP retrofit schemes applied to improve the earthquake performance of deficient columns. In all cases, FRP had a positive impact on global column displacement ductility. See summary Table E-2 for comparisons between researchers. Additionally, the use of steel devices anchored into the footing significantly increased deformation ductility, flexural strength of the columns, and provides better ductile detailing, while minimizing the effects on stiffness.

Table E-2: Summary of Experimental Testing of Concrete Columns with FRP

Researcher	Specimen	ρ_l	N_a (%)	f'_c (ksi)	FRP	Ductility	Failure Mode
Sheikh & Yau (2002)	S-3NT	3.00	30	5.69	N/A	3.0	Bar buckling
	ST-2NT	3.00	30	5.86	(2) GFRP	6.0	Fiber rupture
Iacobucci et. al. (2003)	AS-1NS	2.58	40	4.55	N/A	3.7	Bar buckling
	ASC-2NS	2.58	38	5.29	(1) CFRP	6.1	Fiber rupture
Endeshaw et. al. (2008)	AB-1	1.33	7	4.50	N/A	6.4	Bar buckling/rupture
	FRP-4	1.33	7	4.50	(4) CFRP	7.4	Bar rupture / fiber bulge
Realfonzo & Napoli (2009)	C9-D	1.03	13	4.61	N/A	2.2	Concrete spalling / bar buckling
	C7-D-C	1.03	14	3.84	(2) CFRP	4.9	Fiber/bar rupture, bar buckling

E.2 Testing of Reinforced Concrete Walls Using FRP

This section covered three experiments involving concrete shear walls and FRP retrofit schemes. Each retrofit sought to improve some combination of shear strength, displacement ductility, energy dissipation, flexural strength, base anchorage, and/or lap splice placement. Most of the retrofitted walls became more ductile compared to their respective control walls without FRP enhancements.

E.2.1 Paterson & Mitchell (2003)

This paper discusses the results from an experiment for a proposed retrofit to use headed bars and carbon fiber wrap for seismic strengthening of shear walls in a 1960s building in Berkeley, California (Mar et al. 2000). Two walls were tested with lap splices at different locations. Figure E-8 shows the two specimens.

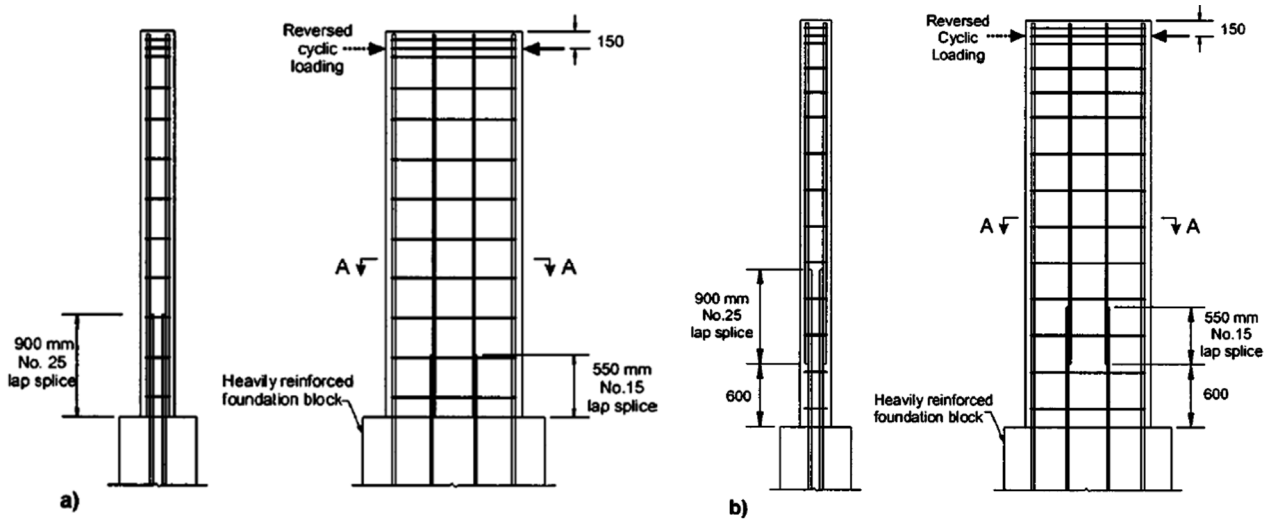

Figure E-8: Specimen (a) W1 and (b) W2, Paterson et al. (2003).

Specimen W1 had a lap splice near the base of the wall. The wall had poor ductility and failed soon after yielding. The wall had a brittle failure where the lap splices occurred, which led to a significant drop in capacity. Specimen W2 had more ductility than W1 because of the delayed response of inelastic deformation in the lap splice region. W2 had a brittle tensile failure at the lap splice region.

The retrofit strategy for W1R used a reinforced collar to add passive confinement where the lap splice of the wall occurred to mitigate the effects of lap splice debonding. The reinforced collar consisted of FRP, headed dowels, confinement steel, and end pins, as shown in Figure E-9(a). Additionally, the rest of the wall was shear strengthened using FRP. As a result of the reinforced collar, the area of concentrated inelastic deformation shifted to the region above the reinforced collar. W1 and W1R had overstrength factors of 1.18 and 1.26, respectively. The deformation ductility increased from 1.5 to 3.8 in W1R.

The retrofit for W2R was FRP with through-wall and end pin confinement reinforcement in the region of inelastic deformation as shown in Figure E-9(b). When compared to W2, W2R experienced an

increase of deformation ductility from 4.0 to 6.3 and no loss of strength due to lap splice failure. Also, W2R had a larger overstrength of 1.31 when compared to W2, which had an overstrength of 1.18.

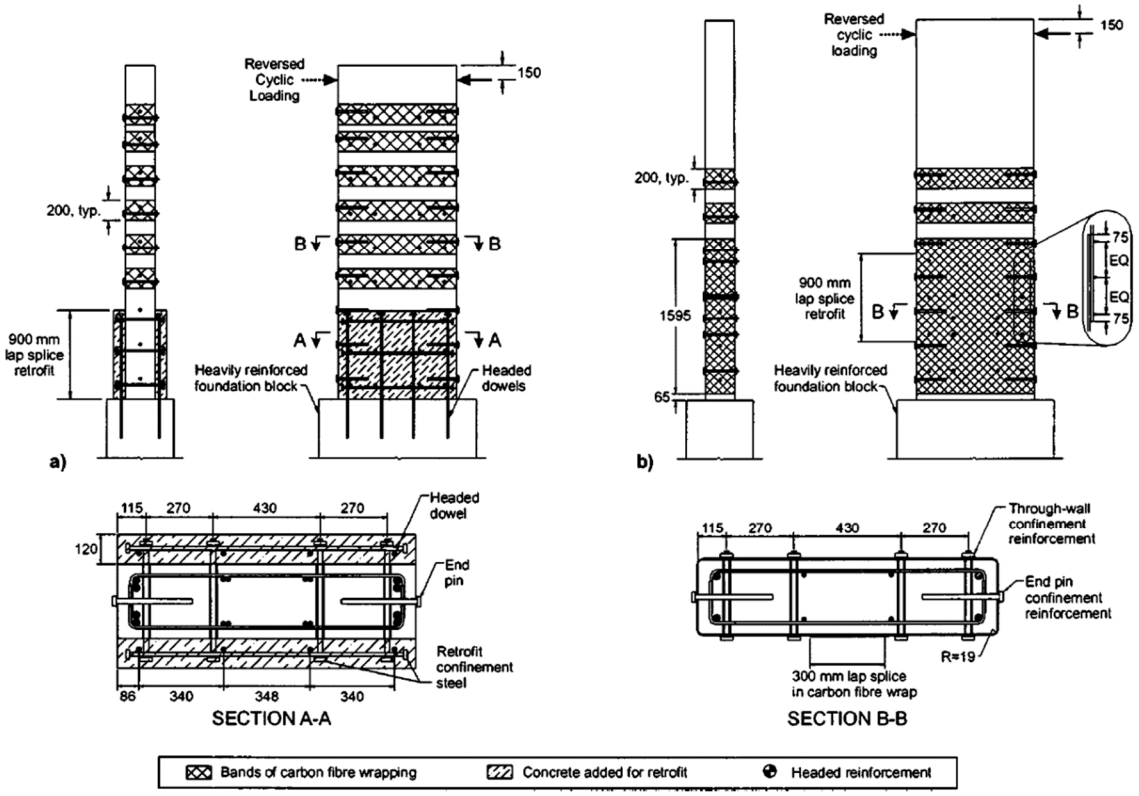

Figure E-9: Retrofit Schemes for (a) W1R and (b) W2R, Paterson et al. (2003).

Both retrofit schemes were effective in increasing deformation ductility and overstrength. Both were effective in providing confinement to prevent lap splice failure in the region of concentrated deformation. However, the increase of overstrength will result in increased design demands on the existing foundation systems. The retrofit for W1R was more invasive than W2R because of the additional shotcrete required but is a viable solution where this is not a concern.

E.2.2 Khalil & Ghobarah (2005)

This paper summarizes the results from an experimental program focused on concrete wall retrofit schemes using FRP and steel rods to improve the ductility, energy dissipation, and shear strength of existing deficient walls. The researchers acknowledge the abundance of rehabilitation testing with FRP in the existing

literature for columns and beams but sought to fill in the literature gap for walls retrofitted with FRP. They did cyclic testing on three walls: specimen CW as the control, specimen RW1 as an FRP only retrofit, and specimen RW2 as a steel and FRP retrofit. Their retrofit schemes were successful at improving the performance of their prototype deficient wall.

For ease of testing, Khalil & Ghobarah modelled the plastic hinge region of their prototype wall and applied loads to replicate the free-body diagram at the plastic hinge (see Figure E-10 below). Cardenas & Magura also implemented this simplification for their walls. Their prototype wall was designed to comply with ACI 318-68 and CSA-77. Figure E-11 shows the reinforcement schemes and dimensions of each specimen.

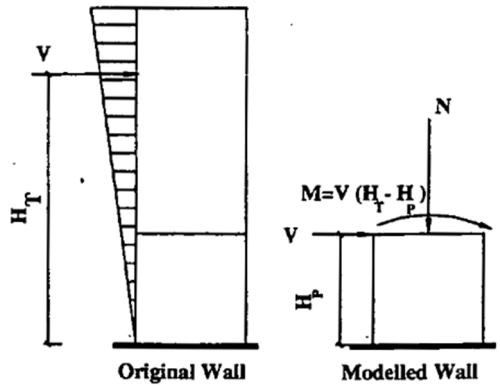

Figure E-10: Prototype wall versus modelled wall, Khalil & Ghobarah (2005).

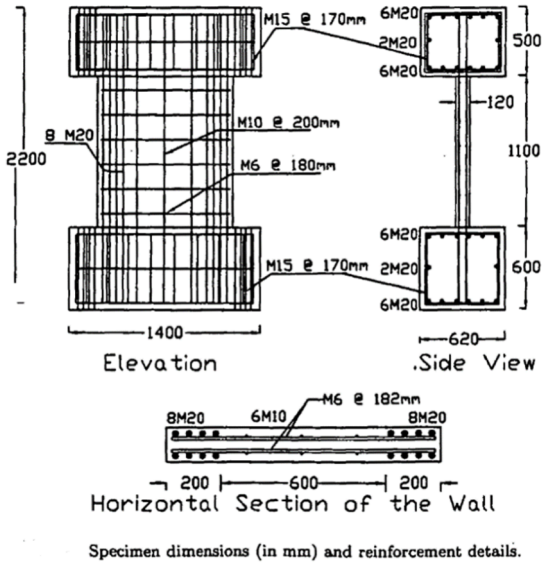

Figure E-11: Reinforcement Steel Layout for Wall Specimens, Khalil & Ghobarah (2005).

The retrofit schemes implemented in this paper are described below and shown in Figure E-12. For specimen RW1, the retrofit was designed to improve the shear strength and displacement ductility of the deficient wall. To improve shear strength, two layers of bidirectional FRP were wrapped around the entire wall, stopping 30 mm from the top and bottom of the wall to allow space for development of the flexural hinge. The ductility-enhancing aspect of the retrofit also implemented FRP but was only concerned with the end column elements of the wall. Similar to transverse ties in a modern boundary element of a concrete wall, the ductility-enhancing retrofit used three layers of unidirectional FRP to confine the highly stressed

concrete end zones by wrapping around the edge elements of the wall (over the bidirectional FRP) in the form of a U-shaped partial hoop. FRP anchors inserted through the wall acted as the fourth side that closed the U-shaped hoops. For specimen RW2, the retrofit concept remained nearly identical to RW1 but implemented steel anchors (threaded rods) instead of FRP anchors.

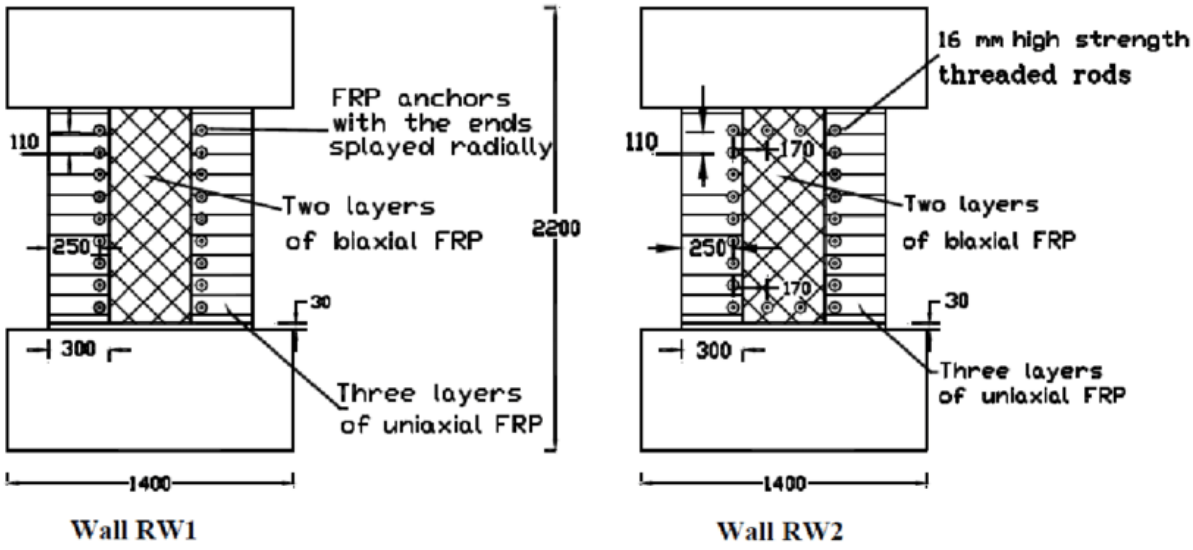

Figure E-12: Retrofit specimen details, Khalil & Ghobarah (2005)

The results of the experiment are summarized below. The control wall specimen CW performed very poorly, failing in shear before theoretical yield occurred. Specimen RW1 reached a displacement ductility of three before failure triggered by longitudinal bar buckling while specimen RW2 reached a displacement ductility of four. Both retrofits also increased the maximum lateral force reached as shown in Figure E-13. Specimen RW2 outperformed RW1 because the steel anchors had a higher shear strength than

the FRP anchors, preventing failure of the retrofit scheme for longer. In general, the retrofits were successful.

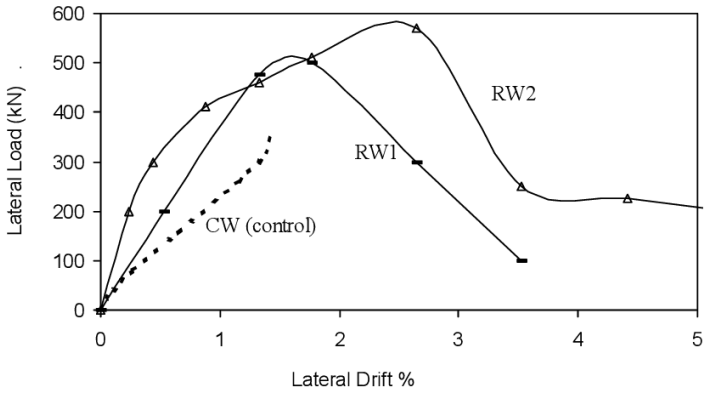

Figure E-13: Lateral force versus experimental drift, Khalil & Ghobarah (2005)

E.2.3 Cruz-Noguez et al. (2015)

Carlos A. Cruz-Noguez et al. summarizes results from experiments performed by Lombard et al. (2000) and Hiotakis et al. (2004) which evaluates seven shear wall specimens using externally bonded FRP as a repair/strengthening measure. This document highlights the performance of the FRP schemes and the effectiveness of two types of FRP anchoring systems. The overall objectives of the experiment were to assess the added flexural strength of FRP to the specimen, gather insight on the different failure mechanisms, and to develop models to predict the strength capacity of shear walls with FRP repair/strengthening.

To limit the parameters of the study to consider only FRP performance, the shear wall specimens were designed to fail in a ductile behavior. The walls were controlled by flexure, meaning that they would fail in flexure before their shear capacities were reached. The test consisted of two baseline walls, which were then repaired, and five strengthened walls. The walls were then divided into two groups to test both anchoring systems. Table E-3 shows the different schemes used in the two-phase experiment.

Table E-3: Summary of Testing Specimens, Cruz-Noguez et al. (2015).

Phase	Anchor type	Type of specimen	Repair/strengthening scheme[a]	Code
1	Angle	Controls	–	CW-1
		Repaired	1V	RW-1
		Strengthened	1V	SW1-1
		Strengthened	2V+1H	SW2-1
2	Tube	Control	–	CW-2
		Repaired	1V	RW-2
		Strengthened	1V	SW1-2
		Strengthened	2V	SW2-2
		Strengthened	3V+1H	SW3-2

[a] *n*V = wall reinforced with *n* layers of unidirectional CFRP on each side in the vertical direction; *m*H = wall reinforced with *m* layers of unidirectional CFRP on each side in the horizontal direction.

The experimental setup included no axial loads, although an axial stress equal to $0.1b_wt_wf'_c$ was assumed for the sectional analysis. The specimens were subjected to an in-plane, quasi-static, cyclic loading sequence of lateral load applied to the top of the structure. FRP was only applied to the face of the wall and was not wrapped around the edges to mimic in-field limitations.

It was observed that the FRP repaired walls were able to recover 87% of the original stiffness. FRP strengthened walls were able to achieve 151% of the original stiffness. The walls with the highest deformation ductility of 9.1 had two vertical layers and one horizontal layer of FRP (SW2-1). Walls with a single layer of vertical FRP achieved a ductility of 9.0 (RW-1, SW1-1, RW-2, SW1-2). Walls with three vertical and one horizontal layer of FRP had a ductility of 8.3 (SW3-2). Walls with two vertical layers had a ductility of 5.5 (SW2-2). It is noted that horizontal FRP reinforcement attributed significantly to the deformation ductility of the walls.

The anchoring system is important in developing the tensile forces in the vertical layers of FRP into the foundation. Two systems were tested – one using angles and the other using a pipe, as shown in Figure E-14. The FRP sheets were able to carry tensile stresses after debonding from the concrete surface due to FRP being anchored to the base. Additionally, the FRP had an average 11% lower flexural capacity than predicted, which is a result of the imperfect bond conditions.

In summary, FRP is effective in recovering elastic stiffness and increasing flexural capacity in repair situations. Likewise, FRP is effective in increasing stiffness and flexural capacity in strengthening situations. Walls with additional horizontal FRP layers performed better, when compared to those without horizontal FRP layers. Additionally, it is noted that anchoring system is crucial in development of the ultimate stresses in the FRP and preventing premature debonding of the FRP.

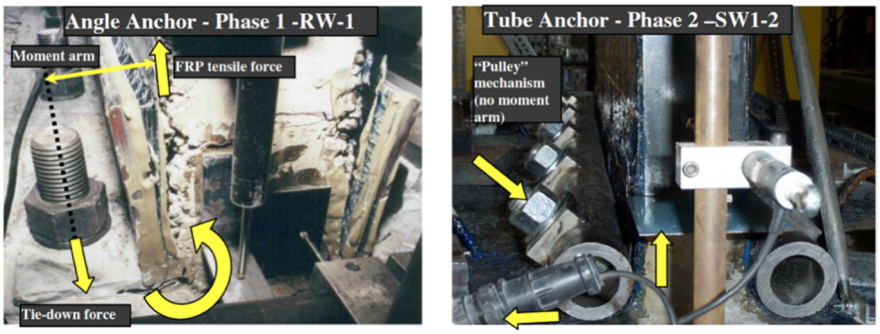

Figure E-14: FRP Anchoring Phases.
(Left) Angle Anchor and (Right) Tube Anchor, Cruz-Noguez et al. (2015).

E.2.4 Summary of Experimental Testing of Concrete Shear Walls with FRP

This section covered three different experiments involving concrete shear walls and FRP retrofit schemes. Each retrofit sought to improve some combination of shear strength, displacement ductility, energy dissipation, flexural strength, base anchorage, and/or lap splice placement. Most of the retrofitted walls became more ductile compared to their respective control walls without FRP enhancements. This information gives insight into how FRP can be used to retrofit concrete walls and how effective it can be when implemented correctly. See Table E-4 for a summary table of comparisons between experiments.

Table E-4: Summary of FRP retrofitted wall tests.

Researcher	Specimen	ρ_l	N_a (%)	*CSAR*	*SS*	f'_c (*ksi*)	FRP	Ductility	Failure Mode
Paterson & Mitchell (2003)	W2	0.74	0	4.0	3.1	4.8	N/A	4.0	Lap Splice
	W2R	0.74	0	4.0	3.1	4.5	(1) CFRP	6.3	Bar Rupture
Khalil & Ghobarah (2005)	CW	4.58	3.3	8.3	2.3	5.5	N/A	< 1.0	Shear
	RW1	4.58	3.3	8.3	2.3	5.5	(3) CFRP	3.0	Bar Buckling
Carlos A. Cruz-Noguez et al. (2015)	CW1	N/A	0	15	1.2	5.8	N/A	4.0	Conc. Crush
	SW2-1	N/A	0	15	1.2	5.8	(2) CFRP	9.1	Bar Rupture

F. Organization of Authorship

The following table of contents indicates authorship of each chapter/section of the document. Initials "RdS" indicate Rory de Sevilla's majority authorship, and initials "JL" indicate Jerry Luong's majority authorship. "Both" indicates that both authors contributed equally to the respective chapter/section.

(BOTH) COMMITTEE MEMBERSHIP

(BOTH) ABSTRACT

(BOTH) ACKNOWLEDGMENTS

(BOTH) LIST OF TABLES

(BOTH) LIST OF FIGURES

(RdS) LIST OF SYMBOLS

1.1. (RdS) Background

1.2. (BOTH) Objective and Scope

1.3. (BOTH) Organization of Contents

2.1. (RdS) Earthquake Damage of Lightly Reinforced Concrete Shear Walls

2.2. (JL) Progression of Structural Wall Detailing in ACI 318

2.3. (RdS) Testing of Lightly Reinforced Concrete Shear Walls

2.4. (JL) Performance of Modern Concrete Shear Walls

2.5. (BOTH) Discussion of Literature Review

3. (RdS) WALL DESIGN & MATERIALS

4. (RdS) TEST SETUP & WALL CONSTRUCTION

5. (JL) WALL TESTING

6.1. (RdS) ASCE 41-17 Analysis

6.2 (RdS/JL) Priestley Analysis

6.3 (JL) PEFORM-3D Analysis

7. (BOTH) CONCLUSIONS & FUTURE WORK

(BOTH) APPENDIX